A Mathematical Model of CA1 Hippocampal Neurons with Astrocytic Input

by

Katie Ferguson

A thesis
presented to the University of Waterloo
in fulfillment of the
thesis requirement for the degree of
Master of Mathematics
in
Applied Mathematics

Waterloo, Ontario, Canada, 2009

I hereby declare that I am the sole author of this thesis. This is a true copy of the thesis, including any required final revisions, as accepted by my examiners.

I understand that my thesis may be made electronically available to the public.

Abstract

Over time astrocytes have been thought to function in an auxiliary manner, providing neurons with metabolic and structural support. However, recent research suggests they may play a fundamental role in the generation and propagation of focal epileptic seizures by causing synchronized electrical bursts in neurons. It would be helpful to have a simple mathematical model that represents this dynamic and incorporates these updated experimental results. We have created a two-compartment model of a typical neuron found in the hippocampal CA1 region, an area often thought to be the origin of these seizures. The focus is on properly modeling the astrocytic input to examine the pathological excitation of these neurons and subsequent transmission of the signals. In particular, we consider the intracellular astrocytic calcium fluctuations which are associated with slow inward currents in neighbouring neurons. Using our model, a variety of experimental results are reproduced, and comments are made about the potential differences between graded and "all-or-none" astrocytes.

Acknowledgements

I would like to express my deep gratitude to my supervisor, Dr. Sue Ann Campbell. Her mathematical expertise and outstanding work ethic have been an inspiration to me throughout this project. Her encouragement and support continues to play an essential role in my research. I express many thanks for her tireless reading of this thesis and her detailed and constructive comments.

I acknowledge the partial financial support provided by the Department of Applied Mathematics through the graduate teaching assistantships.

I would like to express my gratitude to the professors and researchers in the Applied Mathematics Department, who have inspired me for many years. A special thanks to my graduate committee: Dr. Sue Ann Campbell, Dr. Brian Ingalls, and Dr. Marek Stastna.

I would also like to thank my father, sisters, and Justin, who have selflessly supported me throughout these years. I express my thanks to my sister, Amanda, for proof-reading endlessly without complaint. I am deeply grateful to my mother, who supported me throughout my life, and continues to be my greatest inspiration.

Dedication

This thesis is dedicated to my mother, Patti Ferguson.

Contents

List of Tables

List of Figures

Chapter 1

Introduction

Focal epileptic seizures affect millions of people worldwide, and are characterized by excessive and often synchronous neuronal discharges (World Health Organization, 2001). Tian et al. (2005) suggests that these seizures may actually be caused by pathologies in astrocytes, and not in neurons as was once thought. This may greatly influence the target of anti-eptileptic drugs, which currently focus on suppressing neuronal transmission. A simple mathematical model, which incorporates these new experimental results, would be helpful to examine the dynamics involved in the excessive discharges. Thus we created a two-compartment mathematical model (based on a reduction of Traub et al.'s (1991) 19-compartment model) of a CA1 pyramidal neuron, a neuron which is often the focus of seizure generation. To model the astrocytic input, we consider a synaptic current which is mediated by intracellular astrocytic calcium fluctuations. We aim to reproduce a variety of experimental results, and we discuss the physiological relevance of our model as well as its limitations.

1.1 Outline of thesis

The structure of this thesis is as follows. In Chapter 2, we discuss the necessary background biology. We start with a brief description of epilepsy, and then consider the components of the brain on multiple levels. We discuss in detail the cellular components of the brain (i.e. neurons and glial cells), and how they communicate with each other. In Chapter 3, we give a review of neuron electrophysiology. We comment on the methods of measurement used for excitable cells, and represent the cell as an R.C. circuit. We consider the dynamics of the currents and their respective conductances, which are involved in action potential generation. Finally, we derive the Hodgkin-Huxley equations for a squid giant axon. In Chapter 4, we give a literature review of the four articles which most influenced our project. First we review an article by Traub et al. (1991), in which a 19-compartment model of a hippocampal pyramidal neuron is created. Second we discuss an article by Pinsky and Rinzel (1994), in which a reduced two-compartment model for a CA3 neuron

is derived from Traub et al.'s (1991) model. Third, we review an article by Tian et al. (2005), in which an astrocytic basis of epilepsy is implied. Finally, we review Parpura and Haydon's (2000) article, in which the physiological astrocytic calcium signalling involved in neuronal modulation is considered. In Chapter 5, we consider an isolated neuron model of a CA1 hippocampal neuron. We describe the importance of model reduction, and how this reduction was accomplished. We create a mathematical description of the isolated neuron, and show that the characteristic behaviour of a CA1 neuron is reproduced. We analyse the bursting mechanics, determining the key parameters involved in such behaviour. In Chapter 6, we couple the CA1 neuron model with other neurons through an excitatory AMPA synapse, and discuss the results. In Chapter 7, we model the astrocytic influence on the CA1 neuron through an NMDA synapse. We consider the calcium signalling from astrocytes to be essential to the activation of the synapse, and model this intracellular astrocytic calcium concentration in a variety of ways. We reproduce many different experimental findings from both Tian et al. (2005) and Parpura and Haydon (2000), and discuss the results. In Chapter 9, we summarize our findings, discuss the physiological relevance of our model as well as its limitations, and directions that such research may take in the future.

Chapter 2

Physiology Background

Epilepsy is a neurological disorder that affects people of all ages worldwide. It is identified by recurrent unprovoked seizures, which are characterized by an excessive discharge (and often synchronization) of a large group of electrical impulses in the brain. Thus we begin this chapter with a brief description of this disease and its epidemiology. Although we will model the dynamics of these synchronized electrical signals on the cellular level, the effects of these cells on the rest of the brain must be considered. Therefore we will continue with a brief summary of the structural and functional organization of the brain, increasing in complexity and focus until we can properly describe the cells we plan to model. There are many ways to classify different regions of the brain, but we have chosen to do so using the principal of "functional localization": we break down the brain into components based on both function and the region in which it is located (Martin, 2003).

2.1 Epilepsy

Approximately 50 million people worldwide are affected by epilepsy (World Health Organization, 2001), a neurological disorder which is primarily identified by re-occuring unprovoked seizures. Although characterized by its seizures, symptoms of epilepsy vary significantly among patients, and thus epilepsy is often thought of as a group of disorders rather than a single disease (Milton and Jung, 2003). Head trauma, degenerative disease, infection, hemorrhage, and genetic dispositions are all possible causes of epilepsy (Vinters et al., 1993), and thus epilepsy affects people of all ages and economic status (Milton and Jung, 2003). The mortality of the population with epilepsy increases two to three fold compared to the general population, with the majority of epilepsy-related deaths involving suicide (associated with depression), trauma associated with seizures, sudden unexpected death in epilepsy (SUDEP), and status-epilepticus (where the brain is in a continuous state of seizure) (Hitiris et al., 2007).

Seizures are created by the excessive discharge of electrical activity in the brain, and are often categorized by their place of origin and their severity. This abnormal

electrical activity can be detected by an Electroencephalogram (EEG), which is the most common diagnotic tool when detecting epilepsy (Milton and Jung, 2003). The process involves measuring the electrical activity of the brain cells by placing sensitive recorders on the patient's scalp. It is very difficult to localize the origin of some seizures, and these are called generalized seizures, whereas others originate in a specific location in the brain, and are known as partial seizures. According to Williamson et al. (1997a), those who suffer from partial epilepsy comprise over 50% of all epileptic patients. Partial seizures can be further categorized into those in which consciousness of the patients remains throughout the seizure, called partial simple seizures, and into those in which consciousness is lost, called partial complex seizures (Milton and Jung, 2003). Antiepileptic drugs, also known as "anticonvulsants", are able to successfully treat approximately $70 - 80\%$ of patients with epileptic seizures (when the medication is available) (Milton and Jung, 2003). Patients with reoccuring epileptic seizures which do not respond well to medication (or sometimes even surgery) are often said to have Medically Intractable Epilepsy (MIE). In MIE, seizures become more frequent over time (known as the "boom-bust" cycle), and less receptive to anticonvulsant medication (Milton and Jung, 2003). The most common type of MIE is called Temporal Lobe Epilepsy (TLE), which is characterized by a particular type of partial seizure originating in a portion of the brain known as the temporal lobe (Milton and Jung, 2003). Temporal Lobe Epilepsy is especially hard to treat (Williamson et al., 1997b), and patients with this type of epilepsy comprise approximately 80% of those suffering from partial epilepsy. Patients with TLE can be categorized into those with Lateral Temporal Lobe Epilepsy (LTLE), and those with Mesial Temporal Lobe Epilepsy (MTLE). Those suffering from MTLE comprise the majority of patients who are unresponsive to antiepileptic medication (Babb and Brown, 1987). Surgery, although often quite effective according to Wieser and Williamson (1993), is a less appealing option due to the risks involved. Seizures involved in MTLE often originate deep in the temporal lobe in structures known as the hippocampus and the amygdala, regions which are well known for their involvement in memory consolidation and emotions (Martin, 2003). In particular, much recent research on MTLE has involved a specialized type of cell found in the hippocampus, called a CA1 pyramidal neuron, which is highly succeptible to strong electical discharges (Duvernoy, 2005). We will first consider the function and location of the regions of the brain involved in MTLE.

2.2 Divisions of the brain

We consider the brain of a vertebrate: along with the spinal cord it composes the central nervous system (CNS). Together the CNS and the peripheral nervous system (PNS) control behaviour and sensory information processing. In fact, the brain also contains components that regulate heart beat, balance and other unconscious but life-saving functions. How does it do so? The brain is composed of two main types of cells: nerve cells (called neurons), and glial cells. These cells are connected

with each other in many ways, creating a complex network that relays information in the form of electrical and chemical signals. In fact, the influence of glial cells on neurons has received much recent attention from researchers interested in the dynamics behind the generation of seizures. Of course, before this cellular level is discussed in further detail we must first understand the larger components of the brain.

The brain can be organized into two components: the forebrain (or the prosencephalon) and the brain stem (Martin, 2003). The brain stem is responsible for many important functions such as cardiac and respiratory functioning, and simple sensory processing such as pain. The forebrain is of greater interest when considering Temporal Lobe Epilepsy, however, since it encompasses the regions of the brain known as the cerebrum (known also as the telencephalon), and the interbrain (or the diencephalon) (Martin, 2003). The interbrain includes the thalamus, hypothalmus, and other important structures known for their involvement in consciousness and processing of metabolic and sensory information. The thalamus in particular is an important relay centre which processes information from the cerebrum. It is the cerebrum, however, that includes the temporal lobe, and thus the hippocampus. This is our primary stucture of interest, as it contains an area called Corpus Ammonus 1 (CA1), which is made up of the specific type of brain cell that is known for its irregular electrical discharges (Duvernoy, 2005). The main components of the cerebrum are the cerebral cortex and the basal ganglia (Carlson, 2001). A summary of this organization of the brain is shown in Figure 2.1.

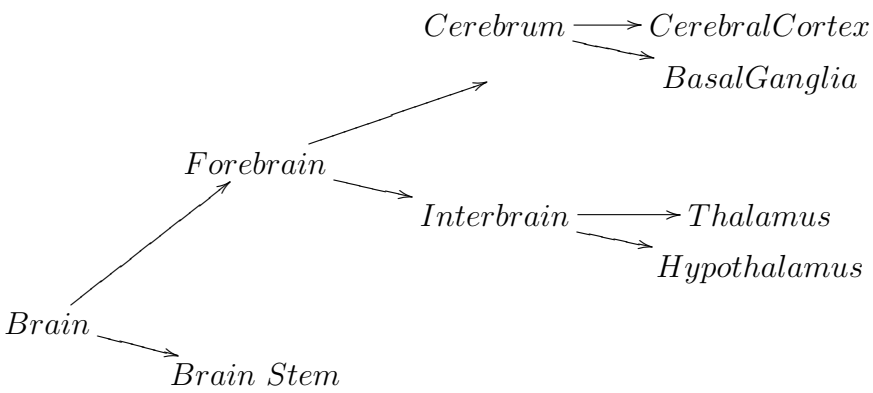

Figure 2.1: A summary of some of the primary functional components of the brain.

2.3 Cerebral cortex

The cerebral cortex composes the largest and most developed part of the human brain, and includes structures such as the amygdala (thought to be responsible for emotion), the hippocampal formation (thought to be involved in learning and memory), and the neocortex cortex (involved in higher functioning) (Martin, 2003). The

cerebral cortex is composed of grooves, called sulci and fissures, and convolutions, called gyri. Since the majority of the surface area is found in the grooves, this composition greatly increases its surface area (by approximately three times) (Carlson, 2001). For example, in a human cerebral cortex, the surface area is approximately 2360 cm^2, with a thickness of only about 3 mm. Thus a large network of neurons is possible within a small volume of cortical tissue.

The cerebral cortex is often divided into four main regions: the frontal lobe, the parietal lobe, the occipital lobe, and the temporal lobe. These lobes are named after the cranial bones which overlie them, and are separated by primary sulci and fissures such as the Central Sulcus (dividing the frontal and parietal lobes). The location and shape of these structures are shown in Figure 2.2. The cerebral cortex receives information from the sensory organs, and although information is shared amongst the lobes, each lobe is primarily responsible for the processing of different aspects of the sensory information. For example, the frontal lobe contains the primary motor cortex, which controls movement, and is involved in decision making and planning. The parietal lobe contains the primary somatosensory cortex, which is responsible for processing spatial information, whereas the occipital lobe contains the primary visual cortex, and is responsible for the processing of visual information. Finally, the temporal lobe contains the primary auditory cortex, and is responsible for the perception and localization of sounds (Martin, 2003). The temporal lobe also contains the hippocampal formation, and the amygdala: crucial components of the limbic system. The limbic system is composed of interconnected structures which are primarily involved in memory, emotion and motivation (Carlson, 2001). As mentioned, the hippocampal formation is of particular interest when studying seizures originating in the mesial temporal lobe.

2.4 Hippocampal formation

The hippocampal formation received its name from Arantius (in 1587) when he compared its shape to a mythical creature known as a hippocampus or sea horse (Duvernoy, 2005). The hippocampal formation plays an integral role in the limbic system, and is known for its strong influence in learning and consolidation of long-term memory. Damage to the hippocampal formation may lead to impairments in semantic memory (knowledge of facts), and episodic memory (memory of spatial and temporal events), but patients are often able to retain implicit memories involving well-learned actions or facts (Martin, 2003). The hippocampal formation helps regulate emotion, especially that of pain, and is thought to influence mechanisms of drug addiction (Duvernoy, 2005). It may influence motor reactions involved in emotion, and regulation of hypothalamic functions (such as the secretion of hormones) (Duvernoy, 2005). The hippocampal formation is usually larger in higher species, and many believe this is because of increased capabilities in learning and memory (Duvernoy, 2005).

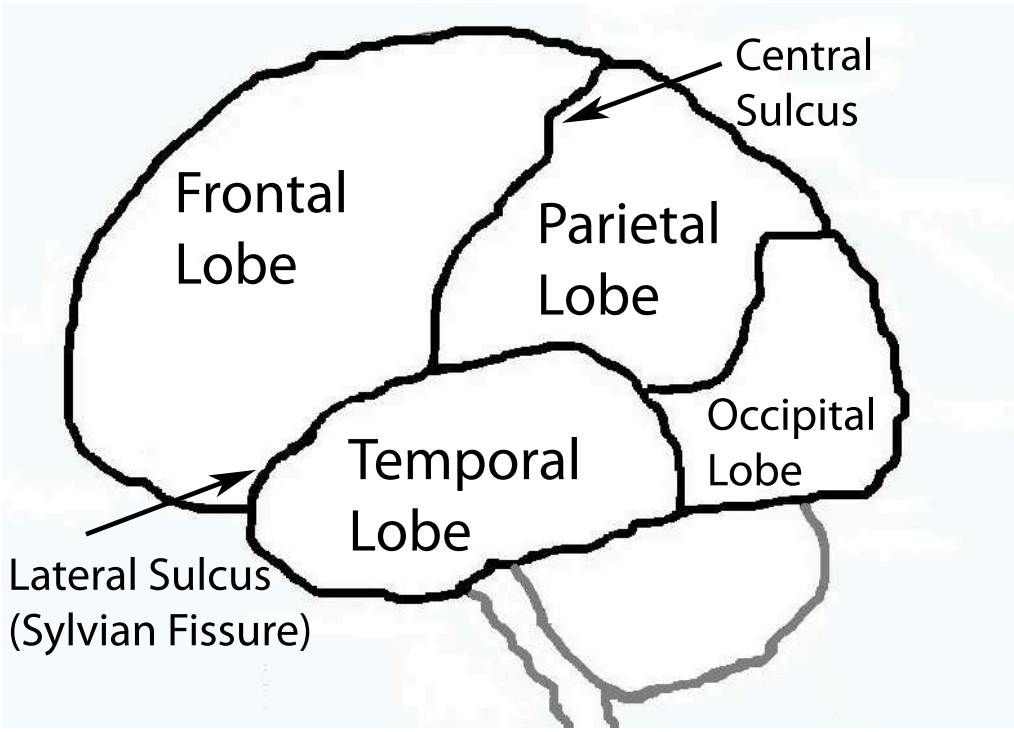

Figure 2.2: The cerebral cortex is often categorized into four lobes: the frontal lobe, the parietal lobe, the occipital lobe, and the temporal lobe. The division for these lobes are determined by prominent sulci, fissures, and gyri, such as the Sylvian Fissure and the Central Sulcus. The structures in gray denote the cerebellum and a part of the brainstem known as the medulla.

Located in the medial temporal lobe, the hippocampal formation is composed of the hippocampus proper, the subiculum, and the dentate gyrus (DG). This composition is variable, as many do not include the subiculum in the structure of the hippocampal formation (Martin, 2003). The hippocampus proper is categorized into four regions called Cornu Ammonis 1, 2, 3, and 4 (abbreviated by CA1, CA2, CA3, and CA4). Cornu Ammonis, meaning "Ram's Horn", was named because of its curved shape. It is densly packed with neurons called "pyramidal neurons" because of their triangular cell body. The dentate gyrus and the hippocampus proper are rolled together, forming a spiral cross-section, shown in Figure 2.3(a). The entorhinal cortex (EC) serves as the primary input to the hippocampal formation, and these pathways are called "perforant pathways". The most prominant input from the EC is to the granuale cells in the DG (Martin, 2003). From the DG, the neurons communicate with pyramidal cells of the hippocampal proper region CA3. The CA3 region relays to the CA1 region through a set of fibers called Schaffer collaterals. CA1 then sends the information as direct output, as well as to the subiculum. These long output fibers, known as axons, intertwine to create a structure called the fornix. The output fibers from the subiculum send information to the mammillary bodies in the hypothalamus (see Figure 2.3(b)), which eventually relay back to the EC. Thus a circuit is formed, called the "trisynaptic circuit" (Martin, 2003). The fornix fibers from the CA1 region relay information to the septal nuclei, a reward center for the brain. These main projections in the hippocampal formation are summarized in Figure 2.4. The CA1 region is of particular interest when concerned with seizure generation, since damage to the CA1 region is the most common form of mesial temporal sclerosis: neurological damage which is commonly found in patients with temporal lobe epilepsy. However, the research community is still unsure whether this damage is the cause or result of hippocampal seizures (Duvernoy, 2005).

2.5 Neurons

The neuron is considered to be the brain's primary functional cellular unit (Martin, 2003). Neurons use the exchange of chemical and electrical signals to process and transmit information, and there are estimated to be approximately 100 billion neurons in the human brain (Carlson, 2001). Most neurons (including those in the hippocampus) are electrically excitable, using an electrical impulse called an action potential to communicate with each other. These impulses have a stereotypical amplitude and shape, and are created by a difference in potential across the cell membrane. Information is carried through rate and timing of these action potentials. (These impulses will be discussed in more detail in chapter 3). Although neurons vary in function, their general components remain consistent: each neuron is composed of dendrites, a soma, an axon, and axon terminals. A typical neuron is depicted in Figure 2.5, and its main components are labelled. Most neurons are multipolar, and thus have one axon and multiple dendrites. However, some neurons

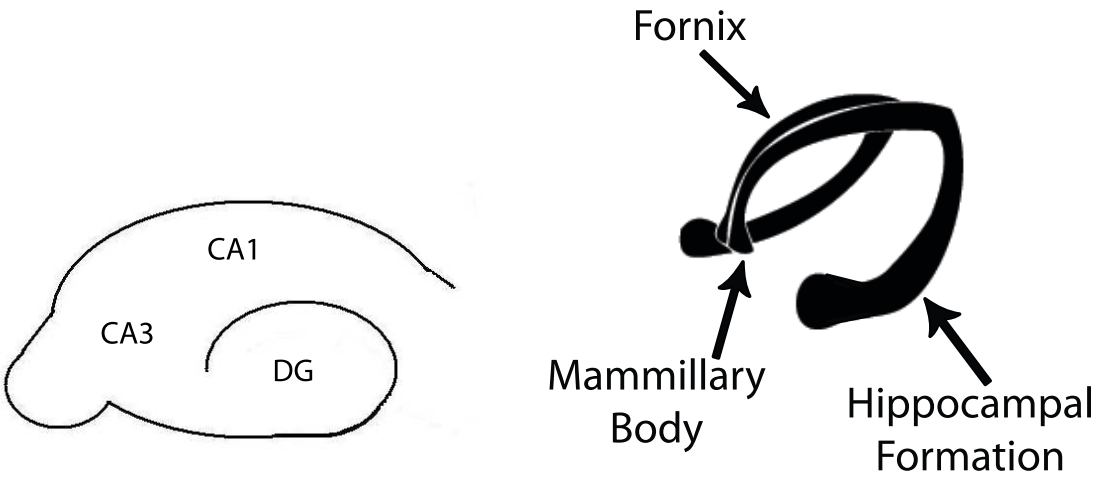

(a) (b)

Figure 2.3: (a) A cross section of the hippocampal formation, showing how the dentate gyrus and the hippocampus proper are rolled together. (b) The hippocampal formation has a curved c-shape. The output from the CA1 regions and the subiculum form the fornix, which connects with the mammillary bodies.

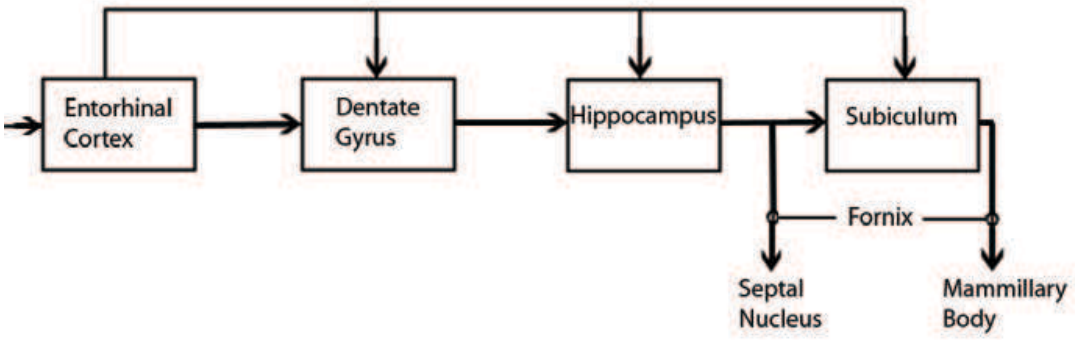

Figure 2.4: The main projections of the hippocampal formation, showing the primary input as the entorhinal cortex. The hippocampal formation is composed of the dentate gyrus, the hippocampus (or hippocampus proper), and the subiculum.

are bipolar, with one axon and one dendrite, or unipolar, with one branch from the soma which splits into both an axon and a dendrite.

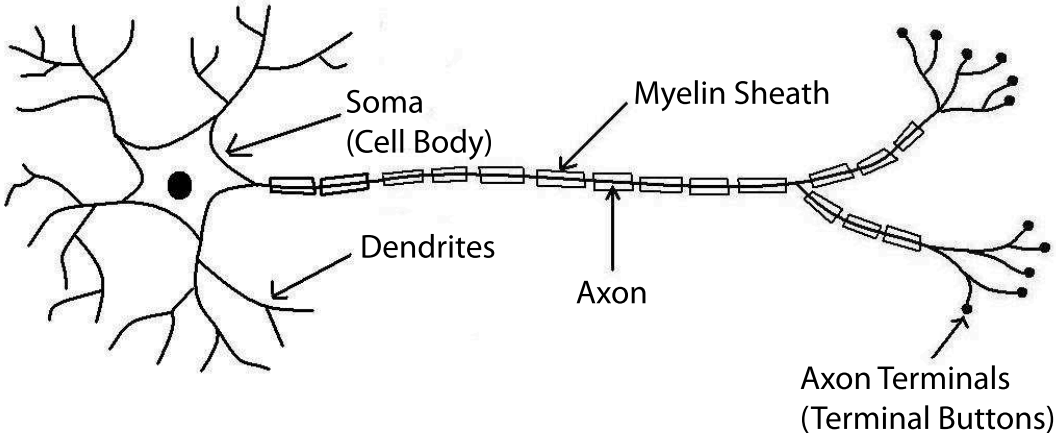

Figure 2.5: A depiction of a typical neuron. The dendrites (with their many branches), the soma, the axon and the axon terminals are labelled. The myelin sheath, which wraps around the axon and insulates it, is also labelled.

Dendrites typically receive signals from other neurons and relay them to the soma. It is appropriate that dendrites were named after the word "dendron", Greek for tree, as they often have a large branching structure which enables them to receive signals from many different sources (Carlson, 2001). They are usually passive, but this is not always the case: the dendrites of the hippocampal CA1 neurons can produce their own action potentials, called dendritic spikes. However, the threshold for the excitation of these spikes is rather high (Carlson, 2001). The signals from all the dendritic branches are integrated into the cell body of the neuron, called the soma. The shape of the soma varies depending on the function of the neuron. For example, CA1 neurons are called "pyramidal" because of their triangular shape. These neurons have two main branches of dendritic trees: one branch at the apex of the neurons (called apical dendrites), and one at the base of the neurons (called basilar dendrites) (Duvernoy, 2005). The soma contains the nucleus (which produces ribosomes for protein synthesis and chromosomes for production of DNA), and mitochondria (which is responsible for the production of energy in the form of ATP - adenosine triphosphate) (Carlson, 2001). The interior of the soma is composed of a substance called cytoplasm, and the cell works to keep it at a much different ionic composition than the extracellular fluid (fluid outside of the cell membrane). The cell membrane is made up of a lipid bilayer, with proteins forming channels and pumps to enable the cell to discriminate between ions and maintain this desired ionic composition. Once the signals are integrated into the soma, the electrically excitable soma "decides" whether it will send a signal or not. That is, if the integrated signal is strong enough, it will send an electrical signal (in the form of an action potential) down the axon, beginning at the portion of the axon closest to the soma (called the initial segment). Axons can be very long

(up to a meter or longer in humans), and thus to maintain this potential difference the long axons are often covered by an insulating layer known as a myelin sheath (Carlson, 2001). This lipid sheath ensures the fast speed of transmission of these signals, and enables the cell to use less energy to maintain the signal: the axon then acts as a cable until it reaches a gap between the sheaths. This gap is called the Node of Ranvier, and allows the difference in the intracellular and extracellular ionic composition to restore the action potential to its full amplitude. The axons are usually passive, and carry the signal to the axon terminals (also known as the terminal buttons). The axon may branch at the ends many times in order to send the signal to many potential receivers, but the signal remains the same strength in all branches (Carlson, 2001). At the ends of these branches lie small knobs (the axon terminals), where a chemical known as a neurotransmitter is released into a gap (called a synaptic cleft) between the axon terminal and the neighbouring cell. By releasing these neurotransmitters, the neurons are able to communicate with neighbouring cells by exciting or inhibiting them. Thus the information from an electrical signal is relayed chemically through what is called a chemical synapse. There are also electrical synapses, and the distinction between the two are described in the next section.

2.6 Synapses

The word synapse comes from the Greek word "sunaptein", which literally means "join together". Cells relay information to each other through a synapse in the form of an electrical or a chemical signal. In electrical synapses (also known as gap junctions), two cells are physically connected, allowing an electrical signal to be passed between them. The two cells are found in very close proximity, and their cell membranes share a common channel, and therefore a common ionic composition. Thus a depolarizing or hyperpolarizing potential across one membrane will create a similar signal across the other. Glial cells, which will be discussed in section 2.7, often communicate in this way. However, chemical synapses involved in communication with CA1 neurons have received much recent attention (Parpura and Haydon, 2000), so it is important to provide a more detailed description of how these synapses function. This summary will be based on a description from Carlson (2001). We will refer to the cell sending the signal as the presynaptic cell, and the cell receiving the signal as the postsynaptic cell.

2.6.1 Chemical synapses

Chemical synapses allow cells to relay signals by releasing chemicals into a small gap known as the synaptic cleft. This gap is variable in size, but is usually around 20 nm wide, and lies between the presynaptic and postsynaptic cells. Where do these chemicals come from? The Golgi apparatus in the presynaptic soma produces "synaptic vesicles" - vesicles containing chemicals called neurotransmitters. These

vesicles are transported to the axon terminal by fast axoplasmic transporters (i.e. transporters in the axon cytoplasm) called kinesin. The transporters move the vesicles down thick bundles of proteins which run the length of the axon, known as microtubules. The process is an active one, thus requiring energy in the form of ATP (adenosine triphosphate). The vesicles, filled with neurotransmitters, are transported down the axon into the axon terminals. Clusters of protein molecules are found on the presynaptic membrane, as well as on the surface of the synaptic vesicles. These protein clusters can bind together, and the synaptic vesicles are "docked" on the cell membrane. Axon terminals contain many voltage-dependent calcium channels. Therefore when an electrical signal reaches the terminal, the membrane is depolarized and the calcium channels open. Since the calcium is kept at a much higher concentration in the extracellular space, it quickly diffuses into the cell. This calcium binds to the clusters of protein molecules, and force the protein molecules to separate, creating a hole in the cell membrane known as a "fusion pore". Thus the neurotransmitters are released into the extracellular space. Everytime the synaptic vesicle joins with the presynaptic membrane, the axon terminal increases in size. This is regulated through a process called pinocytosis, in which pieces of the membrane are pinched off into the cytoplasm. This process provides a method of recycling, as the small pieces of pinched off membrane are used to create more synaptic vesicles.

Once the neurotransmitters are released into the synaptic cleft, they diffuse across and join with receptors on the postsynaptic membrane. Each neurotransmitter has a complementary shape to the receptor with which it binds, ensuring that specific neurotransmitters bind to specific receptors. When a chemical binds to a receptor in such a way, it can be referred to as a ligand, which in Latin means "to bind". This process is summarized in a cartoon shown in Figure 2.6. The receptors may be ionotropic or metabotropic: ionotropic receptors open neurotransmitter-dependent ion channels directly, whereas metabotropic receptors act indirectly and require metabolic energy. Once activated, a metabotropic receptor can respond in a variety of ways. Initially, the neutransmitter-bound metabotropic receptor activates a special protein bound to the membrane, called a G-protein. However, this activated G-protein may in turn activate a specific ion channel, or may activate a target enzyme. The activated enzyme may then produce a second messenger to open the ion channel. This metabotropic process is obviously more complicated than an ionotropic process, and requires more energy, but its effects last longer and may affect ion channels over larger distances.

The ion channels which open begin a series of events which may depolarize or hyperpolarize the postsynaptic membrane depending on whether the neurotransmitter is excitatory or inhibitory. There are four major types of ion channels which open due to neurotransmitter reception: sodium, potassium, chloride and calcium. When the sodium channels open, an excitatory post synaptic potential (EPSP) results (the cell is depolarized), and when potassium channels open an inhibitory post synaptic potential (IPSP) arises (the cell is hyperpolarized). An EPSP greatly increases the chances that the neuron will generate an action potential. If the cell

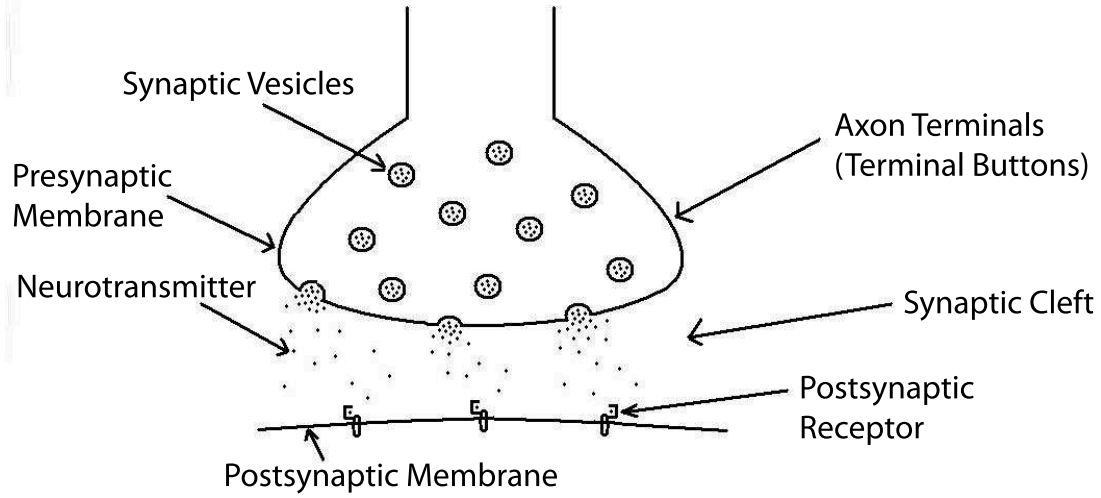

Figure 2.6: A cartoon showing the process involved in a chemical synapse. For simplicity, the presynaptic voltage-dependent calcium channels are not shown. Once these channels open, calcium rushes in, causing the protein clusters which join the synaptic vesicles with the presynaptic membrane to separate. The neurotransmitters are released into the synaptic cleft, and bind to postsynaptic receptors.

membrane is depolarized, then the opening of chloride channels will produce an influx of chloride ions, serving to repolarize the membrane. Therefore, chloride is said to neutralize the EPSP. Activated calcium channels results in an EPSP, which are often accompanied by important biochemical and structural changes. It is possible that some synapses of a neuron receive excitatory signals, and others inhibitory: the neuron integrates these signals and responds appropriately. The whole chemical synaptic process happens quite quickly. After the receptors release the neurotransmitter into the extracellular space, and the postsynaptic receptors are activated, the neurotransmitters are released and transported quickly back into the axon terminal of the presynaptic cell. For a particular neurotransmitter known as acetylcholine (ACh), enzymes are released into the synaptic cleft to destroy the chemicals (called enzymatic deactivation).

There are many different types of neurotransmitters, producing variable effects. Glutamate and acetylcholine are two common excitatory neurotransmitters, whereas γ-Aminobutyric acid (GABA) and glycine are common inhibitory neurotransmitters. Others, such as dopamine and serotonin, have various effects (Martin, 2003). Two distinct GABA receptors have been identified: the fast activating, fast deactivating ionotropic $GABA_A$ receptors are known to activate chloride channels, and the metabotropic $GABA_B$ receptors activate potassium channels. According to Carlson (2001), glutamate is the main excitatory neurotransmitter found in the central nervous system. There are four main types of glutamate receptors: the ionotropic NMDAr (N-methyl-D-aspartate receptors), the ionotropic AMPAr (α-amino-3-hydroxyl-5-methyl-4-isoxazole-propionate recep-

tors), the ionotropic kainate receptors, and the metabotropic glutamate receptors (mGluR). Excitatory synapses between neurons most often involve AMPAr. These are fast activating and fast deactivating receptors that respond to α-amino-3-hydroxyl-5-methyl-4-isoxazole-propionate (AMPA), a synthetic amino acid which mimics the effects of glutamate. These receptors control sodium channels and produce EPSPs. Similarily, N-methyl-D-aspartate (NMDA) is a synthetic substance derived from an amino acid, which is a selective agonist for these particular channels which are now called NMDAr. These receptors are fast activating, but slow deactivating, and are unique in that they are ligand dependent and voltage dependent. The NMDAr activate calcium and sodium channels. However, the calcium channels are initially blocked by magnesium, which naturally moves from the extracellular space and binds to a binding site deep in the calcium channel. Thus when the receptors are activated by gluatamate (or aspartate), the calcium channels open but calcium can not enter the cell. If, however, the neuron is depolarized, then the magnesium is released, and the ion channel is free to admit calcium into the cell. The calcium depolarizes the cell, and may initiate important structural or biochemical changes. These NMDA receptors are found in great numbers in the hippocampal formation, especially in the CA1 area.

2.7 Glial cells

Another type of cell is found in the brain - the glial cell - and they outnumber neurons by 10:1 (Martin, 2003). Glial cells are best known for their structural, functional and metabolic support, and have been considered to be the glue that physically holds the brain together. They are known to insulate neurons so that communication remains private and messages stay clear, to provide nutrition to neurons, and to remove dead cells. There are two major groups of glial cells: microglia and macroglia (Martin, 2003). Microglia play a phagocytic role, meaning that they remove dead or dying cells, destroy unwanted microorganisms, and aid in the repair of injured cells. Macroglia can be separated into four types: astrocytes, oligodendrocytes, Schwann cells, and ependymal cells. The oligodendrocyte's main function is to produce myelin for neurons in the central nervous system, whereas the Schwann cells produce myelin for neurons in the peripheral nervous system, and perform some phagocytotic activity. The ependymal cells help produce cerebral spinal fluid, whereas the astrocytes are known to provide physical support and perform phagocytotic activity. Although for many years glial cells were thought to perform auxillary functions, they are now considered to play a much larger role. In particular, the astrocyte is thought to influence neuronal signalling in the CA1 area of the hippocampus proper, and may even play a crucial role in the generation of seizures.

2.7.1 Astrocytes

Astrocytes are "star-shaped", and although they do not have dendrites nor axons, their many long processes that extend from their soma enable them to have many levels of communication (Carlson, 2001). They are most known for their structural support and phagocytotic activity, however they also provide nutrition. Astrocytes can help regulate the chemical composition of the extracellular space, by taking in and releasing chemicals which must be kept at particular levels. Astrocytes surround somatic and dendritic membranes as well as many surrounding capillaries, and thus are thought to extract glucose from the capillaries and break it down to lactate for neuronal uptake, which neurons use for metabolic energy (Carlson, 2001). Their long branches also surround neuron-neuron synapses, and help prevent scrambling of signals by insulating the neurons.

Due to their absence of a sufficient number of sodium channels, astrocytes are not electrically excitable as most neurons are. This has contributed to their lack of attention over the years, as their membrane potential is difficult to measure. However, with modern imaging techniques, scientists have been able to learn much more about these cells. In fact, they are now known to communicate with both neurons and other astrocytes (Carlson, 2001). Astrocytes interact with neurons by wrapping around synapses, and are thought to monitor up to 90% of cells in the cerebral cortex (Carlson, 2001). For this reason, and since they are known to have a variety of both ionotropic and metabotropic neurotransmitter receptors, they are thought to modulate neuron activity. In particular, electrically excited neurons are able to signal astrocytes through their synaptic release of glutamate. Astrocytes have metabotropic glutamate receptors (mGluRs) on their membrane, which become activated when the neuronal glutamate diffuses through the synaptic cleft. When these receptors are activated, a messenger protein called Inositol Triphosphate (IP3) is released into the astrocytic cytosol. This protein activates the IP3 receptors that are found on the membrane of internal calcium stores, namely the endoplasmic reticulum (ER). Once activated, calcium is released into the intracellular space (Nadkarni and Jung, 2005). Astrocytes usually communicate with each other through gap junctions and therefore are directly connected. Thus one activated astrocyte will result in waves of calcium across neighbouring astrocytes. However astrocytes communicate directly with neurons, modulating neuronal activity through chemical synapses. Thus one activated astrocyte will be able to access and affect a multitude of neurons. Astrocytes most commonly use glutamate to communicate with neighbouring neurons. The increase in the internal astrocytic calcium concentration leads to glutamate release into the synaptic cleft, activating the neuronal NMDA receptors and producing an excitatory effect. Since astrocytes can modulate neuronal activity, perhaps pathologies in these cells (instead of in neurons), play a role in seizure generation. In fact, many studies have recently been done to understand the effect of astrocytes on pyramidal neurons found in the hippocampus (Parpura and Haydon, 2000; Tian et al., 2005). It has been implied that upregulation of mGluRs on the membrane of astrocytes can lead to excessive

activity of neighbouring neurons (Nadkarni and Jung, 2005).

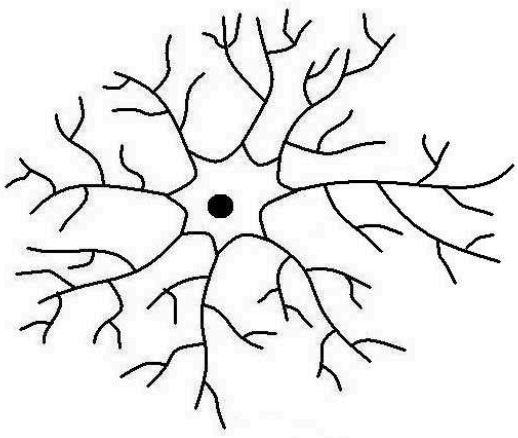

Figure 2.7: A drawing of a typical astrocyte. Its long processes permit it many levels of communication, both with other astrocytes and with neurons.

2.8 Discussion

Epilepsy affects many people worldwide, and yet the cause of epileptic seizures remains a mystery. Epilepsy is a diverse disease with variable symptoms affecting a variety of brain structures. Therefore to obtain a better understanding of seizure generation, it is important to focus on a particular type of epilepsy and the corresponding structures involved. We concentrate on mesial temporal lobe epilepsy (MTLE), as it is the most common form of medically intractable epilepsy (MIE), and thus very difficult to treat. In this form of epilepsy, the hippocampus is often the focal point of seizure generation, resulting in potential deficiencies in memory and learning. In particular, neurons known as CA1 neurons receive attention for their ability to easily produce excessive electrical discharges. Astrocytes have also been a focus in recent research, as they play a role in modulating the behaviour of these neurons. The function and structure of the neurons, the glial cells, and the synapses through which they communicate, have been reviewed. A better understanding of how all the parties involved communicate and affect each other is essential for more effective treatments and eventually a cure for this deadly disease.

Chapter 3

Neuron Electrophysiology

Fundamental to most nerve cells is the action potential: an all-or-none pulse of voltage that is produced near the cell body and propagated down the axon. This electrical impulse is the primary mode of communication for a neuron, carrying information quickly and efficiently. Through a series of equations, Hodgkin and Huxley have created a means of describing the ionic mechanisms that generate these action potentials (Hodgkin and Huxley, 1952d). These equations have been used in our two-compartment model of the CA1 pyramidal neuron, so a brief overview is required. Before we can outline the principal characteristics of the Hodgkin and Huxley model, we must understand some important concepts. Firstly, what makes a cell "excitable" (ie. able to attain an action potential)? Secondly, what techniques have been used to measure the properties of these cells? Next, what are ion channels, and how do they work? Hodgkin and Huxley were unaware of the existence of individual ion channels when their model was developed, but for a solid understanding of the dynamics of a cell, we will discuss the conductances of these ion channels and the currents that pass through them (instead of simply the overall permeability of the membrane). Throughout each section in this chapter, we will discuss the influences of each of these properties on the production of an action potential. Since Hodgkin and Huxley based their model around the concepts of electrophysiology, the idea of a cell represented as an R.C. circuit will be introduced. Then, once the necessary background information has been discussed, a summary of the Hodgkin and Huxley model of action potential generation will be provided.

3.1 Excitable cells

The cell membrane is composed of a phospholipid bilayer, with hydrophilic polar heads facing the extracellular and intracellular space, and hydrophobic non-polar tails (which face each other). This bilayer serves as a very thin insulator, preventing ions and other solutes from crossing. That is, it separates charges from the intracellular and extracellular space, acting as a capacitor. To provide the cell with a means of controlling the influx and efflux of ions, the membrane contains pore-like

proteins called ion channels and ion pumps. The ion channels use passive transport to allow ions to move along their electrochemical gradient into or out of the intracellular space, whereas ion pumps use energy (known as active transport) to move the ions against their electrochemical gradient. These channels and pumps can discriminate between the ions (although not perfectly), allowing one particular ion to cross the membrane and not the others. The movement of these ions through their respective channels or pumps causes an ion flux, which has an immediate effect on the potential across the membrane. Since the ion channels have been shown to play a crucial role in generating an action potential (Hille, 1992), we will concentrate on the dynamics of these channels, and not the pumps.

Most cells maintain a constant potential across the membrane when no stimulus or synaptic input is applied. That is, the cell works to keep a constant difference in electrical potential between the intracellular and extracellular space. This is called the cell's "resting potential". It is customary to define the potential across a membrane (E_m) as the difference between the intracellular potential (E_i) and the extracellular potential (E_e) such that

$$E_m(t) = E_i(t) - E_e(t) \tag{3.1}$$

where t represents time. To determine E_m, the following approach is often used. A very thin glass micropipette electrode attached to an amplifier is sent into the extracellular space. The amplifier is set to zero, and the electrode is advanced until it enters the cell. An immediate change in recording will be seen, and this is the resting membrane potential (Hille, 1992). Experiments by Cole and Curtis (1939) and by Hodgkin and Huxley (1952d) demonstrated that when at rest, the membrane potential for a cell is negative ($E_i < E_m$). The specific potential varies depending on the cell (usually from $-30\ mV$ to $-90\ mV$), but most excitable cells have a resting potential of about $-60\ mV$ to $-70\ mV$ (Fall and Keiser, 2002). When a stimulus or synaptic input is applied, the electrical response of the nerve cell is not necessarily proportional to the signal it received. This is because nerve cells are "excitable cells". That is, when a small signal is received by the cell, a small perturbation in the membrane potential occurs. However, if an excitatory stimulus is applied that surpasses a particular threshold, a large non-linear depolarization results that is determined by the cell properties, and not the impulse received. This burst of electrostatic energy is called an action potential, and has a consistent amplitude and stereotypical shape. Information is conveyed by varying the time and rate of these pulses (called "spike trains"). A typical action potential and its properties are shown in Figure 3.1.

To understand an action potential, one must consider the forces that interact to create the membrane potential. The cell membrane acts as a boundary between the extracellular fluid and the cell's intracellular fluid. Both these substances contain a vast number of ions, and so electrical forces and forces of diffusion are in constant conflict. Walther Nernst, a German physical chemist, formulated an equation to determine the equilibrium potential for these ions - the balance between electrical

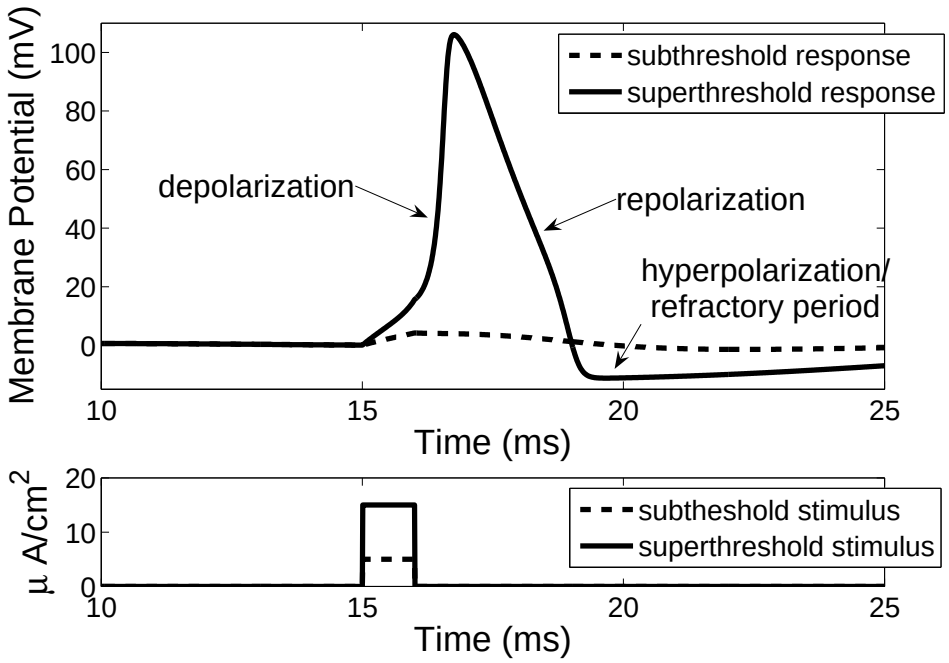

Figure 3.1: Top: An excitable cell undergoes an action potential when it is depolarized past a threshold. The key properties of an action potential are labeled. Bottom: The subthreshold and superthreshold stimuli applied.

attraction and diffusion due to concentration gradient. Consider two ions, chloride (Cl^-) and potassium (K^+), which are in a solution on either side of a membrane which is semi-permeable to K^+ (i.e. only K^+ is permitted to cross the membrane). Say that the left side of the membrane has a high concentration of this solution, and the right side has a low concentration of the solution. Because of this concentration difference, K^+ will initially flow from high concentration to low concentration by diffusion. Since Cl^- is unable to move across the membrane, the electrical charge will no longer be balanced. The right side of the membrane will become more positive, and the left more negative. The electrical potential gradient will cause K^+ to be pulled to the negative side. Thus the equilibrium in this case is a balance of both diffusion and electrical attraction. Each ion has a different equilibrium, called the Nernst potential, or the reversal potential. The Nernst Equation is given by:

$$E_{Nernst} = \frac{RT}{zF} ln \frac{[ion]_{out}}{[ion]_{in}} \tag{3.2}$$

where R is the universal gas constant, F is Faraday's constant, T is the absolute temperature in Kelvin, and z is the valence of an ion (or the charge number of the electrode reaction). For more information on the Nernst equation, see Hille (1992). Since this Nernst potential is derived using thermodynamics, the membrane potential will tend towards this value regardless of its initial starting potential. How does

one describe current when ions flow across the membrane? Goldman (1943) and Hodgkin and Katz (1949) derive a current-voltage relation, describing the current across a particular ion channel S (denoted I_S), with respect to the membrane potential (E_m) and the concentration of ions in the intracellular and extracellular space ($[C_i]$ and $[C_o]$ respectively). This relation is known as the "Goldman-Hodgkin-Katz Current Equation" (or GHK current equation), and is given by:

$$I_S = \frac{P_S z_S{}^2 F^2 E_m}{RT} \frac{([C_i] - [C_o]e^{-z_s E_m F/(RT)})}{1 - e^{-z_s E_m F/(RT)}} \tag{3.3}$$

where P_S is the permeability of the membrane, z_S is the valence of the ion, F is Faraday's constant, R is the gas constant, and T is the temperature in Kelvin. It is interesting to note that when the membrane potential, E_m, is the Nernst potential for the ion S, then $I_S = 0$. To derive this GHK current equation, they made the assumption that the electric field across the membrane is constant. For a full derivation and explanation of this equation, see Goldman (1943) and Hodgkin and Katz (1949). This relation between current and voltage leads us to contemplate which ion channels are fundamental to the production of an action potential. Moreover, how do they individually affect the membrane potential? Before these problems are addressed, the methods used to measure the voltage and current of an excitable cell will be summarized.

3.2 Methods of measurement

Throughout history, a few innovative methods changed the way we look at excitable cells. In particular, the voltage-clamp technique enabled scientists to observe the influence of an applied step of voltage on the currents flowing in and out of the cell. On the other hand, the current clamp enabled them to observe how an applied current may influence the membrane potential. Finally, the patch clamp technique allowed scientists to isolate a single ion channel and observe its dynamics. This discussion follows Guevara (2003) and describes these three methods, along with a brief description of how the squid giant axon was used to further our understanding of action potentials.

3.2.1 The voltage clamp technique

The voltage clamp technique, developed by Cole (1949), Marmont (1949), and Hodgkin, Huxley, and Katz (1949), enables one to control the voltage in a cell membrane through a feedback loop. One external electrode and two internal electrodes are needed for this method. First, electrodes are placed into both the extracellular and the intracellular space. These are called "voltage wires", and they determine the difference in potential across the membrane. Secondly, a "current wire" is placed inside the membrane, and injects a current into the cell. The electrodes

are attached to an amplifier so that once the membrane potential is recorded, the amplifier compares the actual potential with the desired fixed membrane potential. The error between the two determines the input from the amplifier into the current wire, and an appropriate signal is fed back to maintain the desired fixed voltage. The input current is thus equal to the ionic current passing through the membrane at the clamped potential. Using this technique, an increase in injected current can be applied to step the membrane potential up from one fixed value to another. For example, the membrane potential can be stepped up from its resting potential to a superthreshold potential, and the resulting response from the ion channels can be recorded (Figure 3.2).

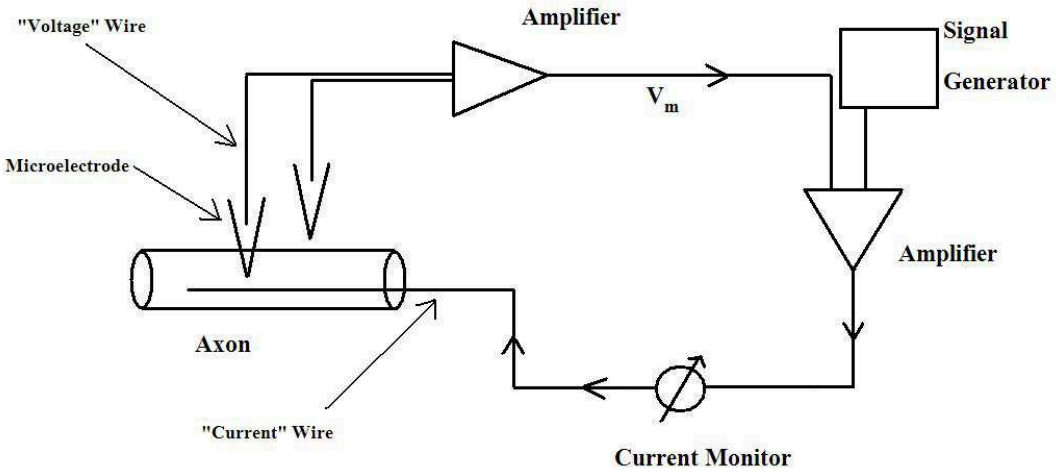

Figure 3.2: A voltage clamp. The membrane potential is measured (by the voltage wires) and fed into an amplifier. The actual potential is compared with the desired membrane potential, and a signal is sent back through the current wire as negative feedback to maintain the desired potential.

The voltage clamp technique was originally used on the squid giant axon. This is a giant axon, found in the stellate nerve of the squid (the North Atlantic squid is used in North America), which is used to initiate movement when escaping from predators. Thus the conduction velocity must be quite fast. This is achieved by the axon's extremely large diameter (up to 1 mm), and therefore low resistance to the signal propagation. This large diameter also permits a much easier insertion of the internal electrode. In fact, during the voltage clamp experiments with the squid giant axon, the electrodes are inserted longitudinally into the axon. This clamped the squid axon uniformly along its length, ensuring isopotentiality along this portion of axon. Therefore the total current response of that portion of the axon can be attributed to one membrane potential. Currents are generally measured in $\mu A/cm^2$.

3.2.2 The current clamp technique

The current clamp technique provides scientists with a means of determining how current affects the membrane potential. The set up is similar to that of the voltage clamp, but instead the voltage is permitted to vary and the current is clamped. Therefore if natural changes in current (or an applied current) causes a change in the membrane potential, the amplifier will record these changes. Using this mechanism and an appropriate stimulation, an action potential can be produced and examined. It is important to note that current flowing into the cell is taken to be negative, and current flowing out is taken to be positive, by convention.

3.2.3 The patch clamp technique

The patch clamp technique is used to study single ion channels found on a patch of membrane of an excitable cell. A glass micropipette (with a tip diameter on the order of 1 μm) is pressed against the surface of the membrane, and is suctioned to provide a strong seal. The micropipette is filled with liquid which is similar in composition to the bath solution (or extracellular fluid). An electrode is placed inside the micropipette solution to conduct current, and is attached to an amplifier. Then the electrical activity through the membrane is recorded. It is possible to isolate only one ion channel in the clamped patch of membrane. In this case, the opening and closing of the ion channel can be recorded. The recordings show that in the "open" state, a fixed amount of current is able to flow through the channel. The Nobel prize in Physiology or Medicine was awarded to Neher and Sakmann in 1991 for their development of the patch clamp technique (in the late 1970s and early 1980s).

3.3 The current-voltage relations of ion channels

The voltage clamp and current clamp techniques allowed the currents involved in an action potential to be disected and analysed. Hodgkin and Huxley (1952a) were able to identify which ion channels were fundamental to the production of an action potential in the squid giant axon. This section follows Hille (1992). We outline how Hodgkin and Huxley identified the principal channels, their current-voltage relations, how these relations affect an action potential, and how the ionic currents can be modeled mathematically.

3.3.1 Ions involved in an action potential (in the squid giant axon)

Hodgkin and Katz noticed that during an action potential, the peak membrane potential of a squid giant axon approached that of the Nernst potential of sodium

($E_{Na} \approx 50\ mV$) (Hodgkin and Katz, 1949). Therefore they proposed the "sodium hypothesis". That is, they proposed that during an action potential, the membrane became much more permeable to sodium. Thus, with sodium in a much higher concentration in the extracellular space than inside the cell, sodium would rush in, and the membrane potential would climb toward the sodium Nernst potential. To test their hypothesis, they reduced the extracellular sodium chloride and found that the action potential was also reduced (but not the resting potential). If the extracellular sodium was removed entirely, the cell became reversibly inexcitable (i.e. no action potential could be obtained) (Hodgkin and Katz, 1949). They asserted that potassium ions also played a lead role in generating an action potential, as on the downstroke, the potential approached that of the potassium Nernst potential ($E_K = -90\ mV$). With potassium in a much higher concentration inside the cell, these dynamics seemed reasonable. Thus Hodgkin and Katz (1949) identified sodium (Na^+), potassium (K^+) and a small voltage-independent leak current to be the fundamental currents involved in the generation of an action potential in a squid giant axon. These findings concur with current experimental data achieved using present technology (Hille, 1992).

Using the voltage clamp technique, Hodgkin and Huxley (1952a) proposed a method of determining how each ion contributed to the total ionic current. They measured the ionic currents obtained from stepping the voltage up from the resting potential of $-65\ mV$ to $-9\ mV$. This current was attributed to both the influx of sodium and the efflux of potassium. They then replaced 90 % of the sodium in the bath solution (or extracellular fluid) with ions which could not permeate the membrane, and again recorded the ionic currents over the same step of voltage. As sodium and potassium were determined to be the only strong influences on an action potential, and most of the sodium had been replaced, they attributed this leftover current to the efflux of potassium ions. Then, the difference between the two currents gave them the inward current due to sodium. Using Hodgkin and Huxley's model (outlined in section 3.6), these results have been simulated (Figure 3.3).

To consider the individual influences of the sodium and potassium currents on an action potential, Hodgkin and Huxley (1952a) measured these currents while the squid giant axon underwent a step of voltage, and plotted the results (see Figure 3.4). These currents were simulated using the Hodgkin-Huxley model in section 3.6. It is interesting to note that the sodium current rose and fell (even though the voltage was clamped), but the potassium current did not. This led Hodgkin and Huxley to consider how these ion currents affect the membrane permeability.

3.3.2 How ion currents affect membrane permeability

Hodgkin and Huxley (1952b) wished to determine how these ionic currents altered the membrane permeability. That is, was a conductance-based model justified? To answer this question, they sought to test their theory of an "independence relation": that the permeability of the membrane to a particular ion was not affected

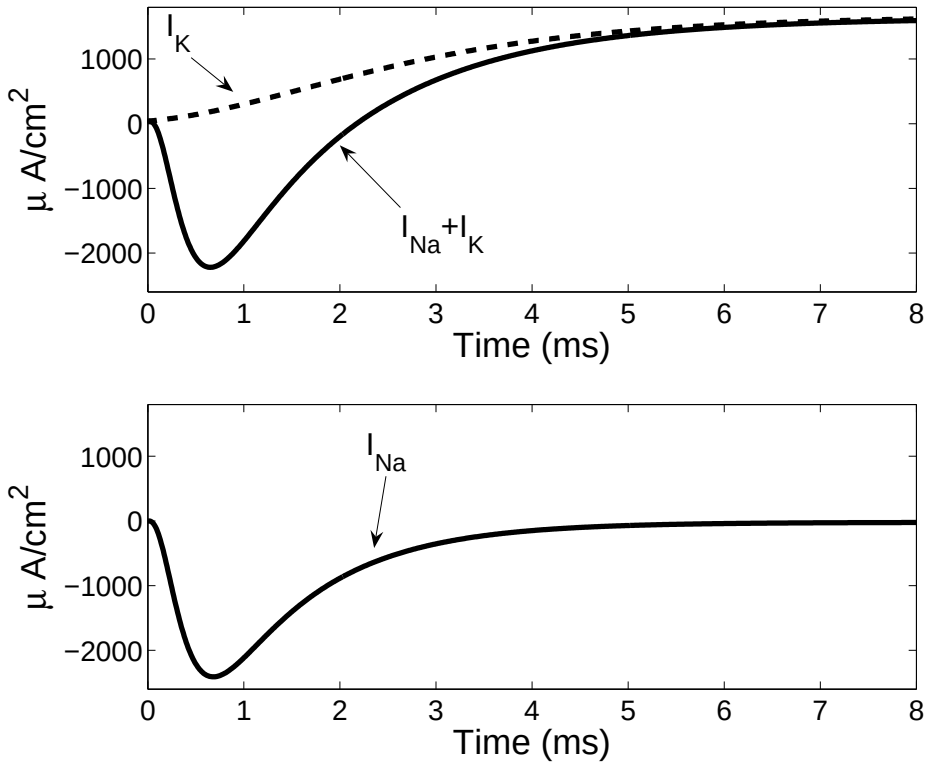

Figure 3.3: A method proposed by Hodgkin and Huxley (1952a) to separate the total ionic current during a step of voltage into the inward current of sodium and the outward current of potassium. The sodium in the extracellular fluid was replaced with impermeant choline ions, and the current was measured over the same step in voltage. This current could be attributed to the efflux of potassium alone. Then the difference between the two currents gave the inward current of sodium. Results were simulated using Hodgkin and Huxley's model (described in section 3.6).

by the presence of other ions. They first depolarized the membrane significantly such that the permeability to sodium ions was high. They then stepped up the voltage, and immediately measured the change in current (before the membrane had time to change permeability: within $10-30\ \mu s$). Hodgkin and Huxley (1952b) discovered that the current-voltage relation was approximately linear. Similarly, if the same experiment was performed such that the membrane was first depolarized for high potassium permeability, a linear current-voltage relation would again result. Therefore a conductance-based model was justified, and Ohm's law could be

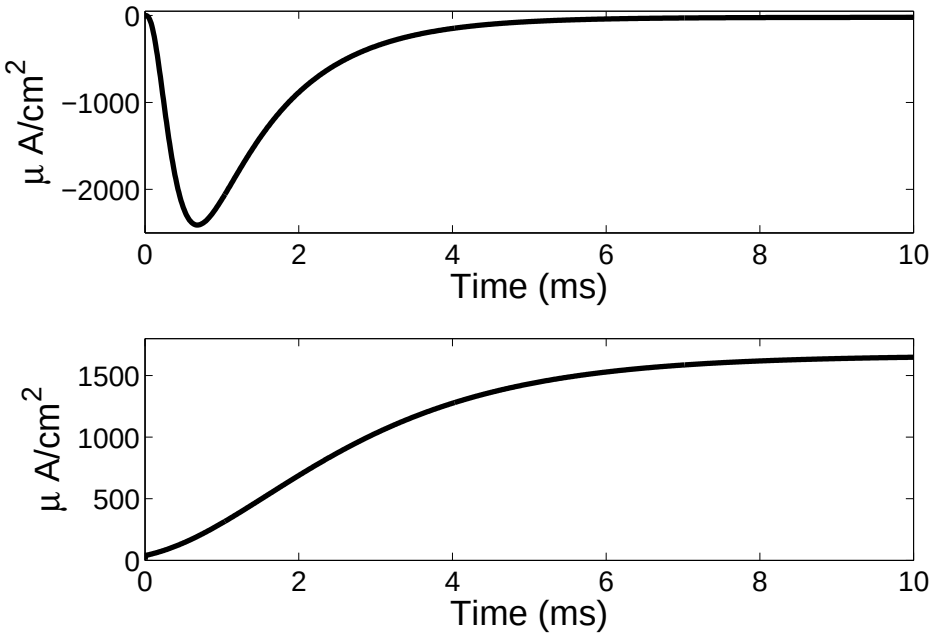

Figure 3.4: The voltage is clamped at $V_m = 60\ mV$. The sodium current has a fast increase and decrease in size, whereas the potassium current increases slowly and monotonically. Note that the sodium current is negative because of its direction of flow (into the intracellular space).

used to descibe these conductances:

$$g^*_{Na}(V_m) = \frac{I_{Na}}{E_m - E_{Na}} \tag{3.4}$$

$$g^*_K(V_m) = \frac{I_K}{E_m - E_K} \tag{3.5}$$

$$g^*_L = \frac{I_L}{E_m - E_L} \tag{3.6}$$

$$\tag{3.7}$$

where g^*_{Na} and g^*_K represent the voltage-dependent (and hence time-dependent) conductance for the membrane permeability to Na^+ and K^+ ions respectively, g^*_L represents the constant conductance for the leak, I_{Na}, I_K and I_L represent the ionic currents, E_m is the membrane potential, and E_{Na}, E_K and E_L are the Nernst potential for these ions. To simplify the mathematical analysis, this Ohmic relation is often written (Hodgkin and Huxley, 1952a) as:

$$g_{Na}(V_m) = \frac{I_{Na}}{V_m - V_{Na}} \tag{3.8}$$

$$g_K(V_m) = \frac{I_K}{V_m - V_K} \tag{3.9}$$

$$g_L = \frac{I_L}{V_m - V_L} \tag{3.10}$$

Such that

$$V_m = E_m - E_r \tag{3.11}$$

$$V_{Na} = E_{Na} - E_r \tag{3.12}$$

$$V_K = E_K - E_r \tag{3.13}$$

$$V_L = E_L - E_r \tag{3.14}$$

where E_r is the absolute value of the resting potential. Thus V_m, V_{Na}, V_K and V_L are taken to be their displacement from the resting potential, $V_{rest} = 0\ mV$. Ohm's law is useful when the current-voltage relation is linear, but some currents (such as calcium) are less linear than others. In these cases, the GHK equation (Equation 3.3) may be used instead of the Ohmic approximation, where permeability P_S can represent the conductance.

3.4 The cell as an R.C. circuit

The study of the change in current and voltage in a cell led to the depiction of the cell as an electric circuit. Hodgkin and Huxley (1952d) described such a model based on their commonly used squid giant axon. Basic laws of physics were used to represent the relationship of a cell with its external surroundings. This was done based on three major concepts. Firstly, they recognized that the cell membrane is an insulating lipid bilayer, through which current cannot directly flow. By accumulating a charge of electricity, the membrane acts as a capacitor. Secondly, the selective permeability of the membrane controls the current flow by providing resistance, acting as an electronic resistor. Finally, the extracellular and intracellular potential difference creates a source of electrical energy, performing as a battery. Hodgkin and Huxley (1952d) then represented their squid giant axon as a parallel R.C. circuit (Figure 3.5), allowing laws of electric circuits to be used.

Ohm's law relates current, voltage and resistance (equations (3.8)-(3.10)). Since the membrane functions as a capacitor, the current across the membrane, I_{cap}, is given by:

$$I_{cap} = C_m(\frac{dV_m}{dt}) \tag{3.15}$$

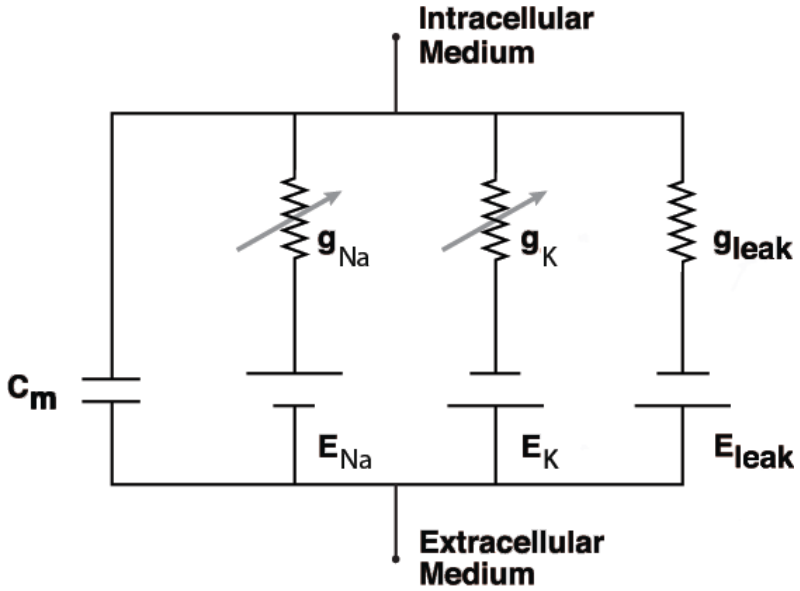

Figure 3.5: The squid giant axon represented as an R.C. circuit. The arrows denote the voltage dependence of the sodium and potassium conductances.

where C_m is the membrane capacitance, and V_m is the potential across the membrane (defined in equation (3.11)). By Kirchoff's law, the capacitive current must be equal to the ionic current and any applied currents. Recalling that our convention for the direction of positive current flow is outwards, we have

$$\begin{aligned} I_{cap} &= -I_{ion} + I_{applied} && (3.16) \\ &= -I_{Na} - I_K - I_L + I_{applied} && (3.17) \end{aligned}$$

where I_{ion} is the sum of all ionic currents, which according to Hodgkin and Katz (1949) involved sodium, potassium, and a leak current, and where $I_{applied}$ represents any applied current. Combining equations (3.8)-(3.10), (3.15), and (3.17), we have

$$C_m \frac{dV_m}{dt} = -g_{Na}(V_m)(V_m - V_{Na}) - g_K(V_m)(V_m - V_K) - g_L(V_m - V_L) + I_{applied} \quad (3.18)$$

which provides us with a means of describing the membrane potential. The question remains: how can these voltage-dependent conductances be represented mathematically? Hodgkin and Huxley (1952a) used the voltage clamp technique to study the independent sodium and potassium currents with respect to a depolarizing step. In particular, they were interested in how the permeability to these ions change with voltage and time.

3.5 The conductances g_L, g_{Na} and g_K

Hodgkin and Huxley were able to separate and examine the sodium and potassium ion currents which flowed across the membrane during a depolarization of the cell (Hodgkin and Huxley, 1952a), as described in the previous section. Using Ohm's law, i.e. equations (3.8)-(3.10), and their their knowledge of the ion currents obtained from their voltage clamp experiments, they were able to plot the conductances for sodium and potassium for a fixed voltage over time. This section describes the dynamics of these sodium and potassium and leak conductances, and the Hodgkin and Huxley model used to represent them. This discussion follows Hille (1992), Nelson and Rinzel (1998), and Hodgkin and Huxley (1952a).

From these voltage clamp experiments, Hodgkin and Huxley noticed that the sodium conductance behaved quite differently from the potassium conductance. When the membrane potential was held under a depolarizing step of voltage, the sodium conductance increased quickly, reached a peak, and then decreased at a slower rate. However, under this same depolarization, the potassium conductance increased approximately ten times slower than the sodium conductance (Hille, 1992), and maintained this increased value. Thus the sodium conductance is said to have a fast activation and slower inactivation, whereas the potassium conductance is said to undergo a very slow activation, and no inactivation (Hodgkin and Huxley, 1952a). If the depolarization is removed when the membrane has very high sodium permeability (i.e. it is at the peak of its upstroke), before the sodium conductance has a chance to inactivate, then the sodium conductance returns to rest quickly and exponentially. If the depolarization is removed when permeability to potassium is high, then the current decays slowly and exponentially. Hodgkin and Huxley did this same experiment for a variety of depolarizations, to determine the overall behaviour of the ion channels (Hodgkin and Huxley, 1952a). They noted that as the depolarization increased, the conductance for sodium and potassium became larger, and increased at faster rate. However, these conductances were found to saturate at some maximum value. Therefore, the conductance of each ion can be represented as its maximum conductance times the fraction of the maximal conductance that actually occurs. Again, we note that Hodgkin and Huxley were unaware of the existence of individual ion channels when their model was developed, but their reasoning remains accurate. For simplicity, we will discuss the conductances in terms of these ion channels instead of the overall permeability. We consider each ion channel to have a small number of "gates" regulating the flow of ions across the channel. These gates can be in one of two states: a permissive state and a non-permissive state. If all the gates are in the permissive state, then the ion channel is in its open state, and ions can pass through. However, if even one of the gates are in the non-permissive state, then the ion channel is considered closed, and no ions can be transported across the membrane (Nelson and Rinzel, 1998). Since we are dealing with a whole population of ions, we can consider a "gating variable" to be the fraction of gates in the permissive state, and thus will be a dimensionless number between zero and one. The next step is to see if our gating variables give

us an accurate expression of our ionic conductances. We begin by examining our potassium conductance.

3.5.1 The potassium conductance

We know that the potassium conductance is characterized by its slow activation under a constant depolarization, with no inactivation. This conductance curve follows an s-shape upon depolarization, and decreases exponentially upon repolarization. We let the potassium activation gating variable be expressed by 'n'. Since the permissivity of the gates are only dependent on the membrane potential V_m (and thus indirectly on time), then n can be modeled with first order kinetics:

$$(1-n) \underset{\beta_n}{\overset{\alpha_n}{\rightleftharpoons}} n \tag{3.19}$$

where $(1-n)$ is the fraction of gates in the non-permissive state, n is the fraction of gates in the permissive state, and α_n and β_n are the rate constants under which this transformation occurs. Then this can be expressed mathematically as:

$$\frac{dn}{dt} = \alpha_n(1-n) - \beta_n n \tag{3.20}$$

Hodgkin and Huxley (1952a) then defined the time constant τ_n and the steady state value n_∞ as:

$$\tau_n = \frac{1}{\alpha_n + \beta_n} \tag{3.21}$$

and

$$n_\infty = \frac{\alpha_n}{\alpha_n + \beta_n} \tag{3.22}$$

Using equations (3.21), and (3.22), we can rearrange equation (3.20) to get:

$$\frac{dn}{dt} = \frac{n_\infty - n}{\tau_n} \tag{3.23}$$

Using the initial condition $n(t=0) = n_0$, this problem can be solved to give

$$n = n_\infty - (n_\infty - n_0)e^{-t/\tau_n} \tag{3.24}$$

Then considering the known conductance curves for a membrane potential clamped at some uniform value, V_c, Hodgkin and Huxley attempted to fit this curve by finding the values τ_n, n_∞ and the initial n_0 (Hodgkin and Huxley, 1952a). They let $g_K = \bar{g}_K n$, where $\bar{g}_K$ is the maximal potassium conductance. Thus to fit this

curve for n to their conductance curve, they must first scale their gating variable by the maximal conductance for potassium. Hodgkin and Huxley found that they could not fit the s-shaped part of the potassium conductance curve well with their gating variable. Rather, they could achieve a much better fit using n^4 (Hodgkin and Huxley, 1952a). Therefore, the opening of the potassium channels can be considered to be dependent on four independent gates, all of which must be in the permissive state in order to open the channel. Thus the potassium conductance can be expressed as:

$$g_K = \bar{g}_K n^4 \tag{3.25}$$

Then, from Ohm's law (equation 3.9), the potassium current can be expressed as:

$$I_K = \bar{g}_K n^4 (V_m - V_K) \tag{3.26}$$

3.5.2 The sodium conductance

The sodium conductance undergoes a fast activation and a slow inactivation under a uniform depolarization. Recall that the peak conductance increases with increased depolarization, and the activation and inactivation become faster. To model this dynamic with one gating variable, Hodgkin and Huxley would have been required use at least a second order differential equation. Instead, they chose to use two gating variables, an "activation variable", m, and an "inactivation variable", h, and therefore were able to maintain first order kinetics (Hodgkin and Huxley, 1952a).

$$(1-m) \quad \underset{\beta_m}{\overset{\alpha_m}{\rightleftharpoons}} \quad m \tag{3.27}$$

$$(1-h) \quad \underset{\beta_h}{\overset{\alpha_h}{\rightleftharpoons}} \quad h \tag{3.28}$$

This can be expressed as:

$$\frac{dm}{dt} = \alpha_m(1-m) - \beta_m m \tag{3.29}$$

$$\frac{dh}{dt} = \alpha_h(1-h) - \beta_h h \tag{3.30}$$

Then as before,

$$\frac{dm}{dt} = \frac{m_\infty - m}{\tau_m} \tag{3.31}$$

$$\frac{dh}{dt} = \frac{h_\infty - h}{\tau_h} \tag{3.32}$$

where

$$\tau_m = \frac{1}{\alpha_m + \beta_m} \tag{3.33}$$

$$\tau_h = \frac{1}{\alpha_h + \beta_h} \tag{3.34}$$

and

$$m_\infty = \frac{\alpha_m}{\alpha_m + \beta_m} \tag{3.35}$$

$$h_\infty = \frac{\alpha_h}{\alpha_h + \beta_h} \tag{3.36}$$

Hodgkin and Huxley set out to fit the sodium conductance curve as they did previously with potassium. They first needed the conductance curves for the gating variables when the membrane potential is clamped at some uniform value, V_c. Thus, it would be helpful if they had a means of separating these activation and inactivation gating variables. This was achieved by measuring the inactivation by a "two-pulse experiment" (Hille, 1992). In this technique, the membrane is held under a constant depolarization so that full inactivation occurs. The membrane is then immediately repolarized to its resting potential, and remains there for some variable period of time. Over this short period of time, some of the channels recover from the inactivation, and some do not. The membrane is again depolarized (to the same value as before), and it becomes evident what fraction of the channels have recovered from the inactivation. Varying the interval between the two pulses provides scientists with a time course for the inactivation (see Hille (1992) for more details).

Then Hodgkin and Huxley were able to fit their sodium conductance activation and inactivation curves in the same manner as before (with the potassium conductance). That is, they fit the values τ_m, τ_h, m_∞, h_∞, at some clamped membrane potential V_c, and fit the initial values $m(t=0) = m_0$ and $h(t=0) = h_0$, when

$$m = m_\infty - (m_\infty - m_0)e^{-t/\tau_m} \tag{3.37}$$

$$h = h_\infty - (h_\infty - h_0)e^{-t/\tau_h} \tag{3.38}$$

by using the relation

$$g_{Na} = \bar{g}_{Na} m^3 h \tag{3.39}$$

Here $\bar{g}_{Na}$ is the maximal potassium conductance (Hodgkin and Huxley, 1952a). Thus the sodium channel is in an open state when all three activating gates are in their permissive state, as well as the one inactivating gate. The sodium current can be expressed, using Ohm's law (equation 3.8), as

$$I_{Na} = \bar{g}_{Na} m^3 h (V_m - V_{Na}) \tag{3.40}$$

3.5.3 A description of the action potential using the sodium and potassium conductances

The sodium and potassium conductances can be used to gain a deeper understanding of the action potential. In Figure 3.6, these conductances, their respective gating variables, and the action potential were all simulated using the Hodgkin-Huxley model in section 3.6. Using this information, we are able to give a more detailed description of the dynamics of an action potential. With enough depolarization, the ionic currents passing through their respective channels will generate an action potential. First, an excitatory stimulus causes voltage-gated sodium channels to open. The sodium gradient forces it to diffuse in, and the cell is depolarized. If the membrane potential crosses a particular threshold, an action potential results. As the cell depolarizes, more voltage-dependent sodium channels open, and the influx of sodium continues to increase. If the sodium channels were the only active channels, the cell would settle at E_{Na}. However, the voltage-gated potassium channels eventually open, causing potassium to flow along its gradient out of the cell. At this time, the voltage-sensitive sodium inactivation channels have already started to close, and the influx of sodium has decreased. At approx $V_m = 100\ mV$, the membrane potential reaches its peak, and the cell begins to repolarize. The repolarization continues as the sodium inactivation channels close, and the potassium channels open. The influx of sodium is now minimal, and the flow of potassium outward is steadily increasing. The membrane potential begins to drop back toward E_K. The voltage-gated potassium channels are also time-dependent: they close slower than the other channels. Therefore even after the cell has repolarized back to resting potential, some potassium channels are still open. Potassium continues to flow out, and the cell membrane becomes "hyperpolarized" (more negative than the resting potential). Thus, for approximately the 1 ms after the channels have fully closed, the threshold to create a new action potential is harder to obtain. This is called the refractory period, and ensures uni-directional propagation of the action potential.

3.5.4 The leak conductance

The leak conductance was very simple for Hodgkin and Huxley to describe in comparison to the sodium and potassium conductances, because it was voltage-independent. From Ohm's law (equation (3.10)), they could immediately describe the leak current as

$$I_L = \bar{g}_L(V_m - V_L) \tag{3.41}$$

where $\bar{g}_L$ is the constant conductance, and V_L is the equilibrium (Nernst) potential for this current. To solve for these constants, Hodgkin and Huxley eliminated the sodium current by putting the axon in a sodium-free bath solution (Hodgkin and

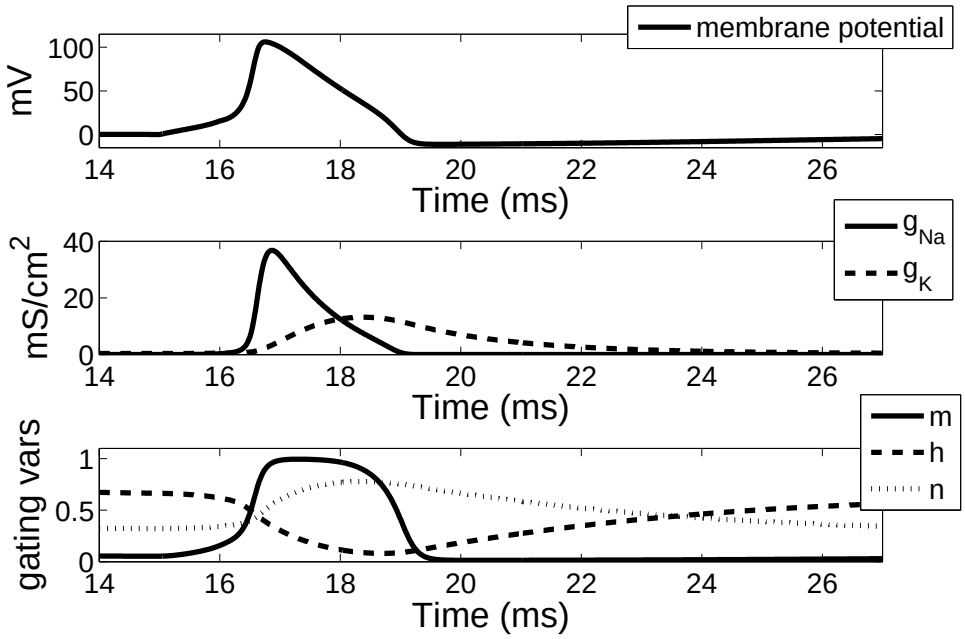

Figure 3.6: Top: An action potential generated by a pulse of applied current (of 15 $\mu A/cm^2$ at $time = 15\ ms$ for one ms). Middle: The sodium conductance rises and falls very quickly, the potassium current rises and falls on a much slower scale. Bottom: The sodium activation and inactivation gating variables (m and h) are shown, as well as the potassium activation gating variable (n). Note that initially, h is high and m is low, but once the membrane is depolarized, h becomes low and m becomes high.

Huxley, 1952a). Using a voltage clamp to maintain a constant membrane potential, Kirchoff's law and the capacitance law (equations (3.17) and (3.15)) give

$$I^*_{applied} = I_K + I_L = \bar{g}_K n^4 (V_m - V_K) + \bar{g}_L (V_m - V_L) \tag{3.42}$$

Then they clamped the membrane potential at two particular voltages: firstly at $V_m = V_K$, the Nernst potential for potassium, and secondly at a very small potential (specifically at $V_m = -84\ mV$). The clamp at $V_m = V_K$ ensured that no potassium current would flow (since it is in its equilibrium), and so they have reduced equation (3.42) to

$$I^*_{applied}(V_K) = \bar{g}_L (V_K - V_L) \tag{3.43}$$

The second clamp reduces equation (3.42) to

$$I^*_{applied}(-84) = \bar{g}_L (-84 - V_L) \tag{3.44}$$

Solving these two equations allowed Hodgkin and Huxley to solve for $\bar{g}_L$ and V_L, and thus they obtained a full mathematical description for this leak current described by equation (3.41). Therefore Hodgkin and Huxley were able to mathematically express all the ionic currents involved in the generation of an action potential. The full model will be summarized in the next section.

3.6 The full Hodgkin-Huxley model of a squid giant axon

From Kirchoff's law and our law of capacitances (equations (3.17) and (3.15)) we know

$$I_{cap} = -I_{Na} - I_K - I_L + I_{applied}$$

and

$$I_{cap} = C_m(\frac{dV_m}{dt})$$

Then using our expressions for the sodium and potassium currents given in the previous section, we have a model for the rate of change of the membrane potential:

$$C_m\frac{dV_m}{dt} = -\bar{g}_{Na}m^3h(V_m - V_{Na}) - \bar{g}_K n^4(V_m - V_K) - \bar{g}_L(V_m - V_L) + I_{applied} \quad (3.45)$$

where C_m is the membrane capacitance, V_m is the membrane potential, $\bar{g}_{Na}$, $\bar{g}_K$, and $\bar{g}_L$ are the maximal conductances for the sodium, potassium and leak channels respectively, V_{Na}, V_K, and V_L are the Nernst potential for the respective ions, and $I_{applied}$ is some applied current. The "Nernst potential" for the leak current was chosen so that the total ionic currents are zero at the resting membrane potential ($V_m = 0\ mV$). All values are taken from Hodgkin and Huxley (1952a) and are shown in Table 3.1.

Parameter	Parameter Value	Unit
C_m	1	$\mu F/cm^2$
$\bar{g}_{Na}$	120	mS/cm^2
$\bar{g}_K$	36	mS/cm^2
$\bar{g}_L$	0.3	mS/cm^2
V_{Na}	115	mV
V_K	-12	mV
V_L	10.613	mV

Table 3.1: Parameter values and units of Hodgkin and Huxley's model Hodgkin and Huxley (1952a)

The gating variables are expressed as in equations (3.29), (3.30), and (3.20):

$$\begin{aligned}
\frac{dm}{dt} &= \alpha_m(1-m) - \beta_m m \\
\frac{dh}{dt} &= \alpha_h(1-h) - \beta_h h \\
\frac{dn}{dt} &= \alpha_n(1-n) - \beta_n n
\end{aligned}$$

where

$$\alpha_m = \frac{0.1(25 - V_m)}{e^{(25-V_m)/10} - 1} \tag{3.46}$$

$$\beta_m = 4e^{-V_m/18} \tag{3.47}$$

$$\alpha_h = 0.07e^{-V_m/20} \tag{3.48}$$

$$\beta_h = \frac{1}{e^{(30-V_m)/10} + 1} \tag{3.49}$$

$$\alpha_n = \frac{0.01(10 - V_m)}{e^{(10-V_m)/10} - 1} \tag{3.50}$$

$$\beta_n = 0.125e^{-V_m/80} \tag{3.51}$$

The values of the α's and β's (again taken from Hodgkin and Huxley (1952a)) were all found at a temperature of 6.3°C. To determine α_n and β_n, the potassium rate constants, Hodgkin and Huxley considered the potassium conductance, g_K. Using a chosen maximal conductance value of $\bar{g}_K = 36\ mS/cm^2$, they used equation (3.25), $g_K = \bar{g}_K n^4$, to calculate n_∞ at various voltages. They determined values for α_n and β_n by using the relations

$$\alpha_n = \frac{n_\infty(V_m)}{\tau_n(V_m)} \tag{3.52}$$

$$\beta_n = \frac{1 - n_\infty(V_m)}{\tau_n(V_m)} \tag{3.53}$$

Hodgkin and Huxley plotted these α_n and β_n values with respect to the membrane potential, V_m. Thus to find continuous curves for the rate constants as a function of the membrane potential, the rate constants were fit to V_m (see equations (3.50) and (3.51). In general, β_n was small compared to α_n, therefore they did not consider it to be essential to have an exact fit. Thus they used the simplest reasonable fit for β_n. The rate constants for the sodium current, given by equations (3.46), (3.47), (3.48), and (3.49), were determined in a similar manner. Thus Hodgkin and Huxley developed a complete mathematical model of the electrical potential of a squid giant axon.

3.7 Discussion

Using first order differential equations, Hodgkin and Huxley (1952a) were able to describe the action potential of a squid giant axon. They did so by describing the change in membrane potential in terms of sodium, potassium, and leak currents, an applied current (or external stimulus), and the membrane capacitance. These ionic currents were described in detail, as were the measurement techniques used to discover them. Hodgkin and Huxley considered the permeability of the membrane and how it affected the action potential. In particular, they noted that the fast activation of the sodium conductance played an integral role in the initiation of an action potential, and the slow activation of the potassium conductance played a large role in the repolarization and hyperpolarization of the membrane. Hodgkin and Huxley's model is a widely accepted model of action potential generation, and is used to describe many different types of cells and their membrane potential. In 1963 they won the Nobel Prize in Physiology and Medicine for their work. We followed their model in our description of a CA1 hippocampal neuron.

Chapter 4

Literature Review

Hippocampal CA1 pyramidal neurons easily produce large electrical discharges, and are thus often the focus of partial seizures in patients with Mesial Temporal Lobe Epilepsy (MTLE). Empirical researchers have focused on these neurons and their synchronous bursting behaviour when examining experimental epileptic-type seizures (referred to as "epileptiform seizures") (Tian et al., 2005). It would be helpful to model their behaviour in a simplified way to be able to qualitatively reproduce the observed behaviour in a physiologically realistic manner. As a starting point, we consider the 19-compartment model of a pyramidal neuron created by Traub et al. (1991), which we will refer to as "Traub's model". Traub et al. (1991) were able to use their model to simulate key characteristics of a CA1 neuron, such as its calcium-dependent potassium channels, its dendritic excitability resulting in dendritic calcium spikes, and its bursting behaviour. However, a more simplified model may be useful to examine the effects of key parameters, to create a network model, or to reduce the computational demand in order to extend the model in other ways. This leads us to consider Pinsky and Rinzel's two-compartment model of a CA3 pyramidal neuron (Pinsky and Rinzel, 1994). They based their simplified model on Traub's model, using Traub's conductance values as a starting point to determine their own. In Chapter 5 we reduce Traub's model of a CA1 neuron in a similar manner. Traub et al. (1991) and Pinsky and Rinzel (1994) both wrote quite intricate articles, examining the CA3 model neuron behaviour in a variety of ways. However, since we are concerned with the behaviour of a CA1 neuron, this review will concentrate on the models themselves, and only mention the key results. For more details, please refer to the articles.

Although CA1 pyramidal neurons are often the focus of epileptiform bursting, some hypothesize that astrocytes are actually responsible for initiating these bursts (Tian et al., 2005). In fact, Tian et al. (2005) suggests that astrocyte pathologies may be the genesis of epilepsy, as well as the target of many anti-epileptic drugs. They examine the enduced seizure activity of a large group of neurons, while eliminating neuronal communication by applying a series of channel blockers. They find underlying slow depolarization shifts of the neurons, which result from increased calcium concentrations in the astrocytic cytosol. These depolarizations may be the

root of excessive neuronal discharges. We use our model to reproduce many of Tian et al.'s experimental observations, and thus a brief summary of their experiments is required. Finally, we consider the changes in the astrocytic calcium concentrations in more detail, following (Parpura and Haydon, 2000). Parpura and Haydon examine how slow inward currents (which cause the slow neuronal depolarization shifts) are initiated by the astrocytic release of the glutamate, which are in turn caused by increased astrocytic intracellular calcium levels. Therefore, the four most important articles for this thesis, by Traub et al. (1991), Pinsky and Rinzel (1994), Tian et al. (2005), and Parpura and Haydon (2000), are reviewed.

4.1 "A Model of a CA3 Hippocampal Pyramidal Neuron Incorporating Voltage-Clamp Data on Intrinsic Conductances", Traub et al. (1991)

Traub et al. were particularily interested in modeling hippocampal pyramidal neurons because of their dendritic excitability, bursting behaviour, and because as a population, these neurons are succeptible to synchronized epileptiform bursting. They created a 19-compartment model of a pyramidal neuron, focusing their attention on CA3 neurons, but considering CA1 neurons as well. This review will concentrate on their 1991 work with CA1 neurons. Their goal was to create a physiologically realistic model which could reproduce the behaviour of a pyramidal neuron in a network and when isolated, and make accurate predictions about pyramidal neuron behaviour.

Traub et al.'s 1991 model was composed of 19 cylindrical compartments: eight compartments representing the basilar dendrites, ten representing the apical dendrites, and one representing the soma. The compartments were numbered 1 through 19, as can be seen in Figure 4.1. Although the cylindrical shape of the soma was not realistic, the somatic membrane area was reasonable. The basilar dendrites were represented by cylindrical compartments which were equivalent in size (as were the apical dendrites), and the ends of the dendritic compartments were sealed. Each dendritic compartment represented 0.1λ, where λ is the length of the core conductor. That is, since Traub et al. assumed extracellular isopotentiality, $\lambda = \sqrt{(R_m/R_i)(d/4)}$, where R_m and R_i represent the membrane resistance and the intracellular resistivity of the cytoplasm respectively, and d is the diameter of the cylinder. Therefore, since the dendritic compartments were sufficiently small, the model maintained its physolological relevance.

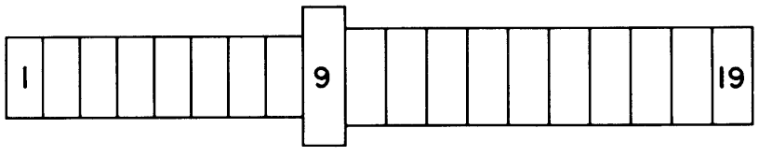

Figure 4.1: A schematic representation of the Traub 19-compartment model. Compartments are labelled 1 through 19, with the soma at compartment 9, the basilar dendrites on the left (1 through 8), and the apical dendrites on the right (10 through 19). The figure was reproduced from Traub et al. (1991).

4.1.1 The ionic currents and conductance densities

By assuming that the dendrites contained the same ionic channels as the soma, and that the dendrites had significant calcium dynamics (based on calcium imaging done on the dendrites), Traub et al. chose a (non-unique) distribution of ionic conductance densities for both the CA3 and the CA1 neurons. Each compartment contained six active ionic conductances: the sodium conductance (g_{Na}), the calcium conductance (g_{Ca}), the delayed rectifier potassium conductance ($g_{K(DR)}$), the A-type of transient potassium conductance ($g_{K(A)}$), the long duration calcium-dependent afterhyperpolarizing potassium conductance ($g_{K(AHP)}$), and the short-duration voltage and calcium-dependent potassium conductance ($g_{K(C)}$). The conductance densities they chose for CA1 are shown in Table 5.1 in section 5.2. Considering the difference in potential across the membrane for each compartment (V_k), measured with respect to the resting potential of $-60\ mV$, Traub et al. used Kirchoff's law to give:

$$C_k \frac{dV_k}{dt} = \gamma_{k-1,k}(V_{k-1} - V_k) + \gamma_{k+1,k}(V_{k+1} - V_k) - I_{ionic,k}$$

where C_k is the membrane capacitance of compartment k (in nF), $\gamma_{l,k}$ is the conductance between compartments l and k (in μS), V_i for $i = k-1, k, k+1$ are the membrane potentials of compartment i with respect to the resting membrane potential $V_{rest} = -60\ mV$, and $I_{ionic,k}$ is a sum of all the ionic currents for compartment k (including the leak current and the synaptic current) (in nA). Then considering the six active currents and their Hodgkin-Huxley type gating variables, $I_{ionic,k}$ can be written as:

$$\begin{aligned} I_{ionic,k} &= \bar{g}_{L,k}V_k + I_{synaptic,k} + \bar{g}_{Na}m_k^2 h_k(V_k - V_{Na}) + \bar{g}_{Ca}s_k^2 r_k(V_k - V_{Ca}) \\ &\quad + \bar{g}_{K(DR)}n_k(V_k - V_K) + \bar{g}_{K(A)}a_k b_k(V_k - V_K) + \bar{g}_{K(AHP)}q_k(V_k - V_K) \\ &\quad + \bar{g}_{K(C)}c_k \times min(1 + \frac{\chi_k}{250}) \times (V_k - V_K) - I_{injected,k} \end{aligned}$$

where $\bar{g}_{j,k}$ represents the maximal conductance for j in the compartment k and V_j represents the reversal potential for j, where $j = L,\ Na,\ Ca,\ K(DR),\ K(A)$,

$K(AHP)$, or $K(C)$. The synaptic current in compartment k is given by $I_{synaptic,k}$. Note that the calcium and voltage dependent potassium current, $I_{K(C)}$, depends on χ_k, the intracellular calcium in a shell beneath the membrane for compartment k (as does the gating variable for $I_{K(AHP)}$, q). Then an expression for the production of χ_k is given by:

$$\frac{d\chi_k}{dt} = -\phi_k I_{Ca,k} - \beta_\chi \chi_k$$

The variable χ_k is dimensionless since the depth of the shell of calcium is unknown. The constant ϕ_k scales the inward calcium current into the production of intracellular calcium, and varies depending on the compartment. The inverse time constant, $\beta_\chi = 0.075\ ms^{-1}$, was determined experimentally.

4.1.2 The synaptic currents

Traub et al. considered two different types of excitatory synaptic currents: those initiated by quisqualate (QUIS), and those initiated by N-methyl D-aspartate (NMDA). The QUIS currents were only considered to affect compartments 3 and 15, compartments which were 0.6λ away from the soma in either the apical or the basilar direction, and the NMDA currents were only considered to affect compartment 15. The QUIS current was a fast excitatory current given by $c_{QUIS}te^{-t/2} \times (V_k - V_{QUIS})$ where $V_{QUIS} = -60\ mV$ was the reversal potential, and $c_{QUIS} = 4\ nS$. This current was activated when the presynaptic cell spikes, i.e. when its somatic membrane potential exceeds 20 mV (Traub et al., 1992). However, the NMDA current was more complicated to model, as it is a slow decaying voltage-dependent and magnesium-dependent (as well as ligand-dependent) current. Therefore, Traub et al. described the NDMA current by :

$$I_{NMDA} = g(t) \times \frac{1}{1 + \frac{[Mg^{2+}]}{3} \times e^{-0.07(V_k - \xi)}} \times (V_k - V_{NMDA})$$

where $V_{NMDA} = -60\ mV$ is the reversal potential, $\xi = -60\ mV$, $[Mg^{2+}] = 2\ mM$, and $g(t)$ is the ligand-dependent conductance which peaks at 2 ms and decays over $100 - 150\ ms$. Similarily, the NMDA current is activated when the presynaptic membrane potential exceeds a threshold of 20 mV (Traub et al., 1992).

4.1.3 The gating variables

The Hodgkin Huxley gating variables for the ionic currents can be described by first order kinetics. Therefore the gating variable x in compartment k (x_k) can be described by:

$$\frac{dx_k}{dt} = \alpha_x(\Psi_k)(1 - x_k) - \beta_x(\Psi_k)x_k$$

where α_x and β_x are the rate constants involved, and $\Psi = V_k$ (or χ_k for the gating variable q). Traub et al. assume for simplicity (and because a lack of data) that the kinetics of the gating variables are the same in the soma and the dendrites, and thus α_x and β_x do not depend on the compartment. Then if the steady state value $x_\infty = \alpha_x/(\alpha_x + \beta_x)$ and the time constant $\tau_x = 1/(\alpha_x + \beta_x)$ are known, the values of α_x and β_x can be determined.

4.1.4 CA1 cell model behaviour

To determine that their CA1 model captured the characteristic behaviours of a CA1 pyramidal neuron, Traub et al. performed a series of simulations. They found that, in accordance with experimental data, the behaviour of the neuron depended on where it was stimulated. When an applied current of $< 1\ nA$ was given to the somatic compartment, the neuron model exhibited a train of action potentials in its soma, and subthreshold depolarizations in the distal dendrites. An application of the same current into the proximal dendrites, 0.3λ from the soma, resulted in similar behaviour, but with slightly larger subthreshold depolarizations in the dendrites. However, if a current with the same magnitude was applied to the distal dendrites (for example, 0.6λ away from the soma), the distal dendrites exhibited a full calcium spike associated with a somatic burst. If a large current was applied ($> 1.15\ nA$) to either the soma or the dendrite, a somatic burst and a full calcium spike were exhibited. Traub et al. commented on a key difference between the behaviour of the CA1 neurons and the CA3 neurons: under a steady applied current, the CA1 neurons do not physiologically exhibit periodic bursting. The model also was able to make predictions about cell behaviour which were later verified. One of such predictions was the ability of a burst in one CA3 neuron to initiate a burst in a neighbouring neuron. Another is that a burst in a single neuron can synchronize bursting in an entire network.

4.2 "Intrinsic and Network Rhythmogenesis in a Reduced Traub Model for CA3 Neurons" Pinsky and Rinzel (1994)

Pinsky and Rinzel modeled a CA3 hippocampal pyramidal neuron by reducing Traub's 19-compartment model (Traub et al., 1991) to a two-compartment model. In doing so, they were able to maintain much of the same behaviour as in Traub's model, such as the major currents and gating kinetics, but greatly reduced the number of variables. Pinsky and Rinzel identified six major currents involved in the electrical behaviour the CA3 neuron: a sodium current (I_{Na}), a delayed rectifier potassium current (I_{K-DR}), a calcium dependent potassium current (I_{K-C}), a afterhyperpolarizing potassium current (I_{K-AHP}), a calcium current (I_{Ca}), and a

leak current (I_L). They did not include Traub's seventh current, I_{K-A}, as according to Traub et al. (1991), it did not greatly contribute to the model. Pyramidal neurons in the hippocampus often have excitable dendrites as well as excitable somas, and their ion channels have significantly different conductances depending on the distance from the soma (Traub et al., 1991). They identified the maximal conductance densities of the currents by performing current clamp experiments on the neurons in vitro (Traub et al., 1991). In the Traub model, the fast currents, such as the sodium and delayed rectifier potassium current, were found primarily in the soma and proximal dendrites, whereas the calcium and calcium dependent currents were found primarily ($\approx 62\%$) in the distal dendritic currents. Based on this criteria, Pinsky and Rinzel lumped Traub's 19-compartments into two compartments, a "somatic compartment" and a "dendritic compartment". Compartmental models are created based on the assumption of spatial homogeneity in the compartments. With this assumption, each compartment can be calculated separately, but the cable behaviour of the neuron remains accurate. However, the compartments used by Pinsky and Rinzel corresponded to a length of 0.5λ or more, a much larger length than would allow such an assumption to be made. Therefore their results must be thought of as phenomenological, rather than physiological.

Pinsky and Rinzel connected their two compartments through a coupling conductance, g_C. The potential across the membrane was measured with respect to a reference potential of $-60\ mV$, and was given by V_S and V_D for the somatic and dendritic compartments respectively. They let p be the proportion of the cell membrane area taken up by the soma ($1-p$ for the dendritic compartment), and added applied currents I_S and I_D to the somatic and dendritic compartments respectively. A schematic representation of the Pinsky and Rinzel model is shown in Figure 4.2.

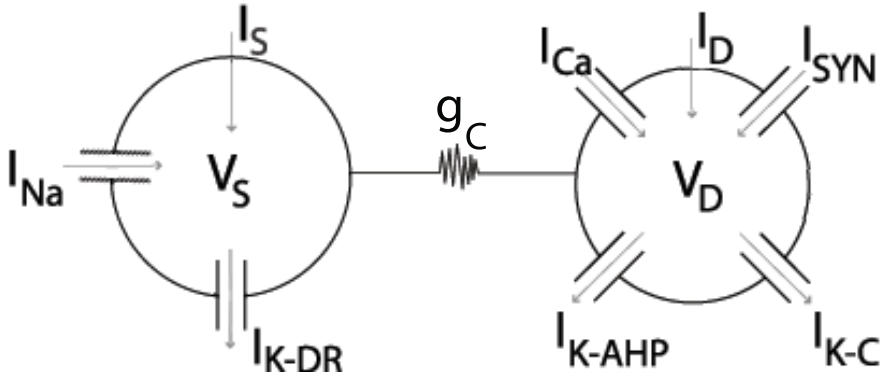

Figure 4.2: A schematic representation of Pinsky and Rinzel's two-compartment CA3 neuron model. This picture was drawn based on Fig. 1A of Pinsky and Rinzel (1994, pg. 42).

Then by Kirchoff's Law,

$$\begin{aligned}
\frac{dV_S}{dt} &= \frac{1}{C_m}\Big\{ - I_{leak,S}(V_S) - I_{Na}(V_S,h) - I_{K-DR}(V_S,n) \\
&\quad + \frac{g_c}{p} * (V_D - V_S) + \frac{I_S}{p}\Big\} \\
\frac{dV_D}{dt} &= \frac{1}{C_m}\Big\{ - I_{leak,D}(V_D) - I_{K-AHP}(V_D,w) - I_{Ca}(V_D,s) \\
&\quad - I_{K-C}(V_D,[Ca^{2+}],c) + \frac{I_{SYN}}{(1-p)} \\
&\quad + \frac{g_c}{1-p} * (V_S - V_D) + \frac{I_D}{1-p}\Big\}
\end{aligned}$$

where C_m represents the membrane capacitance. Each current was described as a function of their membrane potentials (either V_S or V_D), their maximal conductance strengths, and their respective Hodgkin-Huxley like gating variable. Pinsky and Rinzel used current densities, with units $\mu A/cm^2$. Therefore, to calculate the applied currents, I_S and I_D, from Traub et al.'s (1991) model, they divided by the total area of Traub's neuron model. As in the Traub et al. (1991) model, the calcium and voltage dependent potassium current, I_{K-C}, and the calcium dependent after-hyperpolarizing potassium current, I_{K-AHP}, were also functions of the amount of calcium in a "shell" beneath the membrane ($[Ca^{2+}]$). As the thickness of this shell is unknown, the scaling constant (ϕ), used to convert the inward calcium current into the concentration of intracellular calcium, is given with units $cm^2/(\mu A \cdot ms)$ so that $[Ca^{2+}]$ remains a dimensionless number. Then the calcium concentration in this intracellular shell was described by:

$$\frac{d[Ca^{2+}]}{dt} = -\phi I_{Ca} - \beta_{[Ca^{2+}]}[Ca^{2+}]$$

where $\phi = 0.13$, and $\beta_{[Ca^{2+}]} = 0.075$ is the inverse time constant with which $[Ca^{2+}]$ degrades. Note that due to convention, a calcium current flowing into the neuron is negative, and thus for production of $[Ca^{2+}]$, a scaling constant of $-\phi$ is required. By describing these currents as a function of their maximal conductances and gating variables, we have:

$$I_{K-AHP}(V_D,w) = \bar{g}_{K-AHP} w (V_D - V_K)$$

and

$$\begin{aligned}
I_{K-C}(V_D,[Ca^{2+}],c) &= \bar{g}_{K-C} c \chi([Ca^{2+}])(V_D - V_K) \\
\text{where} \qquad \chi([Ca^{2+}]) &= min(1, \frac{[Ca^{2+}]}{250}),
\end{aligned}$$

V_K is the reversal potential for potassium, and the maximum conductances are given by g_{K-AHP} and g_{K-C}. The gating variable for I_{K-AHP}, i.e. w, is dependent on $[Ca^{2+}]$. Similarily, the I_{K-C} current is dependent on both a voltage-dependent gating variable, c, and a $[Ca^{2+}]$ dependent gating variable, $\chi([Ca^{2+}])$. The gating variable $\chi([Ca^{2+}])$ was chosen (Traub et al., 1991) based on the experimentally determined maximum magnitude of intracellular calcium concentration of 250. The currents which are only dependent on the potential across the membrane are given by:

$$\begin{aligned} I_{leak,s}(V_S) &= \bar{g}_{leak}(V_S - V_{leak}) \\ I_{leak,d}(V_D) &= \bar{g}_{leak}(V_D - V_{leak}) \\ I_{Na}(V_S, h) &= \bar{g}_{Na} m_\infty^2 h(V_S - V_{Na}) \\ I_{K-DR}(V_S, n) &= \bar{g}_{K-DR} n(V_S - V_K) \\ I_{Ca}(V_D, s) &= \bar{g}_{Ca} s^2(V_D - V_{Ca}) \end{aligned}$$

where V_i represents the reversal potential for the particular channel $i = leak,\ Na,\ K,\ Ca$. Then, assuming the gating variables follow first order kinetics, i.e.,

$$(1 - y) \underset{\beta_y(U)}{\overset{\alpha_y(U)}{\rightleftharpoons}} y,$$

the dynamics of the gating variables are given by

$$\begin{aligned} \frac{dy}{dt} &= \frac{y_\infty(U) - y}{\tau_y(U)} \\ &\text{where} \qquad y_\infty(U) = \frac{\alpha_y(U)}{\alpha_y(U) + \beta_y(U)} \\ &\text{and} \qquad \tau_y(U) = \frac{1}{\alpha_y(U) + \beta_y(U)} \end{aligned}$$

$$\text{with} \qquad U = \begin{cases} V_S & \text{for } y = h, n \\ V_D & \text{for } y = s, c \\ [Ca^{2+}] & \text{for } y = w \end{cases}$$

4.2.1 The synaptic currents

Pinsky and Rinzel considered two synaptic currents, found only in their dendritic compartment: a fast rising, fast decaying AMPA (α-amino-3-hydroxyl-5-methyl-4-isoxazole-propionate) current and a fast rising, slow decaying NMDA (N-methyl D-aspartate) current. Pinsky and Rinzel used a similar form for their synaptic

currents as Traub et al. (1991), but modelled the connection to the presynaptic cell using gating variables. The NMDA current is voltage and magnesium dependent, as well as ligand dependent, and was given by

$$I_{NMDA} = \frac{\bar{g}_{NMDA} S_i(t) \times (V_D - V_{SYN})}{1 + 0.28e^{-0.062(V_D - 60)}}$$

where $\bar{g}_{NMDA}$ is the maximal NMDA conductance, $V_{SYN} = 60\ mV$ is the NMDA reversal potential, and V_D is the membrane potential of the dendritic compartment. Then the gating variable, $S_i(t)$, was expressed as:

$$S_i' = \sum_j H(V_{S,j} - 10) - S_i/150$$

where $H(x)$ is the Heaviside function such that $H(x) = 1$ for $x \geq 0$, and $H(x) = 0$ otherwise. The sum is taken over all cells j which synapse onto the cell i, and $V_{S,j}$ is the membrane potential of the somatic compartment of cell j. Therefore, if the voltage from a presynaptic cell is greater than the threshold of 10 mV, then the fraction of open gating channels increases. In accordance with the slow decaying NMDA channel, the degradation time constant is large (150 ms). The AMPA current was thought to be the main synchronizing current for the cells, and was given by:

$$I_{AMPA} = \bar{g}_{AMPA} W_i(t)(V_D - V_{SYN})$$

where

$$W_i' = \sum_j H(V_{S,j} - 20) - W_i/2$$

Then

$$I_{SYN} = I_{NMDA} + I_{AMPA}$$

4.2.2 Results

Pinsky and Rinzel found that with the standard coupling parameters, their model exhibited the same key behaviours as the CA3 neuron model in Traub et al.'s (1991) paper. In particular, they found that stimulating the somatic compartment resulted in a train of action potentials, whereas dendritic stimulation resulted in somatic bursting. They analysed this behaviour with respect to the slow variables, q and $[Ca^{2+}]$, and found that these variables (which affected the outward I_{K-AHP} and I_{K-C}) determined the length of the interspike interval. Pinsky and Rinzel then analysed the dynamics of the burst, concluding that it was not simply a series of sodium spikes sitting on a long dendritic calcium-dependent depolarization, but in fact was due to a complex interaction between the dendritic and somatic compartments. They discussed the effects of the coupling parameters, g_C and p, on the model, and noted that for large g_c, the model effectively acted as a single compartment model, and for small g_C, it acted as two isolated models. Thus their

model only exhibited the desired behaviours for a limited range of the coupling parameters. Pinsky and Rinzel also created a network model, by creating 100 two-compartment cell models. Each neuron received input through their synaptic channels from 20 randomly chosen cells. They used this network to describe the significant differences the two synaptic currents and how they modify the network. The fast AMPA currents were primarily responsible for the synchronizing behaviour of the network model, while the slower NMDA current (which is influenced by the level of $\bar{g}_{NMDA}$), determined the sustained bursting behaviour of the network model. Overall, Pinsky and Rinzel created a significantly reduced model based on Traub et al.'s (1991) model, and performed an indepth analysis of the key behaviours exhibited by this model.

4.3 "An astrocytic basis of epilepsy" et al. (2005)

The excitatory neurotransmitter, glutamate, is suspected of playing a key role in seizure generation. In fact, glutamate receptor (GluR) agonists are known to cause excessive neuronal discharges, whereas GluR antagonists suppress them (Tian et al., 2005). Tian et al. decided to examine these excessive and synchronous discharges while eliminating neuronal communication. To do so, they first applied a bath of potassium channel blockers to CA1 pyramidal neurons in rat hippocampal slices. The potassium channel blocker, called 4-aminopyridine (4-AP), is a convulsant known to induce seizure activity in animals and epileptiform bursting in vitro slices. Then they applied a bath of sodium channel blockers called tetrodotoxin (TTX), suppressing neuronal firing. To completely suppress firing, they also applied a variety of voltage gated calcium channel blockers (VGCC blockers). Although excessive bursting was suppressed, they found slow underlying depolarizations, called paroxysmal depolarization shifts (PDSs), which were largely $(70 - 90\%)$ unaffected by TTX and VGCC blockers, and were synchronized among the neurons. These prolonged depolarizations, thought to be the root of the excessive neuronal firing, were obviously not spread by the communication of neurons through chemical synapses. Thus, Tian et al. considered other influences that could cause these PDSs. Two key observations led them to focus their attention on astrocytes. First, activated astrocytes release glutamate into the extracellular space. Second, astrogliosis, an increase in the size and number of astrocytes, is a known characteristic of an epileptic brain (Tian et al., 2005). They hypothesized that glutamate released from activated astrocytes cause these abnormal and prolonged depolarizations, which underly the synchronous neuronal firing in experimental seizures.

To determine how the extracellular glutamate initiates the neuronal action potential independent PDSs, Tian et al. study the activity of a variety of neurotransmitter receptors by applying receptor blockers. First, as before, they generate epileptiform seizures by applying a bath of 4-AP (potassium channel blockers).

They then add TTX and VGCC blockers (sodium and voltage gated calcium channel blockers) to cut off action potential generation, and thus neuronal communication. They found that the action potential independent PDSs were reduced in both frequency and amplitude when APV (2-amino-5-phoshonovalerate), a NMDA receptor inhibitor, and CNQX (6-cyano-7-nitroquinoxaline-2,3-dione), an AMPA receptor inhibitor, were applied. When a series of non-selective metabotropic glutamate receptors (mGluRs) were inhibited, the PDSs were not affected. Thus the glutamate that causes these PDSs activates ionotropic glutamate receptors. In particular, the majority of the PDSs ($\approx 57\%$) were affected by the combination of TTX and APV (where only $\approx 26\%$ were affected by TTX and CNQX), implying that NMDA receptors activated on the neuronal membrane were responsible for the majority of experimental seizure generation in neurons. As well as glutamate receptors, neurons have a number of glutamate transporters on their membrane, which are responsible for the reuptake of glutamate from the synapse. To rule out the possibility of inverted transport of glutamate, Tian et al. applied glutamate transport inhibitors and found that the frequency and amplitude of the PDSs increased significantly. In addition, to confirm that the astrocytic release of glutamate was not simply a response to excessive neuronal firing from the bath of 4-AP, Tian et al. added TTX to the bath before 4-AP, and the PDSs were only reduced slightly.

Since seizures can be generated in a variety of ways, Tian et al. (2005) wanted to test their theory that seizures are induced by PDSs caused by glutamate released from astrocytes. Thus, they used multiple methods to initiate seizure activity, and applied TTX to measure the resulting action potential independent PDSs. First, they removed magnesium (Mg^+) from the extracellular space, which was known to excite a large group of neurons by removing the Mg^+ block from NMDA receptors. The majority of PDSs remained present after the application of TTX, whereas APV and CNQX (the NMDA and AMPA receptor inhibitors) blocked more than 80% of the depolarization shifts. Second, they considered bicuculline and penicillin, which were also known to initiate seizures. Instead of activating excitatory receptors, they were thought to repress inhibitory $GABA_A$ receptors. However, Tian et al. suggested that bicuculline and penicillin may actually affect extrasynaptic glutamate receptors, as the application of APV and CNQX significantly reduced the frequency and amplitude of the PDSs. Finally, they considered the effects of a calcium-free solution, and found the same results: TTX insensitive PDSs were generated, and APV and CNQX significantly reduced their frequency and amplitude. Thus their theory that glutamate induced TTX insensitive PDSs seemed reasonable, and they must next determine if these glutamate signals were sent from astrocytes.

To determine how astrocytes were altered by each method of seizure generation, Tian et al. loaded hippocampal slices with a calcium indicator (fluo-4/AM), and viewed these slices using a two-photon laser scanning microscopy. Thus, they were able to determine how the cytosolic calcium levels in the astrocyte change due to the seizure-inducing agents. For each method discussed above, the astrocytic calcium levels were increased, even in the absence of the neuronal action potentials. In fact, in cultured astrocytes, 4-AP initiated the increased cytosolic calcium levels without

the presence of neurons. This is also true for the other seizure inducing agents, and therefore these increased calcium levels are not a direct effect of neuronal activation. In addition, the application of TTX did not affect the astrocytes, because they have a limited number of sodium channels. When Tian et al. photoreleased the caged calcium in astrocytes (i.e. released calcium by administering pulses of light), they found that PDSs were triggered the majority of the time, and when glutamate release from astrocytes was reduced through channel inhibitors, the frequency and amplitude of the PDSs were decreased. Also, the PDSs, which occur synchronously in a large group of neurons, seem to remain in physiologically relevant spatial territories for astrocytes. That is, since astrocytes often use gap junctions to send signals to other astrocytes, cytosolic calcium oscillations of one astrocyte are usually also found in one to three neighbouring astrocytes. Thus, PDSs should be seen in neurons which are neighbouring these astrocytes - i.e. within a small space of $< 50-200\ \mu m$. Electrodes spaced less than 100 μm apart showed that approximately 56% of PDSs were temporally synchronized, whereas electrodes spaced $100-200\ \mu m$ apart showed that only about 4.8% of PDSs were synchronized. Finally, Tian et al. noted that three common anti-epileptic drugs, valproate, gabapentin and phenytoin, inhibited the increase in astrocytic calcium levels which was triggered by the seizure generating agent. This calcium signalling was also depressed when no seizure generating agent was applied, demonstrating that these drugs were directly affecting the astrocytes, and not simply supressing neuronal excitation.

Tian et al.'s study suggests that astrocytic pathologies may be a contributing factor in epileptic seizures, and the excessive neuronal discharges are driven by these pathologies. They hypothesize that calcium signalling from astrocytes causes glutamate to be released into the extracellular space. This glutamate signals the neurons primarily through NMDA receptors, inducing prolonged depolarizations which result in excessive spiking. Perhaps then, anti-epileptic drugs which focus on inhibiting the calcium signalling in astrocytes, instead of supressing neuronal transmission, would be more effective.

4.4 "Physiological astrocytic calcium levels stimulate glutamate release to modulate adjacent neurons" Parpura and Haydon (2000)

Intracellular astrocytic calcium elevations cause glutamate release, which can lead to prolonged neuronal depolarizations through the activation of ionotropic glutamate receptors. Is this astrocytic glutamate release a pathological condition, or do these mechanisms involved in astrocyte-to-neuron signalling occur physiologically as well? This question existed because the level of astrocytic calcium required to signal the release of glutamate, and what concentrations of internal calcium were

physiological as opposed to pathological, were yet to be determined. Parpura and Haydon (2000) attempted to resolve these issues.

Increased astrocytic calcium concentrations were thought to increase astrocytic glutamate release, causing slow inward currents (SIC) on neighbouring neurons (which result in the depolarization shifts seen by Tian et al. (2005)). To examine this effect experimentally, Parpura and Haydon needed to be able to determine and control the intracellular levels of astrocytic calcium. Working *in vitro*, growing single neurons on microislands of astrocytes, they coloaded astrocytes with a calcium indicator, a fluorescence called fluo-3, and the calcium cage NP-EGTA. They found the resting astrocytic calcium level to be 87 nM, and used this and a standard calibration curve to determine the level of fluo-3 when the astrocyte was at rest (F_0). Then using flash photolysis, a train of six UV pulses were administered which significantly increased the astrocytic calcium levels ($\Delta F/F_0 = 186 \pm 29\%$). To confirm that this effect was not a result of damage done to the astrocyte by the UV pulses, they administered the same pulses of light when the astrocytes were loaded with fluo-3, but not NP-EGTA. In this case, no increase in astrocytic calcium levels were seen. Therefore, Parpura and Haydon (2000) determined that flash photolysis could be used to increase the intracellular calcium concentrations in astrocytes. Through these experiments, and their knowledge of the resting calcium levels, they were able to derive a relationship between the fluo-3 and the calcium levels:

$$[Ca^{2+}]_i = 87nM \times e^{0.0094 \times \Delta F/F_0}$$

By recording the neuronal glutamate-dependent currents, Parpura and Haydon examined the relationship between the astrocytic calcium increases and the release of glutamate. By voltage clamping the neurons at -60 mV, they found that the UV pulses led to astrocytic calcium increases, which caused SICs in neurons. If the astrocytes were only coloaded with fluo-3, and not NP-EGTA, then neither calcium increases, nor SICs resulted from the UV pulses. They also tested neurons cultured without astrocytes, and determined that the UV pulses did not themselves produce SICs. Thus they demonstrated a connection between the astrocytic calcium levels and the neuronal SICs. To show that this connection was glutamate dependent, they administered D-AP5 (a NMDA receptor antagonist) and CNQX (an AMPA receptor antagonist), and found that the neuronal SICs were significantly reduced, while the levels of astrocytic calcium were unaffected.

Parpura and Haydon created a number of plots (which will be reproduced using our model in Chapter 7), which demonstrated the relationship between astrocytic calcium concentration and SICs. Interestingly, they found two types of effects resulting from the increase in calcium. Some neurons demonstrated a graded response, while others exhibited an all-or-none response to calcium increases. In these all-or-none responses, once the astrocytic calcium passed a particular threshold, the neuron exhibited a large SIC, which did not change in strength for continued astrocytic calcium increases. Parpura and Haydon were unsure of the underlying cause of these all-or-none responses, hypothesizing that they may be due to a saturation

of the neuronal glutamate receptors, or from the cytosolic calcium signalling a large release of glutamate from the astrocyte. However, they stated that it was not a result of damage to the cell, as multiple pulses of UV stimulated multiple SICs.

To determine if the calcium-enduced SICs were physiologically relevant, or only occured under pathological conditions, Parpura and Haydon administered glutamate receptor agonists and simultaneously monitor the astrocytic calcium levels. They used 50 μM of glutamate, norepinephrine, and dopamine - agonists which were normally found in the hippocampus and which commonly affect metabotropic glutamate receptors on the astrocytic membrane. They found that these agonists caused increases in the astrocytic calcium concentrations well beyond 140 nM, a level above which consistent neuronal SICs resulted. Thus, Parpura and Haydon concluded that the calcium-dependent release of glutamate from astrocytes was a physiological process, which affected neighbouring neurons, and may play a role in synaptic transmission and neuronal modulation.

4.5 Discussion

Hippocampal pyramidal neurons have received much attention in the study of epileptiform bursting. To model these neurons, we have first considered Traub et al.'s (1991) 19-compartment model of a CA3 and CA1 pyramidal cell. Through a series of current-clamp experiments, they came up with a (non-unique) set of conductance densities for each compartment. Their model was able to accurately reproduce the key characteristics of a CA1 neuron, and their detailed model provided them with a description of the discrete cable properties of the neuron. However, a simplified model would be useful to examine the effects of key parameters, to create large networks, or to expand on the model in other ways. Thus we review Pinsky and Rinzel's (1994) two-compartment model of a CA3 neuron. Although they significantly reduced the complexity of the model, they were able to reproduce many of the characterists of the CA3 neuron which Traub had introduced.

How these CA1 neurons initiate the excessive discharge in experimental seizures is essential to our model. Therefore, Tian et al.'s (2005) article on the astrocytic influence of epileptiform bursting was introduced. They did a series of experiments which suggested that increases in intracellular astrocytic calcium caused the release of glutamate. This glutamate was shown to initiate paroxysmal depolarization shifts in neighbouring neurons, which were thought to influence seizure activity. They suggested that if anticonvulsant drugs focused on the increased cytosolic calcium in the astrocytes, the epileptiform bursting may be affected without elimiating neuronal transmission. Then, Parpura and Haydon (2000) performed a series of experiments to determine whether the increased calcium levels occured physiologically, or just pathologically. They suggested that the intracellular astrocytic calcium levels fluctuate naturally, and that astrocytes may modulate normal neuronal behaviour. These four articles give us a good starting point to create a physiologically realistic model of a CA1 neuron.

Chapter 5

An Isolated CA1 Neuron Model

The mechanisms of hippocampal seizures may become clearer with a solid understanding of the epileptiform bursting activity that can be generated in CA1 pyramidal neurons. This understanding will be facilitated by the existence of biologically realistic models that correspond with current empirical data and are able to make accurate predictions. Traub's model (see section 4.1) serves as a good representation of the structure and behaviour of the CA1 pyramidal neuron. It would be helpful, however, to have a further simplified model in order to dissect and analyze the inner workings of the cell. This new model must be simple enough to permit a detailed analysis of the key parameters, and maintain a realistic representation of the cell's kinetics. Furthermore, the correlation between internal astrocytic calcium waves and epileptiform bursting in CA1 neurons requires some attention while modeling the neuronal synapses. We first discuss in more detail why we have chosen to reduce Traub's model, and then how the behaviour of a typical CA1 neuron influences our reduction of the Traub model. Finally we give a more detailed description of the reduced model by producing a schematic representation, and a mathematical model to represent the voltage, the ionic, applied and synaptic currents, and the coupling between the two neurons.

5.1 Why reduce a model?

We aim to reduce the complexity of Traub's CA1 neuron model while maintaining its key characteristics. The reduction can be done in two ways: we can reduce the membrane complexity by decreasing the number of active ion channels, or we can reduce the geometric complexity by decreasing the number of compartments. Using both of these techniques permits us to explore how much of the key behaviour is dependent on the parameters and variables that remain. It also reduces the computational demand of the model, allowing large networks to be created and examined efficiently, and particular ion or synaptic channels to be modeled in more detail. In our analysis we concentrate on the latter of the two.

5.2 The reduction

Our reduced model does not maintain the same level of detail as Traub's 19-compartment model, so we must ensure that the characteristic qualities of the CA1 neuron are retained. It is important when reducing any model to first identify these characteristic behaviours. Traub et al. (1991) finds that the CA1 neuron exhibits trains of action potentials when a small current ($< 1\ nA$) is applied to the soma, but a full calcium spike and burst followed by trains of action potentials when the same small current is applied to the distal dendrites (0.6λ from soma). Thus we immediately recognize a distinction between the electrical properties in different parts of the neuron. In addition, small synaptic excitation leads to afterdepolarization, whereas large synaptic excitation (or a large somatic applied current) leads to bursting and/or a depolarization shift. The dynamics of the bursting behaviour that commonly occurs in CA1 neurons will be examined in detail in section 5.5. However, it is important to note that modeling this behaviour requires the spatial separation of different channel types and the proper current flow between them (Traub et al., 1991). Thus our model must have at least two compartments.

To separate these compartments we observe that the ionic channels are segregated such that their conductance strength varies significantly in the distal dendrites compared to the proximal dendrites and the somatic compartment (Traub et al., 1991). Therefore we used the general approach of Pinsky and Rinzel (1994) by lumping Traub's soma and proximal dendrite compartments (Traub compartments 6 through 12) into one soma compartment, and the distal dendrite compartments (Traub compartments 1 through 5 and compartments 13 through 19) into one dendrite compartment. The assumption that the electrical behaviour of the axon can be neglected is common in compartmental models and has been adopted. Although there is merit in this assumption, as the axon in pyramidal neurons is often electrically passive compared to the dendrites and soma (Traub and Llinás, 1979), Koch (1998) has noted that this idea may require further scientific analysis. A basic assumption of compartmentalized models is that each compartment represents an isopotential section of the neuron. The compartmental dimensions should be small enough (a fraction of the characteristic length, such as 0.1λ) such that the computational error of this assumption is minimal. Since we maintain the same volume/area ratio as Traub, and Traub's compartments have a length of 0.1λ, this gives our lumped compartments a length greater than 0.5λ. Thus, like Pinsky & Rinzel's model (see section 4.2 for more details), our model should be considered as phenomenological rather than physiological.

Each compartment is assumed to have its own active and passive membrane channels, and the two compartments are connected through the coupling parameters g_C, the strength of coupling, and p, the percentage of the cell model's total area taken up by the somatic compartment. These parameters in our two compartment model were taken from Pinsky and Rinzel (1994), which were adopted from the passive cable parameters of Traub's 19-compartment CA3 neuron model. To get an initial estimate for g_C, we consider a single cable of length l to represent

the soma and dendrites of a CA1 neuron. We split this cable into two compartments representing the soma and proximal dendrites in one compartment, and the distal dendrites in the other. We normalize the membrane area by letting p be the proportion of the cell membrane area taken up by the soma, and $1-p$ be the proportion taken up by the dendrite. The coupling conductance should then be $\hat{g}_C = A/(lR_i)$ where A is the cross-sectional area of the cable (πr^2 for radius r), and R_i is the cytoplasmic resistivity (in Ωcm). For our model with normalized total area (A_{tot}=1) we deal with conductance densities (in mS/cm^2). Therefore we divide the core conductance by the surface area of our two compartments ($2\pi rl$). This gives $g_C = r/(2R_i l^2)$. However, using the values in Traub et al. (1991) we obtain $g_C = 0.18\ mS/cm^2$, which is not large enough for the current flow between the two compartments to create the desired bursting behaviour. Thus, similar to Pinsky and Rinzel (1994), we increase our conductance so that $g_C = 1.5\ mS/cm^2$ for most simulations, noting that this is not a purely physical value.

5.2.1 Ion channel segregation

To separate the ion channels into the appropriate compartments we must first determine which ion currents dominate in the distal dendrites, and which dominate in the soma and proximal dendrites. This is done by examining the ion channel conductances determined by Traub et al. (1991) in their 19-compartment model of a CA1 neuron, given in Table 5.1. They found this non-unique distribution of these conductance densities by trial and error, through current clamp experiments on whole neurons and apical dendrites of pyramidal CA1 neurons of rats.

The active maximal conductance densities are represented by $\bar{g}_{Na}$ for sodium, $\bar{g}_{Ca}$ for calcium, $\bar{g}_{K-DR}$ for delayed rectifier potassium, $\bar{g}_{K-AHP}$ for long-duration calcium-dependent potassium, $\bar{g}_{K-C}$ for short-duration voltage and calcium-dependent potassium, and $\bar{g}_{K-A}$ for A-type of transient potassium, whereas the passive leak conductance is represented by $\bar{g}_L$. Traub et al. (1991) states that a model for a CA1 neuron can be obtained by slightly altering the dynamics of the CA3 model – specifically by decreasing the dendritic $\bar{g}_{Ca}$ and $\bar{g}_{K-C}$, and increasing the somatic $\bar{g}_{K-DR}$. Since Pinsky and Rinzel (1994) have successfully captured the dynamics of a CA3 neuron in their reduced model, we also use their conductance densities as a starting point to determine our own.

Pinsky and Rinzel did not represent a calcium channel in their somatic compartment, as they determined that most calcium is found in the dendrites of the CA3 neuron. But according to Traub et al. (1991), the somatic calcium current is larger than the dendritic calcium current in CA1 neurons. Therefore it is essential that we model this current in both compartments. Consequently, the calcium-dependent currents (i.e. those with conductances $\bar{g}_{K-AHP}$ and $\bar{g}_{K-C}$) must be represented in our somatic compartment as well as our dendritic compartment. The conductance

densities of each of the ion channels in our model is shown in Table 5.2. In the following we describe how these conductance densities were determined.

The sodium conductance, $\bar{g}_{Na}$, is restricted to soma and proximal dendrites – compartments 6 through 12 in the Traub model, with the soma represented as compartment 9. This is the same distribution as with CA3, and so we adopt Pinsky and Rinzel (1994) value of $\bar{g}_{Na} = 30\ mS/cm^2$ (the exact value at the soma). In accordance with Traub's (1991) conductance distributions, our sodium channel is only found in the somatic compartment.

For this same reason, we put delayed rectifier potassium channels only in the somatic compartment, with a conductance strength of $\bar{g}_{K-DR}$. Following Traub's (1991) comments on deriving a CA1 neuron model from the CA3 model, we raised the conductance density from Pinsky and Rinzel (1994) chosen value of 15 mS/cm^2 to 17 mS/cm^2.

A calcium conductance density of $\bar{g}_{Ca}$ is present in both our somatic and dendritic compartments, and according to Traub and Llinás (1979), $\bar{g}_{Ca}$ should be slightly stronger in the proximal dendrites (and therefore the somatic compartment) than in the distal dendrites. These values are essential to reproduce the desired bursting, spiking and afterdepolarization behaviour, and thus some adjustments were required. The dendritic $\bar{g}_{Ca}$ from Pinsky and Rinzel's (1994) CA3 model is reduced from 10 mS/cm^2 to $\bar{g}_{Ca,D} = 5\ mS/cm^2$. The somatic conductance is increased from 0 mS/cm^2 to $\bar{g}_{Ca,S} = 6\ mS/cm^2$.

Both the long-duration calcium-dependent potassium conductance density ($\bar{g}_{K-AHP}$) and the short-duration voltage and calcium-dependent potassium conductance strength ($\bar{g}_{K-C}$) depend on the concentration of free calcium beneath the membrane. Since in our model we have calcium currents in both our compartments, these calcium-dependent currents should also be represented in both compartments. From Table 5.1, it is obvious that we should choose $\bar{g}_{K-AHP,S} = \bar{g}_{K-AHP,D} = 0.8\ mS/cm^2$. Determining the conductance density, $\bar{g}_{K-C}$, is not quite as simple. Pinsky and Rinzel (1994) modeled a K-C current only in the dendritic compartent. Traub et al. (1991) represented the conductance strengths in the somatic compartment and proximal dendritic compartments (i.e. compartments 6-12) of both the CA1 neuron model and the CA3 model as the same. Therefore, we adopt Pinsky and Rinzel's value for $\bar{g}_{K-C}$, but place this in our somatic compartment (i.e. $\bar{g}_{K-C,S} = 15\ mS/cm^2$). Traub's CA1 model has less $\bar{g}_{K-C}$ in the distal dendritic compartments than CA3, so we put a smaller conductance strength in our dendritic compartment. Since all the K-C conductances in the distal dendrite compartments for Traub's CA1 model are the same, we let $\bar{g}_{K-C,D} = 5\ mS/cm^2$.

We ignore $\bar{g}_{K-A}$ since it is found only in the Traub's somatic compartment and is quite small. Traub et al. (1991) stated that this effect of this omission is not significant.

Table 5.1: Ionic maximal conductance densities (mS/cm^2) for Traub's CA1 cell model (reproduced from Traub et al. (1991))

Compartment	$\bar{g}_{Na}$	$\bar{g}_{Ca}$	$\bar{g}_{K-DR}$	$\bar{g}_{K-AHP}$	$\bar{g}_{K-C}$	$\bar{g}_{K-A}$	$\bar{g}_{L}$
1	0.0	0.0	0.0	0.0	0.0	0.0	0.1
2	0.0	5.0	0.0	0.8	5.0	0.0	0.1
3	0.0	5.0	0.0	0.8	5.0	0.0	0.1
4	0.0	7.0	0.0	0.8	5.0	0.0	0.1
5	0.0	7.0	0.0	0.8	5.0	0.0	0.1
6	20.0	12.0	20.0	0.8	10.0	0.0	0.1
7	0.0	5.0	5.0	0.8	5.0	0.0	0.1
8	15.0	8.0	10.0	0.8	20.0	0.0	0.1
9(soma)	30.0	4.0	25.0	0.8	10.0	5.0	0.1
10	15.0	8.0	10.0	0.8	20.0	0.0	0.1
11	0.0	5.0	5.0	0.8	5.0	0.0	0.1
12	20.0	17.0	20.0	0.8	15.0	0.0	0.1
13	0.0	7.0	0.0	0.8	5.0	0.0	0.1
14	0.0	7.0	0.0	0.8	5.0	0.0	0.1
15	0.0	7.0	0.0	0.8	5.0	0.0	0.1
16	0.0	5.0	0.0	0.8	5.0	0.0	0.1
17	0.0	5.0	0.0	0.8	5.0	0.0	0.1
18	0.0	5.0	0.0	0.8	5.0	0.0	0.1
19	0.0	0.0	0.0	0.0	0.0	0.0	0.1

Table 5.2: Ionic conductance densities (mS/cm^2) for our reduced CA1 cell model

Compartment	$\bar{g}_{Na}$	$\bar{g}_{Ca}$	$\bar{g}_{K-DR}$	$\bar{g}_{K-AHP}$	$\bar{g}_{K-C}$	$\bar{g}_{L}$
Somatic	30.0	6.0	17.0	0.8	15.0	0.1
Dendritic	0.0	5.0	0.0	0.8	5.0	0.1

5.3 The model

In the previous section we determined the ionic currents present in each compartment and their respective conductance densities. In this section we will expand this to a full model. A schematic representation of our model was developed in accordance with Pinsky and Rinzel's model of the CA3 pyramidal neuron (Figure 5.1). The schematic shows the ionic currents (I_{Na}, I_{Ca}, I_{K-DR}, I_{K-C}, and I_{K-AHP}) present in each compartment, with the direction of current flow represented by an arrow. The applied currents (I_D, I_S), the synaptic current (I_{SYN}), and the coupling conductance (g_C) are also shown. The difference in potential across the membrane is denoted by V_S and V_D for the somatic and dendritic compartments respectively, and represents the deviation (in mV) from the resting membrane potential of $-60\ mV$.

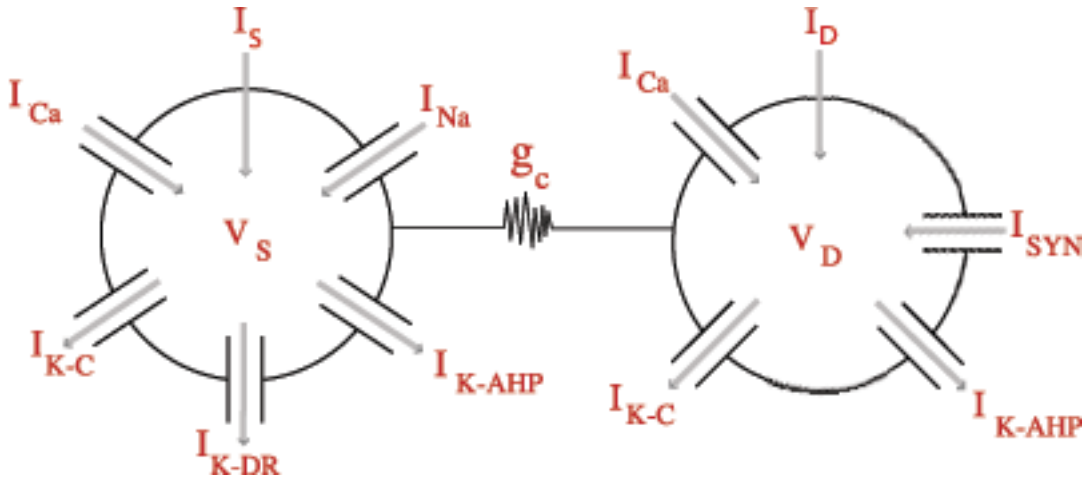

Figure 5.1: A schematic representation of our two-compartment CA1 neuron model.

The somatic compartment has five ionic current channels: sodium and calcium are the inward currents (I_{Na} and $I_{Ca,S}$ respectively), and the outward currents are the delayed rectifier potassium current (I_{K-DR}), long-duration calcium-dependent AHP potassium current ($I_{K-AHP,S}$), and short-duration voltage and calcium-dependent potassium ($I_{K-C,S}$). The dendrite compartment has three ionic current channels: an inward calcium current ($I_{Ca,D}$), and the outward $I_{K-AHP,D}$ and $I_{K-C,D}$. There is a small leak current in both the soma and dendrite compartments. As mentioned, the strength of the coupling between the compartments is controlled by the coupling conductance g_C, and p represents the proportion of the cell area that is taken up by the soma. We use C_m to represent the membrane capacitance in units F/cm^2. All currents in this model have the unit $\mu A/cm^2$ and all conductances have the unit mS/cm^2.

5.3.1 Applied currents

The applied currents, I_S and I_D, model electrode currents that are applied to the somatic or dendritic compartment. We deal with current densities, and thus must divide Traub et al. (1991) applied current by the total area of the Traub model. Thus the values of I_S and I_D are divided by p and $1-p$ respectively, since they are only applied to that proportion of our cell model. In our simulations we will use a variety of applied currents, usually constant, which we have taken from Traub et al. (1991) in the described manner. Unless otherwise stated, we assume that $I_S = I_D = 0\ \mu A/cm^2$.

5.3.2 Ionic currents

Ionic currents are given as a function of their maximal conductance strengths and their corresponding Hodgkin-Huxley-like gating variables, in accordance with Traub et al. (1991). The voltage dependent currents are given by:

$$
\begin{aligned}
I_{leak,S}(V_S) &= \bar{g}_{leak}(V_S - V_{leak,S}) && (5.1)\\
I_{leak,D}(V_D) &= \bar{g}_{leak}(V_D - V_{leak,D}) && (5.2)\\
I_{Na}(V_S, h) &= \bar{g}_{Na} m_\infty^2(V_S) h (V_S - V_{Na}) && (5.3)\\
I_{K-DR}(V_S, n) &= \bar{g}_{K-DR} n (V_s - V_K) && (5.4)\\
I_{Ca,S}(V_S, s_1) &= \bar{g}_{Ca,S} {s_1}^2 (V_S - V_{Ca}) && (5.5)\\
I_{Ca,D}(V_D, s_2) &= \bar{g}_{Ca,D} {s_2}^2 (V_D - V_{Ca}) && (5.6)
\end{aligned}
$$

where V_S and V_D are the membrane potentials for the somatic and dendritic compartments respectively, and V_i is the reversal potential of the specific ion channel that i represents. Sodium has an activation variable, m, and an inactivation variable, h. Since sodium activates almost instantaneously compared to the other variables, its activation variable is represented by the steady state value of m, m_∞, which is voltage dependent.

The activation of the other ion channels depends on the concentration of calcium inside the cell. Following standard practice (Traub et al., 1991), we represent the intracellular calcium concentration in a "shell" beneath the cell membrane as $[Ca^{2+}]_S$ and $[Ca^{2+}]_D$, for the somatic and dendritic compartments respectively. The internal calcium concentration grows as the calcium current flows in, and degrades with a time constant of $1/\beta_{[Ca^{2+}]}$. We do not explicitly model the intracellular release of calcium, and the calcium does not diffuse between compartments. Thus

$$
\frac{d[Ca^{2+}]_i}{dt} = -\phi I_{Ca,i} - \beta_{[Ca^{2+}]}[Ca^{2+}]_i \qquad (5.7)
$$

where $i = S, D$ representing the somatic or dendritic compartment, ϕ is the scaling constant that converts the inward calcium current to the internal calcium concentration, and $\beta_{[Ca^{2+}]}$ is defined above. We chose $\phi = 0.13$ and $\beta_{[Ca^{2+}]} = 0.075\ ms^{-1}$ in accordance with Pinsky and Rinzel (1994) and Traub et al. (1991). The scaling constant, ϕ, was chosen based on numerous simulations by Traub and Llinás (1979), aimed at reproducing the firing rate–injected current curves. The appropriate range for this constant was determined by considering $\phi = c/Ad$, where c was a constant converting current (in nA) to millimoles of divalent ions ($c = 5.2 \times 10^{-12}\ mmol/nC$), A was the area of the soma membrane ($3320\mu m^2$), and $d = 5 \times 10^{-4}\ \mu m$ was the thickness of the thin submembrane shell (Traub and Llinás, 1979). Thus, using this $\phi = c/Ad$ relationship, $[Ca^{2+}]_i$ had dimensions $mmol/(L \cdot m^2)$. However, since the depth of the submembrane shells are yet to be determined, $[Ca^{2+}]_S$ and $[Ca^{2+}]_D$ are given as dimensionless variables, and the relation $\phi = c/Ad$ is only used to determine an appropriate range of values. This leaves the units of ϕ to be $cm^2/(\mu A \cdot ms)$. The ionic K-AHP currents are given by

$$I_{K-AHP,S}(V_S, q_1) = \bar{g}_{K-AHP} q_1 (V_S - V_K) \tag{5.8}$$

$$I_{K-AHP,D}(V_D, q_2) = \bar{g}_{K-AHP} q_2 (V_D - V_K) \tag{5.9}$$

The activation of $K-AHP$ ion channels is calcium dependent, thus the gating variables q_1 and q_2 are a function of $[Ca^{2+}]_S$ and $[Ca^{2+}]_D$ respectively. The $K-C$ ion channels depends on both voltage and the intracellular calcium concentration. The gating variables for these currents are therefore expressed as a product of a voltage-dependent gating variable, c_1 or c_2, and a saturating variable representing the proportion of intracellular calcium with respect to a maximum internal calcium concentration, $[Ca^{2+}]_0$. Traub and Llinás (1979) set $[Ca^{2+}]_0 = 250$ to be the value such that when $[Ca^{2+}] > [Ca^{2+}]_0$ the gating variable takes the maximum value of one.

$$I_{K-C,S}(V_S, [Ca^{2+}]_S, c_1) = \bar{g}_{K-C,S} \times c_1 \times min(1, \frac{[Ca^{2+}]_S}{250}) \times (V_S - V_K) \tag{5.10}$$

$$I_{K-C,D}(V_D, [Ca^{2+}]_D, c_2) = \bar{g}_{K-C,D} \times c_2 \times min(1, \frac{[Ca^{2+}]_D}{250}) \times (V_D - V_K) \tag{5.11}$$

The gating variables h, n, s_1, s_2, c_1, c_2, q_1, and q_2 are of the form:

$$\frac{dy}{dt} = \frac{y_\infty(U) - y}{\tau_y(U)} \tag{5.12}$$

$$\text{where} \qquad y_\infty(U) = \frac{\alpha_y(U)}{\alpha_y(U) + \beta_y(U)} \tag{5.13}$$

$$\text{and} \qquad \tau_y(U) = \frac{1}{\alpha_y(U) + \beta_y(U)} \tag{5.14}$$

$$\text{with} \qquad U = \begin{cases} V_S & \text{for } y = h, n, s_1, c_1 \\ V_D & \text{for } y = s_2, c_2 \\ [Ca^{2+}]_S & \text{for } y = q_1 \\ [Ca^{2+}]_D & \text{for } y = q_2 \end{cases}$$

The rate constants, given by α_y and β_y where y represents each gating variable, are functions of voltage but not time. They were measured empirically and are given below. These rate constants were taken directly from Traub et al. (1991). Note that for $j = 1$, $U = V_S$, and for $j = 2$, $U = V_D$. The time constants are plotted in Figure 5.2.

$$\begin{aligned}
\alpha_m(V_S) &= \frac{0.32 \times (13.1 - V_S)}{e^{(13.1-V_S)/4} - 1} \\
\beta_m(V_S) &= \frac{0.28 \times (V_S - 40.1)}{e^{(V_S-40.1)/5} - 1} \\
\alpha_h(V_S) &= 0.128 \times e^{(17-V_S)/18} \\
\beta_h(V_S) &= \frac{4}{e^{(40-V_S)/5} + 1} \\
\alpha_n(V_S) &= \frac{0.016 \times (35.1 - V_S)}{e^{(35.1-V_S)/5} - 1} \\
\beta_n(V_S) &= 0.25 \times e^{(0.5-0.025V_S)} \\
\alpha_{s_j}(U) &= \frac{1.6}{1 + e^{-0.072\times(U-65)}} \\
\beta s_j(U) &= \frac{0.02 \times (U - 51.1)}{e^{(U-51.1)/5} - 1} \\
\alpha_{c_j}(U) &= \begin{cases} 2 \times e^{(6.5-U)/27} & \text{if } U > 50 \\ (e^{\{((U-10)/11)-((U-6.5)/27)\}})/18.975 & \text{otherwise} \end{cases} \\
\beta_{c_j}(U) &= \begin{cases} 0 & \text{if } U > 50 \\ 2 \times e^{(6.5-U)/27} - \alpha_{c_j}(U) & \text{otherwise} \end{cases} \\
\alpha_{q_j}[Ca^{2+}]_U &= min(0.00002 \times [Ca^{2+}]_U, 0.01) \\
\beta_{q_j} &= 0.001
\end{aligned}$$

The synaptic current, I_{SYN}, represents the currents the CA1 neuron receives from other neurons, interneurons, and glial cells through chemical synapses. We do not consider gap junctional synapses (electrical synapses) in this model. The neuron mostly receives the synaptic signal on its dendrites, so I_{SYN} is modeled in the dendritic compartment. In particular we model the fast-rising and fast-decaying AMPA synapse, the fast-rising, and the slow-decaying NMDA synapse. Then I_{SYN} represents the sum of all the synaptic currents:

$$I_{SYN} = I_{AMPA} + I_{NMDA} + I_{GABA} \tag{5.15}$$

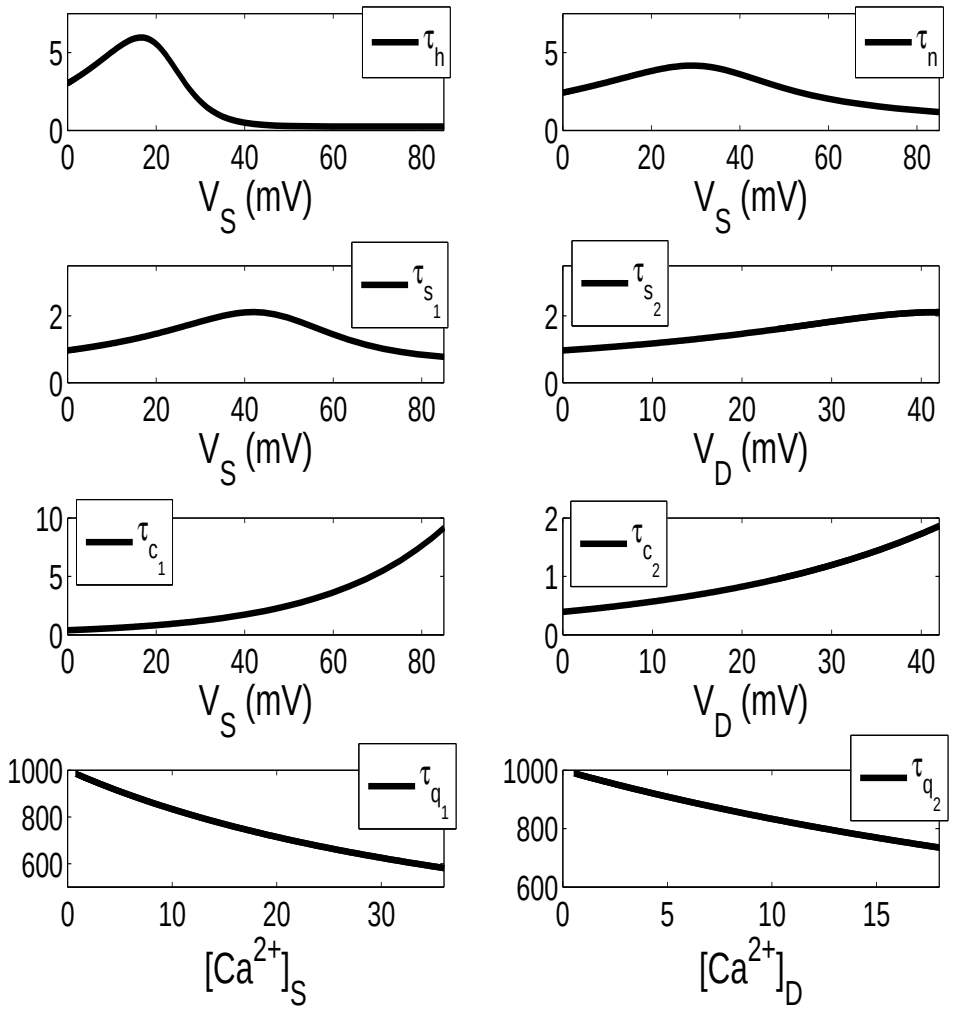

Figure 5.2: The time constants τ_m, τ_h, τ_n, τ_{s_1}, and τ_{c_1} are plotted against V_S. The time constants τ_{s_2} and τ_{c_2} are plotted against V_D, and the time constants τ_{q_1} and τ_{q_2} are plotted against $[Ca^{2+}]_S$ and $[Ca^{2+}]_D$ respectively. Note the long time constants for the calcium-dependent q_1 and q_2 variables.

5.3.3 The membrane potential

Now that the ionic and applied currents have been described, the voltage change for each compartment can be explicitly expressed. For now, we consider the synaptic current to be zero ($I_{SYN} = 0\ mS/cm^2$), meaning that the isolated cell model does not receive input from other excitatory or inhibitory cells. According to Kirchoff's law (section 3.4), the rate of change of the potential across each membrane (soma and dendrite respectively) can be represented as:

$$\begin{aligned}\frac{dV_S}{dt} &= \frac{1}{C_m}\Big\{ - I_{leak,S}(V_S) - I_{Na}(V_S,h) - I_{K-DR}(V_S,n) - I_{Ca,S}(V_S,s_1) \\ &\quad - I_{K-C,S}(V_S,[Ca^{2+}]_S,c_1) - I_{K-AHP,S}(V_S,q_1) \\ &\quad + \frac{g_c}{p} * (V_D - V_S) + \frac{I_S}{p}\Big\} \qquad (5.16)\\ \frac{dV_D}{dt} &= \frac{1}{C_m}\Big\{ - I_{leak,D}(V_D) - I_{K-AHP,D}(V_D,q_2) - I_{Ca,D}(V_D,s_2) \\ &\quad - \frac{I_{SYN}}{1-p} - I_{K-C,D}(V_D,[Ca^{2+}]_D,c_2) + \frac{g_c}{1-p} * (V_S - V_D) + \frac{I_D}{1-p}\Big\} \qquad (5.17)\end{aligned}$$

Unless otherwise stated, the maximal conductances, reversal potentials, coupling parameters and membrane capacitance are as stated in Table 5.3, and the initial conditions are as stated in Table 5.4.

5.3.4 Numerics

The model was implemented in Windows using XPPAUT, an ordinary differential equation solver. The program, XPPAUT, was created to show the dynamics of an excitable membrane (Ermentrout, 2002), and is useful for simulating and analyzing these dynamics. The Runge-Kutta fourth-order explicit method was used with a fixed timestep of 0.05 ms. This classic Range-Kutta method, with a timestep of h, has accuracy of order $O(h^4)$. Consider a differential equation of the form

$$\frac{dx}{dt} = f(t,x)$$

with the initial condition $x(t_0) = x_0$. The Runge-Kutta approximation of $x(t_{n+1})$ can be written as x_{n+1}, where $t_{n+1} = t_n + h$,

$$x_{n+1} = x_n + \frac{h}{6}(k_1 + 2k_2 + 2k_3 + k_4)$$

Table 5.3: The parameter values for our isolated CA1 neuron model.

Parameter	Unit	Parameter Value
$\bar{g}_L$	mS/cm^2	0.1
$\bar{g}_{Na}$	mS/cm^2	30
$\bar{g}_{K-DR}$	mS/cm^2	17
$\bar{g}_{Ca,S}$	mS/cm^2	6
$\bar{g}_{Ca,D}$	mS/cm^2	5
$\bar{g}_{K-AHP,S}$	mS/cm^2	0.8
$\bar{g}_{K-AHP,D}$	mS/cm^2	0.8
$\bar{g}_{K-C,S}$	mS/cm^2	15
$\bar{g}_{K-C,D}$	mS/cm^2	5
$\bar{g}_{NMDA}$	mS/cm^2	0
$\bar{g}_{AMPA}$	mS/cm^2	0
V_{Na}	mV	120
V_{Ca}	mV	140
V_K	mV	-15
V_L	mV	0
V_{EXC}	mV	60
V_{INH}	mV	-15
I_S	$\mu A/cm^2$	-0.25
I_D	$\mu A/cm^2$	-0.25
g_C	mS/cm^2	1.5
p		0.5
C_m	$\mu F/cm^2$	3

Table 5.4: The initial conditions of the variables in our isolated CA1 neuron model. Recall that V_S and V_D are the differences in the membrane potential (for the somatic and dendritic compartments respectively) relative to rest (where $V_{rest} = -60\ mV$). These values were taken from Traub et al. (1991), and from Pinsky and Rinzel (1994).

Variable	Initial Value
$V_S\ (mV)$	-4.6
$V_D\ (mV)$	-4.5
h	0.999
n	0.001
$s_1,\ s_2$	0.009
$c_1,\ c_2$	0.007
$q_1,\ q_2$	0.010
$[Ca^{2+}]_S,\ [Ca^{2+}]_D$	0.2

and

$$\begin{aligned} k_1 &= f(t, x_n) \\ k_2 &= f(t + \frac{h}{2}, x_n + \frac{hk_1}{2}) \\ k_3 &= f(t + \frac{h}{2}, x_n + \frac{hk_2}{2}) \\ k_4 &= f(t + h, x_n + hk_3) \end{aligned}$$

Our model was relatively stiff, due to the fast dynamics of the spiking and the slow dynamics of the interspike interval. However, our fixed timestep of 0.05 ms was sufficiently small, and we were able to accurately capture the desired dynamics.

5.4 Results

Before we consider synaptic influence, we need to ensure that our isolated neuron model simulates the electrophysiological properties of a typical CA1 pyramidal neuron. We compare simulations from our model (where the model is given in the previous section) to those of Traub's model. The primary behaviours of interest of a CA1 neuron are discussed, as well as the range of key variables for which this behaviour is maintained. Since Traub's isolated neuron model is much more detailed than ours, there will inevitably be characteristics of the neuron that Traub's model captures and ours does not. Thus we conclude with a discussion of the limitations of our model.

We must first clearly define an action potential and a burst. Following Pinsky and Rinzel (1994), we define a somatic burst as a depolarization of at least $V_S = 10\ mV$, with a miniumum of three separate peaks. The dynamics of a burst will be discussed more in section 5.5. Again, following Pinsky and Rinzel's (1994) definition, we say an action potential exists when V_S has a maximum of at least $50\ mV$ and a minimum below $5\ mV$.

From section 4.1, we recall Traub et al. (1991) determined that when a current of $< 1\ nA$ ($\approx 2.5\ \mu A/cm^2$) is injected into the soma of a CA1 pyramidal neuron, repetitive somatic firing occurs. The distal dendrites depolarize slightly, and produce subthreshold voltage transients. Stimulation in the proximal dendrites (at 0.3λ from the soma) results in a similar pattern of firing, but with greater depolarization in the distal dendrites. However, if the distal dendrites are stimulated (0.6λ from the soma), then a full dendritic calcium spike associated with a somatic burst is enduced. The somatic burst is followed by repetitive action potentials.

By injecting a sustained current into our somatic compartment (I_S) and later into our dendritic compartment (I_D), we reproduce these results. In Figure 5.3(a), the somatic and dendritic voltage (V_S and V_D respectively) are shown when a

sustained current is applied to the somatic compartment. As expected, a steady train of somatic action potentials is produced with no bursting. Subthreshold dendritic voltage spikes ensue. The interspike interval (i.e. the interval between action potentials) lengthens over time, which is consistent with Traub's (1979) findings for CA1 neurons. When a current of the same strength is applied to the dendritic compartment, our model accurately simulates the dendritic calcium spike and somatic burst, followed by action potentials (Figure 5.3(b)). It is obvious from Figure 5.3 that when a current is applied to the dendritic compartment, the train of action potentials occurs at a lower frequency than when the same current is applied to the somatic compartment. The large dendritic calcium spike triggers the calcium-dependent outward potassium channel $I_{K-AHP,D}$, resulting in a longer afterhyperpolarization (due to the large time constant), and therefore larger interspike intervals. Again, this characteristic CA1 neuron behaviour only occurs for applied currents smaller than approximately 2.5 $\mu A/cm^2$. For the simulations in Figure 5.3, we use a constant applied current of either I_S or $I_D = 1.25\ \mu A/cm^2$ (which translates to approximately 0.48 nA from Traub's model), while the applied current to the other compartment is held constant at $-0.25\ \mu A/cm^2$. We have chosen to hold the current at $-0.25\ \mu A/cm^2$ so that it is slightly below our rheobase – the minimum amount of current required to excite the neuron – which is found to be approximately $-0.175\ \mu A/cm^2$ when $p = 0.5$. We did so in accordance with Pinsky and Rinzel (1994) and Traub et al. (1991), who applied a small negative current to suppress spontaneous firing. The coupling parameters are kept for now at the standard values of $g_C = 1.5\ mS/cm^2$ and $p = 0.5$.

The desired behaviour can be observed when the applied current is in a specific range. For example, when $g_C = 1.5\ mS/cm^2$, $p = 0.5$ and a sustained current is applied to the somatic compartment, the characteristic train of action potentials are produced for $0\ \mu A/cm^2 < I_S < 3.5\ \mu A/cm^2$. However, within this range the frequency of spiking varies significantly, decreasing as the applied current decreases. According to Traub (1979), the minimum firing rate of a typical CA1 neuron with a somatic depolarization is approximately 20 $impulses/sec.$ Thus we restict our range of I_S so our model produces physiologically relevant results, leaving us with $1.25\ \mu A/cm^2 \leq I_S < 3.5\ \mu A/cm^2$. Similarily, when a dendritic current is applied (with the same coupling parameters as stated above), our desired bursting behaviour with subsequent action potentials is produced when $0.5\ \mu A/cm^2 < I_D < 4\ \mu A/cm^2$. This is an approximate range, and of course depends on the particular definition of a burst.

It is important to recognize that, as with Pinsky and Rinzel's model (1994), our model only demonstrates the desired characteristic CA1 behaviour for a limited range of the coupling conductance, g_C. A very large coupling conductance essentially makes our model a single compartment model, and a very small g_C leaves us with isolated compartments. However, if g_C is only slightly reduced then no bursting occurs, and if g_C is slightly increased then aperiodic bursting occurs. In fact, with an applied current of $I_D = 1.25\ \mu A/cm^2$, the desired bursting behaviour

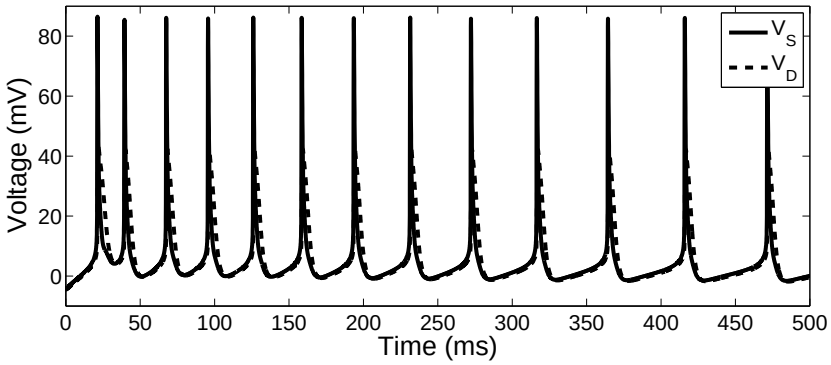

(a) A sustained somatic current of $I_S = 1.25\ \mu A/cm^2$ is applied

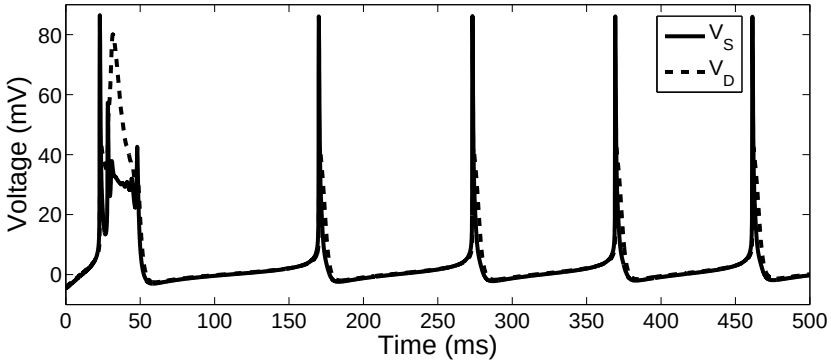

(b) A sustained dendritic current of $I_D = 1.25\ \mu A/cm^2$ is applied

Figure 5.3: The membrane voltage when a (a) somatic and (b) dendritic current is applied. Characteristic qualities of a CA1 neuron are reproduced: (a) A train of action potentials with increasing interspike interval, (b) a burst with a full dendritic calcium spike, followed by repetitive spiking.

is reproduced for $1.35\ mS/cm^2 \leq g_C \leq 1.7\ mS/cm^2$.

Our results were produced with a small negative holding current, following Traub et al. (1991). The holding current prevented spontaneous neural activity in Traub's experiments, and eliminated very low frequency spiking in our model. Without this small current, our model produced the same results with spiking at a very slightly higher frequency. The simulations in the remainder of this thesis are created with this holding current, but have been reproduced without it as well, and the results remain consistent with experimental findings. In the next section, we consider the underlying mechanism behind the generation of a burst.

5.5 Bursting mechanics

As we have shown in the previous section, a moderate sustained current of less than $2.5\ \mu A/cm^2$ applied to the dendritic compartment will cause an initial tran-

sient burst in the somatic compartment followed by a train of action potentials. What causes this transient burst? To explain this qualitatively, we analyze the dynamics of the burst and compare it with a single spike. For simplicity, we examine a single isolated model CA1 neuron with no synaptic input. The coupling parameters are kept at their usual values of $g_C = 1.5\ mS/cm^2$ and $p = 0.5$, and maintaining $I_S = -0.25\ \mu A/cm^2$, a constant applied dendritic current of $I_D = 1.25\ \mu A/cm^2$ is used to create the initial burst followed by the action potential shown in Figure 5.4. We show that the dendritic calcium current, $I_{Ca,D}$, is the primary cause of bursting: more specifically it is the interplay between the outward dendritic currents $I_{K-C,D}$ and $I_{K-AHP,D}$ with the inward dendritic current $I_{Ca,D}$. Since the calcium-dependent potassium currents are essential to the bursting behaviour, we look at the associated variables $[Ca^{2+}]$ and q . In addition, the coupling parameters, g_C and p, are identified as key elements in generating this characteristic behaviour.

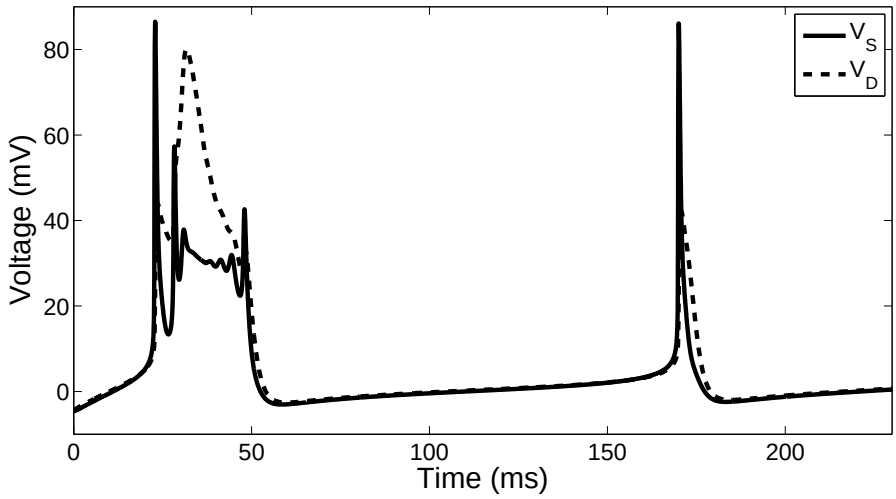

Figure 5.4: A typical transient burst and an action potential is produced from our isolated model when a sustained current of $I_D = 1.25\ \mu A/cm^2$ is applied to the dendritic compartment. The burst is initiated by a somatic spike. The dendritic voltage, V_D, is significantly larger than the somatic voltage, V_S (compared to the single action potential case). The coupling component alternately deplolarizes the two compartments, resulting in a burst. In the case of the action potential, V_S has a full sodium spike but V_D is not large enough to send the somatic compartment into a second spike.

So what is happening in our simulations? Initially, the applied dendritic current (I_D) depolarizes the dendritic compartment, but the dendritic voltage (V_D) is not large enough for a full calcium spike. The coupling between the compartments quickly depolarizes the somatic compartment, enough so that it surpasses its threshold and creates an action potential. This is known as a sodium spike since the somatic sodium current ($I_{Na,S}$) activates at lower voltages than the somatic

calcium current ($I_{Ca,S}$). The key is that if the outward dendritic currents $I_{K-C,D}$ and $I_{K-AHP,D}$ are strong enough to counteract the inward $I_{Ca,D}$ (Figure 5.5, right inset), then the dendritic voltage, V_D, will decrease at approximately the same rate as the somatic voltage, V_S. Thus, the difference in the two voltages will be small, and very little current will be transferred due to coupling. This permits the two compartments to repolarize, and relax to their resting potentials. In this case only an action potential will be produced.

However, if $I_{K-AHP,D}$ and $I_{K-C,D}$ are not strong enough to counteract the inward $I_{Ca,D}$ (Figure 5.5, left inset), the difference between V_D and V_S after the somatic spike is large. The coupling further depolarizes the somatic compartment and a second Na^+-spike occurs. Since the soma has not fully recovered from its initial action potential ($I_{K-DR,S} > 0\ \mu A/cm^2$), this second spike will be partial in size (note the decreased amplitude in the second spike in the burst in Figure 5.4). Although V_D increases due to coupling, it may still not be large enough to surpass the threshold for a full calcium spike. In this case the process continues: the depolarized dendritic compartment sends the somatic compartment into another partial somatic spike — depolarizing the dendritic compartment yet again through the coupling current. This cycle repeats until finally V_D passes the threshold and produces a full dendritic calcium-mediated spike. This broad dendritic spike initiates a strong depolarizing current flow between the compartments. The short time scale does not allow I_{K-DR} to recover, and the soma is "over-driven" — i.e. no somatic sodium spikes can be produced. Once V_S, V_D, and I_{K-DR} have begun to recover, the soma is no longer in over-drive, and a small somatic Na^+-spike may occur. This time the difference in voltage is not enough to initiate another burst sequence, thus V_S and V_D are repolarized.

To determine why our model is much more likely to produce a single transient burst than repetitive bursting, we consider the dynamics of the outward potassium currents $I_{K-C,D}$, and $I_{K-AHP,D}$. Recall that the K-C ion channels activate depending on both the fast voltage-dependent gating variables, c_1 and c_2, and the slower intracellular calcium concentrations, $[Ca^{2+}]_S$ and $[Ca^{2+}]_D$ (section 5.3). Therefore the time constant of this outward potassium channel largely depends on the slow decay time ($1/\beta_{[Ca^{2+}]}$) of the concentration of internal calcium. Similarily, the decay time of the potassium current $I_{K-AHP,D}$ depends on the slow gating variable q_2, which is also a function of $[Ca^{2+}]_D$. Thus the dendritic calcium spikes repolarize in accordance with the time constants of the slow variables $[Ca^{2+}]_S$, $[Ca^{2+}]_D$, q_1 and q_2. The length of the "quiet period" of V_S – when the soma is overdriven – during such a dendritic calcium spike is also determined mainly by these slow variables. From Figure 5.6(b) it is evident that the levels of q_2 are low at the time of bursting, and are significantly elevated during the action potentials. In general, the q_1 and q_2 variables of our CA1 neuron model are initially low, allowing for the characteristic transient burst. High q values permit greater outward flow of I_{K-AHP}, allowing the voltage to recover faster, thereby reducing the probability of bursting. Similarily, the intracellular calcium concentration is low during the initiation of a burst. Increased levels of $[Ca^{2+}]$ activates the $K-C$ channels directly (and

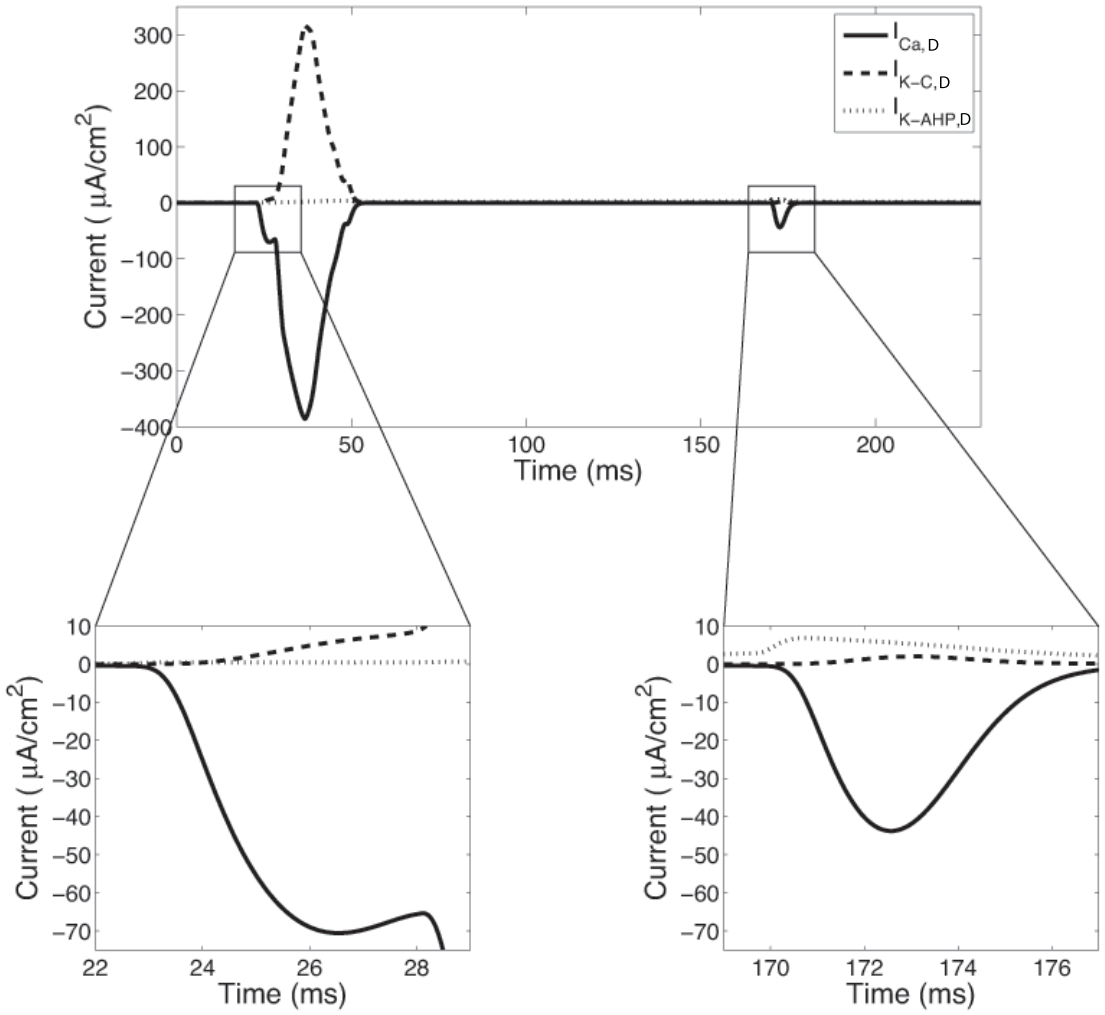

Figure 5.5: The currents $I_{K-AHP,D}$, $I_{K-C,D}$ and $I_{Ca,D}$ are shown during the burst and spike triggered from the applied current of $I_D = 1.25\ \mu A/cm^2$ from Figure 5.4. A magnified view of the currents from the upper figure during the burst (left inset) and the spike (right inset). The outward currents are denoted as positive and the inward as negative by convention. When the outward currents are not strong enough to counteract the effect of the inward $I_{Ca,D}$, a burst is generated. When they are sufficiently strong, a single action potential is generated. Notice the inward $I_{Ca,D}$ is much larger during the burst than the action potential.

$K - AHP$ channels indirectly), permitting the compartmental voltage to repolarize faster. This faster recovery implies a decreased chance of bursting, resulting in single action potentials (Figure 5.6(a)). However, a large dendritic calcium conductance, $\bar{g}_{Ca,D}$, creates a large inward calcium current flow. This makes it difficult for the outward potassium currents to counteract the inward flow, increasing the possibility of a burst.

It is obvious that the coupling parameters, g_C and p, play an essential role in

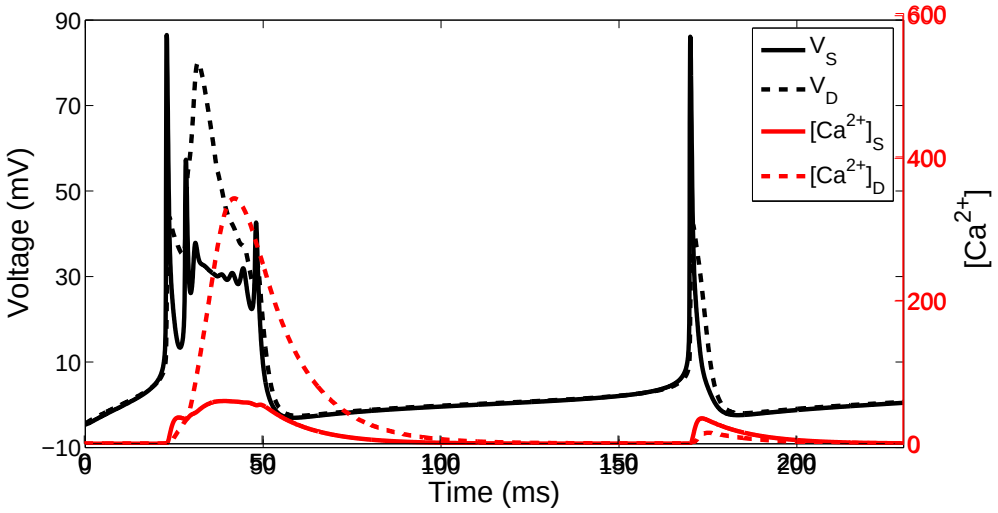

(a)

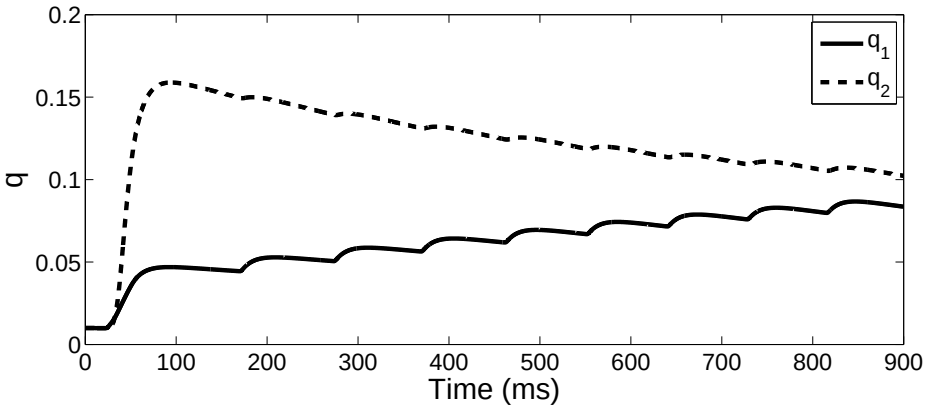

(b)

Figure 5.6: (a) The somatic and dendritic intracellular calcium concentrations, $[Ca^{2+}]_S$ and $[Ca^{2+}]_D$ (in red), overlaying the bursting and spiking from Figure 5.4. (b) q_1 and q_2 for the burst and spike sequence in (a). Therefore an applied dendritic current of $I_D = 1.25\ \mu A/cm^2$ as in Figure 5.4 results in the same voltage burst and spike. It is evident that increased levels of the slow variables $[Ca^{2+}]_S$, $[Ca^{2+}]_D$, q_1, and q_2 decrease bursting activity. The characteristic transient burst occurs because of the initially low q values.

generating bursts. Since the currents are voltage-dependent, they are also dependent on the coupling. Increased coupling results in increased flow of electrotonic current, elevating the q and $[Ca^{2+}]$ levels, as well as the inward current flow. Although the model will be more effective in creating the bursts, it will also recover faster, shortening the length of the burst. Thus, if the coupling parameter g_C is increased, the greater current flow between the two compartments will be more effective in intiating a burst. Similarily, the effects of the two compartments depend

on their proportional size, p: the larger the dendritic compartment is compared to the somatic compartment, the more influence it will have.

5.6 Discussion

Pyramidal neurons from the CA1 region of the hippocampus have been focused on in the study of epileptiform bursts, because of their ability to generate excessive and synchronous electrical discharges. Traub et al. (1991) created a 19-compartment model (discussed in detail in section 4.1), which elegantly described the structure and behaviour of these neurons. However, a simplified model would be useful, allowing one to identify the key parameters, and analyse the mechanisms behind the epileptiform bursting. We used Pinsky and Rinzel's (1994) two-compartment model of a CA3 neuron as inspiration while reducing Traub's model. However, Pinsky and Rinzel's CA3 model and our CA1 model had a few key differences. First of all, the two neurons responded differently to dendritic stimulation. When a moderate dendritic stimulus was applied, a CA1 soma exhibited a burst followed by a train of action potentials, whereas a CA3 soma exhibited repetitive bursting (Traub et al., 1991). This was due to the different calcium dynamics of the two neurons. Unlike a CA3 neuron, the soma and proximal dendrites of a CA1 neuron exhibited larger calcium currents than the distal dendrites. Thus, we had to model the calcium current in both compartments, instead of only the dendritic compartment as in Pinsky and Rinzel's CA3 neuron model (Pinsky and Rinzel, 1994). Finally, in accordance with Traub et al. (1991), the conductances of the ion channels differed between the two models. Therefore, using Pinsky and Rinzel's (1994) CA3 model, and Traub's model and conductance densities, as a starting point, we created a two-compartment model of a CA1 neuron. The mathematical model provided a representation of the membrane potential, the ionic, and applied currents, and the coupling between the two compartments. In this section we considered an isolated cell, and therefore took the synaptic currents to be zero. We were able to reproduce the characteristic behaviours of a CA1 neuron, as described by Traub et al. (1991), and to examine the key parameters involved in the generation of a burst. We found that the coupling parameters g_C and p and the dynamics between the inward dendritic calcium current and the two outward dendritic potassium currents were especially important to the generation of a burst. In addition, the slow parameters, q and $[Ca^{2+}]$, were determined to be essential influences in the length of the interspike interval as well as the generation of a burst.

It is not surprising that there are some characteristics of the CA1 neuron that our reduced model will not capture. When creating such a reduced model, it is important to recognize the level of detail one wishes to obtain. For example, according to Traub and Llinás (1979), about 25% of CA1 neurons produce very small all-or-nothing spikes called "d-spikes". These spikes are small in amplitude (approximately $2-15\ mV$) and peak quickly. They can be produced spontaneously, and are capable of exhibiting bursting. Traub's model accounts for these small

spikes, while our reduced model does not. However, for the purpose of our study, we are not concerned about such a detail.

Chapter 6

A Coupled Neuron Model

To create the basis for a potential network of CA1 neurons, we must first consider how two CA1 neurons communicate with each other. The physiological details of this neuron-neuron communication are given in section 2.6, and thus we just discuss the key points briefly. When excited, the presynaptic neuron releases neurotransmitters into the synaptic cleft to signal its postsynaptic neighbour. According to Pinsky and Rinzel (1994) and Traub (1992), the AMPA synapse is the dominant mechanism involved in the synchronization of two pyramidal neurons. Thus we conclude that the neurotransmitters from the presynaptic cell primarily activate the AMPA receptors on the postsynaptic neuronal membrane. Using this knowledge, we construct an appropriate synapse model which synchronizes coupled cell models under a strong connection, and desynchronizes the coupled models immediately once the strong connection is removed. The influence of an inhibitory interneuron on a CA1 neuron is modeled through a simple $GABA_A$ synapse.

6.1 The AMPA synapse model

The idea of coupling two cell models requires some discussion. We attach a subscript to our variables to denote the appropriate cell to which it belongs. For example, we say V_{S_i} is the i^{th} cell's somatic voltage for $i = 1, 2, ...$ Consider two cells, a presynaptic cell (cell 2) and a postsynaptic cell (cell 1). Using the gating variable W_1 and the maximal conductance $\bar{g}_{AMPA_1}$, we represent the synaptic current due to the AMPA receptors by:

$$I_{AMPA_1} = \bar{g}_{AMPA_1} W_1 (V_{D_1} - V_{EXC}) \tag{6.1}$$

where V_{D_1} is the voltage of the dendritic compartment of the postsynaptic cell, and the reversal potential of the excitatory synapse is given by $V_{EXC} = 60\ mV$ in accordance with Traub (1991). So as not to confuse which synaptic currents are involved in our simulations, the maximal conductances, $\bar{g}_{AMPA_1}$ and $\bar{g}_{AMPA_2}$, are set to be 0.0 mS/cm^2, unless otherwise stated. During a signal (or spike) from

the presynaptic cell, the presynaptic voltage increases. The presynaptic voltage is denoted V_{S_2} and V_{D_2} for somatic and dendritic voltage respectively. If V_{S_2} surpasses some threshold, V_W, then the AMPA current of the postsynaptic cell activates with a time constant of 1 ms. Otherwise, the current will not activate. The activation degrades with a time constant τ_W. Then

$$\frac{dW_1}{dt} = H(V_{S_2} - V_W) - \frac{W_1}{\tau_W} \tag{6.2}$$

where H(x) is the heaviside function $H(x) = \begin{cases} 1 & \text{if } x \geq 0 \\ 0 & \text{otherwise} \end{cases}$,
$V_W = 40\ mV$ and $\tau_W = 2\ ms$ in accordance with Traub (1992) and Nadkarni & Jung (2005).

To maintain a biologically realistic model, the two individual cell models should not be identical. Thus we alter some variables of "cell 2" slightly, while keeping them close to the values for cell 1. Unless otherwise stated, we have $\bar{g}_{Na_2} = 28\ mS/cm^2$, $\bar{g}_{K-AHP_2} = 0.7\ mS/cm^2$, and all other variables stay as stated in section 5.2.

6.2 Results for the AMPA synapse

Before we consider any other synaptic input, we should determine whether this modeled neuron-to-neuron coupling corresponds with the results of Traub et al. (1991). Traub et al. stated that the AMPA synapse is primarily responsible for the synchronization of two neurons. To demonstrate that this characteristic is upheld in our model, we couple two cell models with an AMPA synapse, disregarding all other synaptic input ($I_{NMDA} = 0\ \mu A/cm^2$). Different non-zero input is applied to each of the two cell models ($I_{D_1} \neq I_{D_2}$), but only the second cell model receives AMPA input ($\bar{g}_{AMPA_1} = 0.0\ mS/cm^2$, and $\bar{g}_{AMPA_2} \neq 0.0\ mS/cm^2$). If the second cell model receives weak AMPA input, then the two models will not synchronize (Figure 6.1(a). However, if a significantly strong AMPA input connects the second cell model to the first, then it synchronizes to that cell.

Next, we consider a sinusoidal input, applied to the somatic compartment of both cell 1 and cell 2. We set the frequency and strength of the input to be different for both cell 1 and cell 2, so the cells do not synchronize on their own. Then, if neuron models are connected with a sufficiently strong AMPA conductance, and the first input (I_{S_1}) has a higher amplitude than the second (I_{S_2}), then the second neuron model should synchronize to the first. Physiologically, when AMPA blockers are applied, the neurons are reported to desynchronize rapidly (Traub et al., 1991).

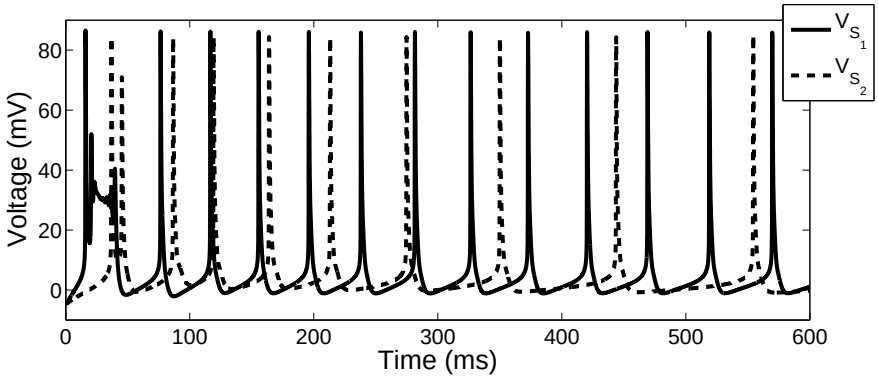

(a)

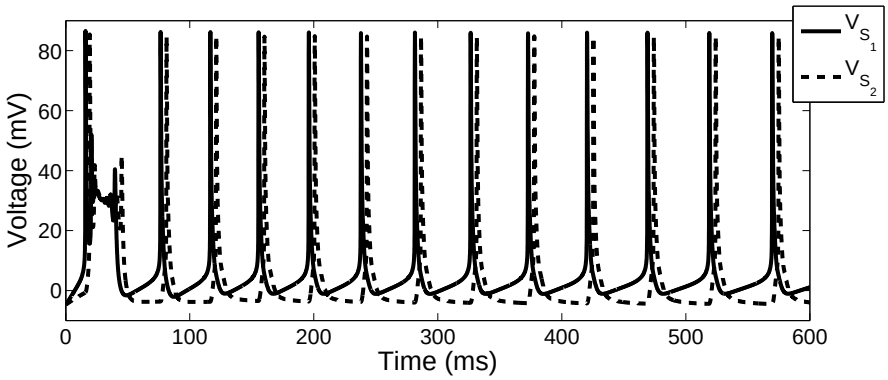

(b)

Figure 6.1: An input of $I_{D_1} = 2.0\ \mu A/cm^2$ and $I_{D_1} = 1.25\ \mu A/cm^2$ is applied. (a) a weak connection : $\bar{g}_{AMPA_2} = 0.04\ mS/cm^2$. The two cell models are not synchronized. (b) a strong connection: $\bar{g}_{AMPA_2} = 0.2\ mS/cm^2$. The two cell models are sychronized.

We show these results in Figure 6.2, by connecting the cells strongly ($\bar{g}_{AMPA_1} = \bar{g}_{AMPA_2} = 0.2\ mS/cm^2$) until $t = 500\ ms$, and weakly ($\bar{g}_{AMPA_1} = \bar{g}_{AMPA_2} = 0.01\ mS/cm^2$) after $t = 500\ ms$. We set the input to be $I_{S_{cell1}}(t) = I_{S_1} sin(2\pi t/100) + I_{S_1} - 0.25$ where $I_{S_1} = 1.25$ so $I_{S_{cell1}}(t)$ fluctuates between -0.25 and 2.25. Similarily we set $I_{S_{cell2}}(t) = I_{S_2} sin(2\pi t/130) + I_{S_2} - 0.25$, where $I_{S_2} = 1.25$, so $I_{S_{cell2}}(t)$ has a slightly different period.

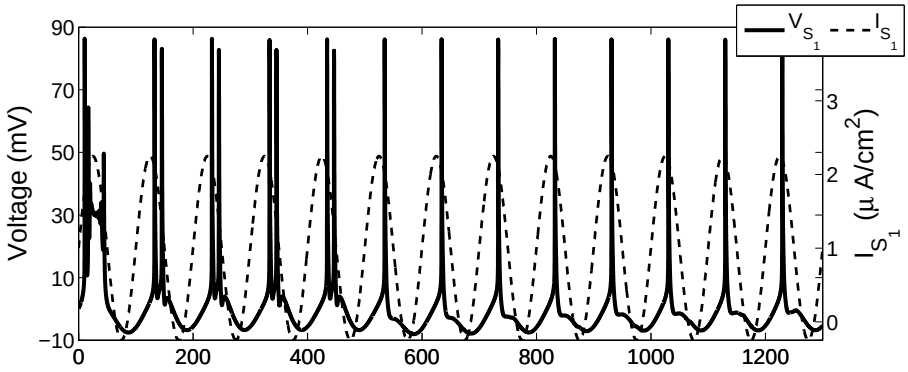

(a)

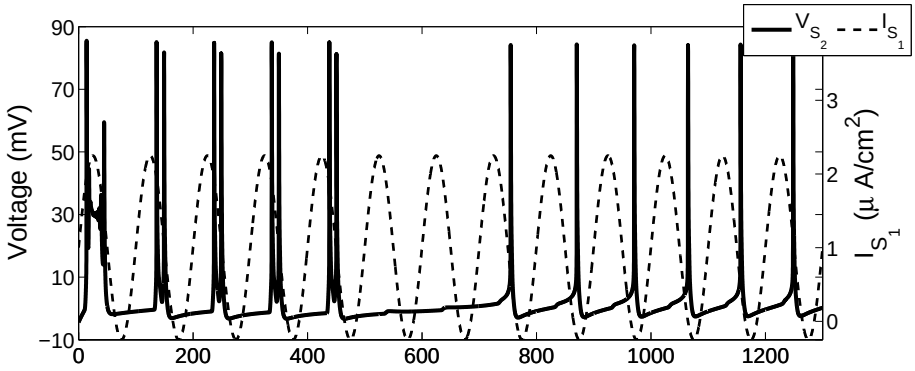

(b)

Figure 6.2: (a) The voltage of cell 1 and its corresponding input, $I_{S_{cell1}}(t)$. Note the synchronization to its input. (b) The voltage of cell 2 and the input from cell 1, $I_{S_{cell1}}(t)$. Cell 2 is synchronized to cell 1 until $t = 500\ ms$, at which point it desynchronizes. At $t = 500\ ms$ the connection goes from strong to weak, and the applied sinusoidal current to cell 2 dominates.

6.3 An inhibitory synapse

Pyramidal neurons often receive input from inhibitory interneurons through a $GABA_A$ synapse. Over the years, it has been suggested that a lack of inhibitory input may initiate seizure generation, and thus is it important to include the interneuron-pyramidal neuron dynamic in our model. However, like Nadkarni and Jung (2005), we find that a lack of inhibitory input is not sufficent for seizure generation.

The $GABA_A$ synapse can be modeled in a very similar manner to the AMPA synapse. We represent the small inhibitory synaptic input from the surrounding interneurons by:

$$I_{GABA_1} = \bar{g}_{GABA_1} G_1 (V_{D_1} - V_{INH}) \tag{6.3}$$

where V_{D_1} is the voltage of the dendritic compartment of the postsynaptic cell, and

the equilibrium potential of the inhibitory synapse is given by $V_{INH} = -15\ mV$ (Traub et al., 1992; Nadkarni and Jung, 2005). The maximal conductance, $\bar{g}_{GABA_1}$ is set to be 0.1 mS/cm^2 in accordance with Nadkarni and Jung (2005). The gating variable, G_1, ideally depends on the voltage of the presyaptic interneuron. In order to avoid modeling this interneuron, we make the assumption that the channels are open at all times. Thus the gating variable is given by $G_1 = 1$, and inhibition in the postsynaptic cell is always present.

Using this model, we find that the influence of the inhibitory interneuron on the CA1 neuron is minimal. It inhibits the neuron by reducing the membrane potential, but its effects are insignificant. That is, we can reproduce all our results with only slight changes to the input values. We conclude that with our model, the inhibitory input is not sufficient to suppress epileptiform bursting, and a lack of this input is not sufficient to cause the bursting.

6.4 Discussion

The AMPA synapse is thought of as the primary method of synchronization between two cells. Although our model is relatively simple, it is a very commonly used representation of the AMPA synapse. Most importantly, it successfully reproduces the desired synchronization results: the two models are synchronized under strong coupling, and desynchronize under weak coupling. This is an essential property of the AMPA synapse, and is useful if a network model is to be produced. However, as always it is important to consider the dynamics one wishes to reproduce. For example, the release of neurotransmitters from the presynaptic cell and their diffusion across the synaptic cleft could be considered in more detail. The influence of an inhibitory interneuron was modeled through a $GABA_A$ synapse, and the effects of the synapse were minimal. This modeled synapse could be improved by including a model of an actual interneuron, rather than assuming that the synaptic channels were open at all times.

Chapter 7

An Astrocytic Influence

Now that we have discussed how two CA1 neurons communicate with each other, we focus our attention on synaptic input from other sources. In particular, we are concerned with the synaptic communication between a CA1 neuron and an astrocyte. In section 4.4 it is discussed in detail how Parpura and Haydon (2000) propose a link between the internal astrocytic calcium concentration (denoted $[Ca^{2+}]_{astro}$) and an inward synaptic current to neighbouring neurons. Tian et al. (2005) take this theory a step further by examining the particular synaptic connections involved. They note that subthreshold depolarizations, known as paroxysmal depolarization shifts (PDSs), occur in neurons when the levels of the internal astrocytic calcium are elevated (see section 4.3 for more details). These PDSs are directly associated with synchronized neuronal bursts, even when communication between the neurons is blocked (Parpura and Haydon, 2000). The theory is that these elevated calcium levels cause the astrocytes to release glutamate into the extracellular space. The glutamate activates a particular type of receptor known as N-methyl D-aspartate (NMDA) receptors on a neuron's dendrite, creating a slow inward current (SIC) into the cell (Parpura and Haydon, 2000). This results in a depolarization in the form of a PDS from the neurons. These PDSs, however, can be significantly reduced by applying a NMDA antagonist known as (2R)-amino-5-phosphonovaleric acid (APV) (Tian et al., 2005), singling out the NMDA synapse as crucial to astrocyte-neuron communication. Since this particular synapse plays such an important role in the communication between a neuron and an astrocyte, we will concentrate on modeling this dynamic.

7.1 The model

Modeling a NMDA synapse is slightly more complicated than modeling an AMPA synapse. This is because it does not depend only on a gating variable, S_1, and a maximal conductance $\bar{g}_{NMDA}$, but also on a voltage- and magnesium-dependent term. The NMDA receptors are blocked by magnesium until a particular membrane

voltage threshold is reached (Martin, 2003). Then the magnesium is released, and the receptor is free to activate. This synaptic current is modeled as

$$I_{NMDA} = \frac{\bar{g}_{NMDA} \times S_1 \times (V_D - V_{EXC})}{1 + 0.28 \times e^{-0.062 \times (V_D - 60)}} \tag{7.1}$$

where V_D and V_{EXC} are defined as in chapter 6, and the denominator represents the magnesium- and voltage-dependent dynamics measured empirically. For our purposes, we set the maximal conductance, $\bar{g}_{NMDA}$, to 0.0 mS/cm^2 (unless otherwise stated) and $V_{EXC} = 60\ mS/cm^2$ as before. We assume that the gating variable S_1 follows first order kinetics. Then, motivated by models for NMDA synapses between neurons, we represent S_1 in a new way:

$$\frac{dS_1}{dt} = \alpha_S f([Ca^{2+}]_{astro})(1 - S_1) - \beta_S S_1 \tag{7.2}$$

Thus S_1 opens with respect to the inverse time constant α_S and a function $f([Ca^{2+}]_{astro})$, which provides the link between the synaptic dynamics and the internal astrocytic calcium concentration, $[Ca^{2+}]_{astro}$. It closes with an inverse time constant β_S. The inverse time constants are given by:

$$\alpha_S = \frac{1}{\tau_{Srise}}, \qquad \beta_S = \frac{1}{\tau_{Sfall}} \tag{7.3}$$

where $\tau_{Srise} = 2\ ms$ and $\tau_{Sfall} = 150\ ms$ represent the fast rise and slow decay of the NMDA synaptic input (Traub et al., 1991).

To determine $f([Ca^{2+}]_{astro})$, we use experimental data which describes how $[Ca^{2+}]_{astro}$ affects the neuronal SIC. In particular, we examine a figure from Parpura and Haydon's paper (Parpura and Haydon, 2000, Fig. 5B). This figure shows how the estimated $[Ca^{2+}]_{astro}$ corresponds with the peak neuronal synaptic inward current when the membrane potential is held at $-60\ mV$. To use this data, we first convert the inward current unit of pA to our current per unit area of $\mu A/cm^2$. Parpura and Haydon (2000) do not specify the surface area of the neurons they used. However, they use hippocampal neurons in their study, and so we calculate the typical total surface area of the neuron model from Traub et al. (1991) — 38584 μm^2. In addition, Parpura and Haydon (2000) mention a key point: the resting level of internal astrocytic calcium is $[Ca^{2+}]_{astro} = 87\ nM$. We add this point to our graph, setting the synaptic inward current of the neuron to zero when the astrocyte is at rest. Thus we determine $f([Ca^{2+}]_{astro})$ by fitting the newly converted plot (Figure 7.1). The program 'Engauge' was used to plot the points accurately, and then MATLAB's 'lsqcurvefit' function was used to fit the curve.

Following Perkel et al. (1981), a sigmoid function of the form

$$g(V_{pre}) = 1/(1 + exp(-(V_{pre} - \theta_{syn})/2)$$

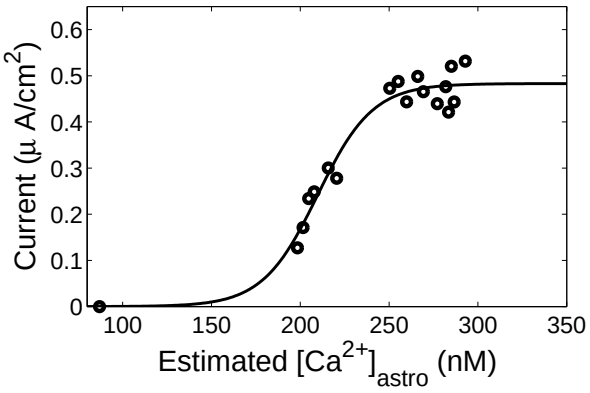

Figure 7.1: A plot of neuronal SICs vs. astrocytic calcium concentration (open circles), and a corresponding fit (solid line). The graph was taken from Parpura and Haydon (2000, Fig. 5B), and a conversion was made to change the inward current to units of $\mu A/cm^2$. The fit was made using MATLAB's "lsqcurvefit" function.

can be used to represent transmitter release, $g(V_{pre})$, based on the presynaptic voltage, V_{pre}. We use a similar method, normalizing $f([Ca^{2+}]_{astro})$ so our gating variable S_1 represents the fraction of open NMDA channels. Then the fit for this graph can be described as

$$f([Ca^{2+}]_{astro}) = \frac{1}{1 + k_1 \times e^{k_2 \times ([Ca^{2+}]_{astro} - k_3)}} \tag{7.4}$$

where $k_1 = 0.0009$, $k_2 = -0.0646$ and $k_3 = 318.5$. For our fit, the squared 2-norm of the residual is 0.0211, which is reasonable for our qualitative simulations.

7.2 The astrocytic calcium and results

We now know how to describe the NMDA synapse as a function of the internal astrocytic calcium concentration, $[Ca^{2+}]_{astro}$. In this section, the $[Ca^{2+}]_{astro}$ is described in a variety of ways, and the resulting simulations for each method are discussed. In these simulations, a maximal conductance of $\bar{g}_{NMDA} = 0.4\ mS/cm^2$ is used, unless otherwise stated. These values are taken indirectly from Traub et al. (1991), as they stated that no cell should have a greater NMDA conductance than 187.5 $nS/cell$ – which translates to 0.49 mS/cm^2 in our model. Although this value is for a CA3 cell, not a CA1 cell, it gives us an appropriate range with which we estimate our $\bar{g}_{NMDA}$. Unless otherwise stated, $\bar{g}_{AMPA} = 0.0\ mS/cm^2$. That is, we are studying a single CA1 cell with astrocytic input.

7.2.1 A step of astrocytic calcium

According to Parpura and Haydon (2000), the $[Ca^{2+}]_{astro}$ decays quite slowly as compared to the slow inward current (SIC) it produces. For simplicity, we begin by adding a single step of calcium, with a long duration (500 ms in the example below) to account for the slow decay. The amplitude of the step can vary to represent a large or small $[Ca^{2+}]_{astro}$, which results in a correspondingly large or small SIC. The Figure below (Figure 7.2) shows how a relatively large step of $[Ca^{2+}]_{astro}$ (250 nM), results in an activated neuron. However, once the $[Ca^{2+}]_{astro}$ returns to its resting value, the neuron immediately returns to rest.

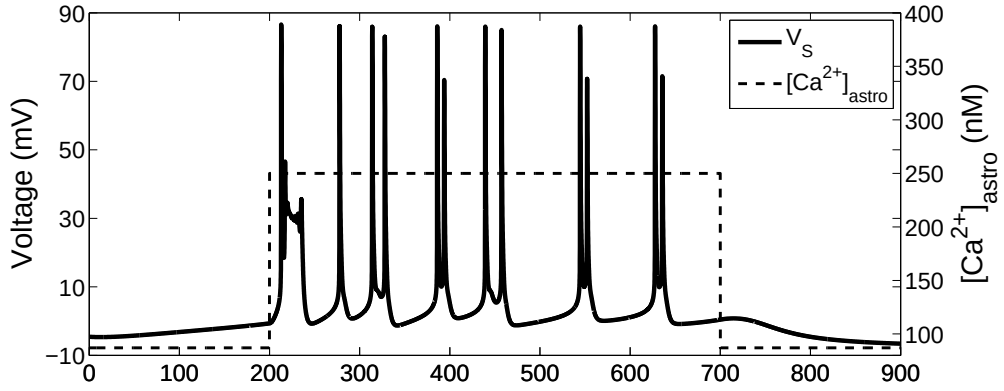

Figure 7.2: A step of $[Ca^{2+}]_{astro}$, 250 nM in amplitude, 500 ms in duration, results in an activated neuron during the step.

It can be shown that a smaller step of $[Ca^{2+}]_{astro}$ results in a smaller depolarization of the cell. However, before we do a detailed analysis of these dynamics, perhaps a better representation of the astrocytic calcium should be considered.

7.2.2 A wave of astrocytic calcium

Tian et al. (2005) give experimental evidence for astrocytic intracellular calcium oscillations. It may be beneficial to examine our neuron model under an such an oscillatory influence. Although the astrocytic waves in theory have very large period (the decay of calcium is extremely slow), we first examine the neuron under a smaller period. This allows us to see the synchronization of the neuron model to the calcium waves, and leads us to consider the synchronization of two CA1 neuron models. First, we consider a single neuron with an astrocytic input, where the $[Ca^{2+}]_{astro}$ is represented by:

$$A \times \sin^2\left(\frac{2\pi t}{T}\right) + 87$$

where $A = 213\ nM$, $T = 280\ ms$ which oscillates between the resting value of

$[Ca^{2+}]_{astro} = 87\ nM$ and $300\ nM$ (Figure 7.3(a)). It is evident that the neuron spikes in synchrony with the calcium oscillations. Then if we consider the neuron to be coupled to a second neuron through an AMPA synapse (see chapter 6), the second neuron will also synchronize with the astrocytic calcium waves (Figure 7.3(b)).

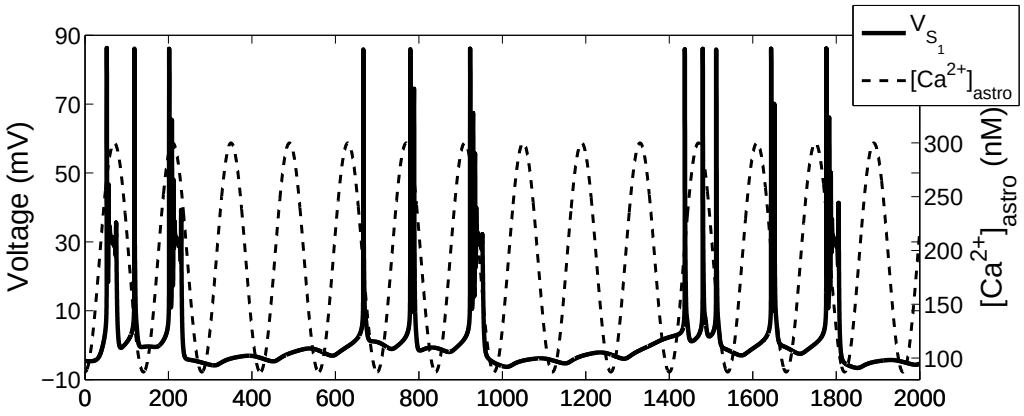

(a) Neuron 1 with astrocytic input. The wave of astrocytic intracellular calcium is represented by the dotted line, V_{S_1} by the solid line.

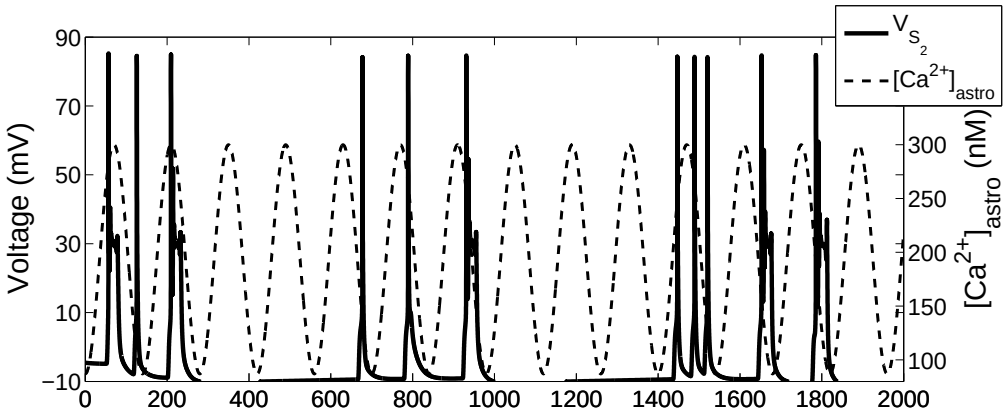

(b) Neuron 2 with AMPA input from neuron 1. The second neuron synchronizes with the astrocytic calcium wave involved in the input to neuron 1.

Figure 7.3: The influence of a wave of $[Ca^{2+}]_{astro}$ on two neurons. In these simulations, $\bar{g}_{NMDA_1} = 0.4\ mS/cm^2$, $\bar{g}_{NMDA_2} = 0.0\ mS/cm^2$, $\bar{g}_{AMPA_1} = 0.0\ mS/cm^2$, and $\bar{g}_{AMPA_2} = 0.2\ mS/cm^2$.

Although an interesting case, this representation of the calcium as a wave may not be entirely realistic. The calcium wave is shown by Parpura and Haydon (2000) to decay exponentially, and at a much slower rate. To create a better model, we turn once again to Parpura and Haydon (2000).

7.2.3 A pulse of astrocytic calcium

Recall (from section 4.4) that Parpura and Haydon (2000) used a particular fluorescence (fluo-3) to identify the amount of internal astrocytic calcium released. Then $[Ca^{2+}]_{astro}$ is expressed in terms of the percentage increase in the fluorescence and of the resting internal calcium level of 87 nM. Using the resting calcium concentration of 87 nM, the resting level of fluo-3 was identified as F_0, and the change in fluo-3 as ΔF. Then, from Parpura and Haydon (2000):

$$[Ca^{2+}]_{astro} = 87 \times e^{0.94 \times \Delta F/F_0} \tag{7.5}$$

where $\Delta F/F_0$ is the percentage increase in fluorescence. To identify $\Delta F/F_0$ we turn to another graph provided by Parpura and Haydon (2000), shown in Figure 7.4.

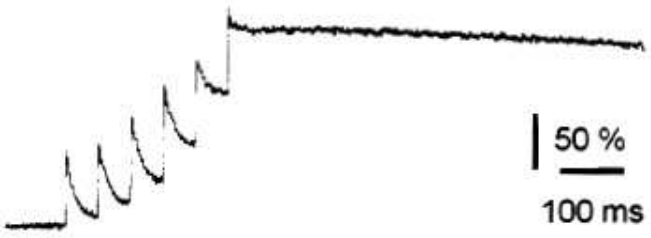

Figure 7.4: Parpura and Haydon (2000, Fig. 2E). A plot of the percentage increase in fluorescence (fluo-3) vs. time (in ms). The increase in the $[Ca^{2+}]_{astro}$ can be expressed using Equation (7.5)

The amount of fluorescence degrades at different rates depending on the initial pulse. In most of the experiments, Parpura and Haydon (2000) gave six consecutive pulses to step the calcium concentration up to an appropriate level. So we examine Figure 7.4 from Parpura and Haydon (2000), but consider a single large pulse and only the final slow degradation. Then we express $\Delta F/F_0$ as:

$$\Delta F/F_0 = pulse \times e^{-k_4(t-t_0)}$$

where $k_4 = 0.0002$ was determined by fitting the degradation of the last pulse in Figure 7.4. The time when the pulse is given is denoted by t_0. Now $[Ca^{2+}]_{astro}$ is expressed as a function of time, giving the NMDA gating variable S_1 as a function of time.

7.2.4 Results with a pulse of astrocytic calcium

By implementing the expression for $[Ca^{2+}]_{astro}$ as a slowly decaying exponential into our model, simulations that correspond with Parpura and Haydon's (2000)

experimental findings are produced. It is evident from Figure 7.5 that increased levels of $[Ca^{2+}]_{astro}$ produce increased neuronal depolarization.

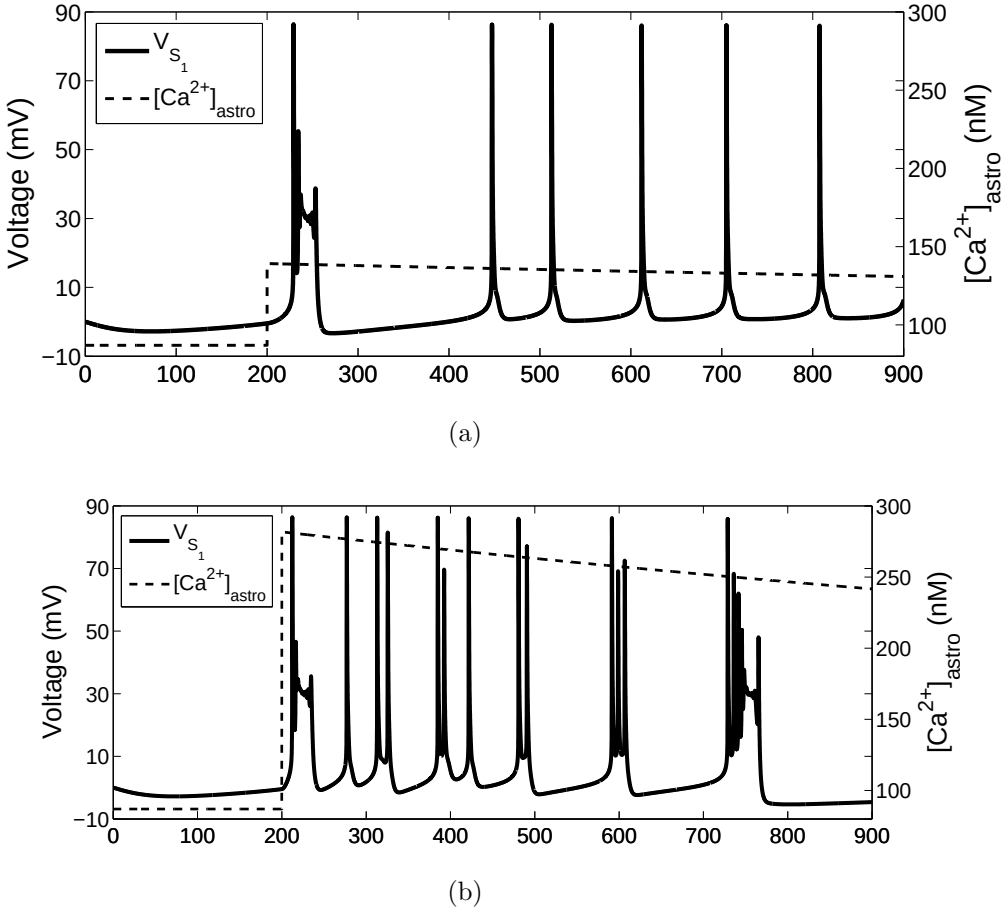

(a)

(b)

Figure 7.5: Different pulses of $[Ca^{2+}]_{astro}$ produces different levels of neuronal depolarization. (a)A weak pulse of $[Ca^{2+}]_{astro}$ produces a weak response from the neighbouring neuron. We use $pulse = 0.5$, which implies the initial $[Ca^{2+}]_{astro}$ is approximately 139 nM. (b) A strong pulse of $[Ca^{2+}]_{astro}$ produces a strong response from the neighbouring neuron. We use $pulse = 1.25$, which implies the initial $[Ca^{2+}]_{astro}$ is approximately 282 nM. In both simulations we use $\bar{g}_{NMDA_1} = 0.4\ mS/cm^2$.

Parpura and Haydon showed that when a pulse of light released $[Ca^{2+}]_{astro}$, a neighbouring neuron obtained a SIC (Parpura and Haydon, 2000, Fig. 3C). In their experiment, the voltage was clamped at its resting value of $-60\ mV$ (Parpura and Haydon, 2000). In our model, since we have normalized the voltage, we fixed V_S and V_D to 0 mV. We attempted to reproduce the SIC that Parpura and Haydon (2000) found resulted from a pulse of $[Ca^{2+}]_{astro}$. To do so, we considered three separate cases. First, we took a peak astrocytic calcium value directly from Figure 7.1. Using $\bar{g}_{NMDA_1} = 0.11\ mS/cm^2$ and $pulse = 0.965$, which implied the initial calcium level of $[Ca^{2+}]_{astro} = 215.5\ nM$, we obtained the SIC in Figure 7.6. This SIC had an appropriate peak magnitude, based on value given in Figure 7.1, and shape, based

on the shape of the SIC in Parpura and Haydon (2000, Fig. 3C). We note that the peak SIC value was not the exact value of the point taken from Figure 7.1, since we used the fit of these points to represent the gating variable, S_1, and not the inward current itself.

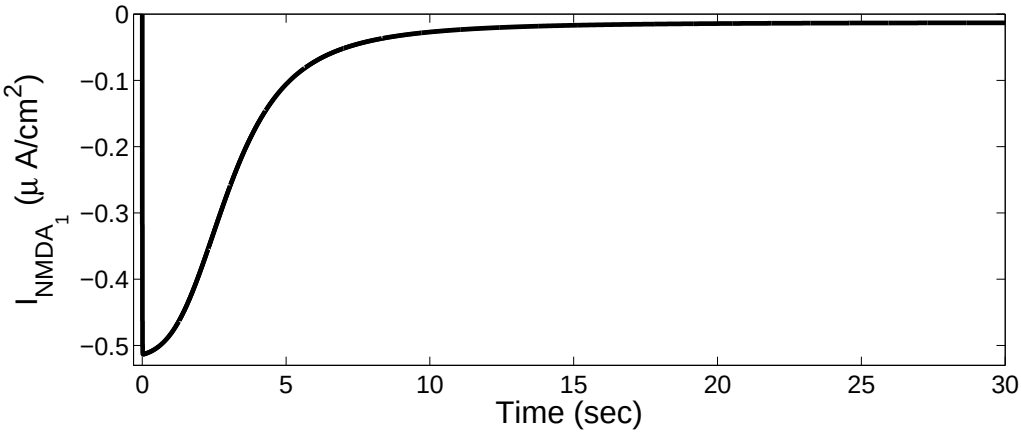

Figure 7.6: Using $pulse = 0.965$, a pulse of $[Ca^{2+}]_{astro}$ with peak 215.5 nM produced a SIC. With $\bar{g}_{NMDA_1} = 0.11\ mS/cm^2$, the SIC had a peak of $-0.514\ \mu A/cm^2$. The resulting peak amplitude of the SIC corresponded closely with that of Parpura and Haydon's Fig. 5B (2000). The shape of the SIC was in agreement with the SIC found in Fig. 3C from Parpura and Haydon (2000).

Second, Parpura and Haydon (2000) stated that an initial astrocytic calcium pulse of $140 \pm 15\ nM$ produced a neuronal SIC with a peak of $-391 \pm 139\ pA$ (which was equivalent to $-1.01 \pm 0.36\ \mu A/cm^2$). To reproduce this finding, we used a small pulse ($pulse = 0.5$) to release 139 nM of $[Ca^{2+}]_{astro}$. Figure 7.7(a) shows that this pulse resulted in a neuronal SIC with the appropriate shape, but with a peak of $-0.19\ \mu A/cm^2$, which was well below the desired range. This occurred because the point given by Parpura and Haydon (2000) did not fall near the fit curve in Figure 7.1: compared to the rest of the points, the given SIC was very large for the magnitude of the calcium pulse. We noted that Figure 7.1 was created by elevating the astrocytic calcium levels in three separate tests. Perhaps the magnitude of the SIC peak was higher in this test because of the particular astrocyte used. Obviously, more information about the astrocytic calcium-SIC relationship, preferably using a larger number of cells, would be helpful to improve our model. In the meantime, we were able to reproduce the desired results by considering a larger maximal conductance, $\bar{g}_{NMDA_1} = 0.5\ mS/cm^2$ (Figure 7.7(b)).

Third, Parpura and Haydon (2000) found that an initial astrocytic calcium pulse of $549 \pm 118.64\ nM$ produced a neuronal SIC with a peak of $-475 \pm 128\ pA$ (which is equivalent to $-1.23 \pm 0.332\ \mu A/cm^2$). To simulate the release of 549 nM of $[Ca^{2+}]_{astro}$, we used $pulse = 1.96$. The resulting SIC is shown in Figure 7.8(a). Both the amplitude of the peak and the shape of the SIC were inconsistent with Parpura and Haydon's Fig. 3C (2000). As in the previous case, the magnitude of

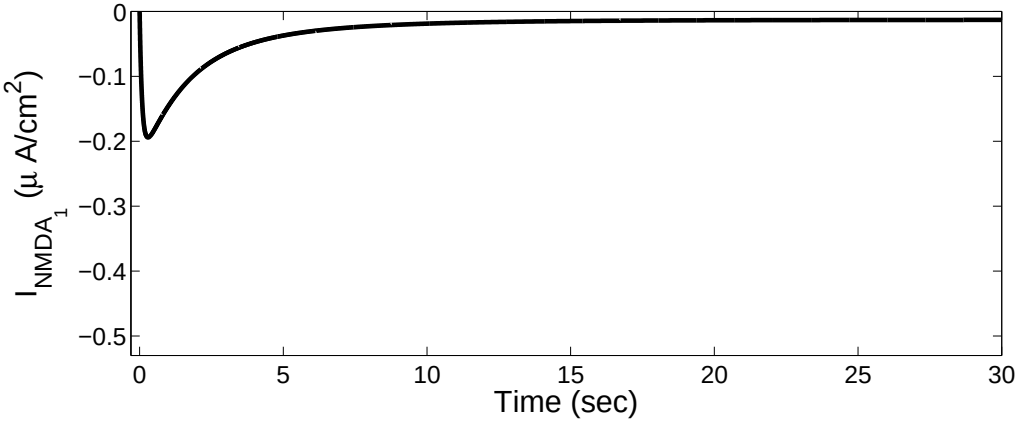

(a)

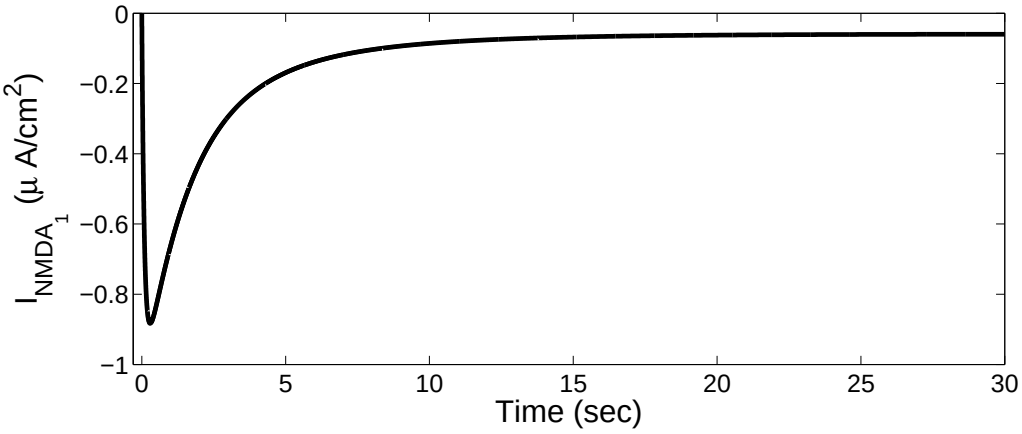

(b)

Figure 7.7: Using $pulse = 0.5$, a pulse of $[Ca^{2+}]_{astro}$ with peak 139 nM enduced a SIC. a) Using $\bar{g}_{NMDA_1} = 0.11\ mS/cm^2$, the SIC had a peak at $-0.19\ \mu A/cm^2$, which was well below the desired range of $-1.01 \pm 0.36\ \mu A/cm^2$. The shape of the SIC was consistent with Parpura and Haydon's (2000) findings in their Fig. 3C. b) The peak amplitude of the SIC could be adjusted to fall within the range given by Parpura and Haydon's (2000) by increasing the maximal NMDA conductance ($\bar{g}_{NMDA_1} = 0.5\ mS/cm^2$). With this new value, the SIC reaches a peak of $-0.88\ \mu A/cm^2$.

the peak current was too small. Again, this may have been due to the particular astrocyte or neuron used for the experiment. The maximal NMDA conductance was increased to $\bar{g}_{NMDA_1} = 0.25\ mS/cm^2$ to adjust the peak value into the appropriate range (Figure 7.8(b)). However, our SIC "peak" was still too flat, due to our lack of information about the astrocytic calcium-SIC relationship for large calcium levels. Recall that Figure 7.1 did not give any information about neuronal inward currents for astrocytic calcium levels above 300 nM. Since we fit Parpura and Haydon's Fig. 5B (2000) with a sigmoid function, any calcium pulse with a peak beyond 300 nM resulted in a SIC with a set maximal value ($-0.52\ \mu A/cm^2$ when $\bar{g}_{NMDA_1} = 0.11\ mS/cm^2$). This maximal SIC value was maintained until the astrocytic calcium level dropped below a particular value (approximately 250 nM), resulting in a plateau shaped "peak". Parpura and Haydon (2000) also stated that when the astrocytes were removed, the same pulse of light did not enduce a response from the neuron. The pulse of light was directly associated with the pulse of $[Ca^{2+}]_{astro}$ in our model, thus when the connection between the astrocyte and the neuron was cut ($\bar{g}_{NMDA_1} = 0.0\ mS/cm^2$), it was obvious that the neuron model did not have any activity.

We were able to reproduce another experimental finding from Parpura and Haydon (2000, Fig. 5A). Parpura and Haydon applied a series of pulses of light to release $[Ca^{2+}]_{astro}$, and measured the corresponding neuronal SIC over time. Since the data was from a single experiment (and not an average over multiple trials), some alterations in our variables were required to reproduce the result. Specifically, in the fit made for Figure 7.1 in Equation 7.4, the variable k_2 was adjusted from -0.0447 to -0.065. Then, using $\bar{g}_{NMDA_1} = 0.11\ mS/cm^2$, the SIC and $[Ca^{2+}]_{astro}$ can be seen as a function of time in Figure 7.9.

Thus we have found that it is reasonable to model $[Ca^{2+}]_{astro}$ as a pulse of calcium, decaying slowly and exponentially over time. The larger the pulse, the larger the neighbouring neuron's depolarization. As in experimental trials (Parpura and Haydon, 2000), once voltage-clamped, the slow inward current resulting from an astrocytic rise in calcium is reproduced with our model (Figure 7.6, 7.7, 7.8). Similarily, if the astrocytic input is cut off, it is obvious that our model will not produce the same neuronal SICs, in correspondence with Parpura and Haydon's experimental data. The characteristic fast rise and slow decay of the NMDA current is captured, and the experimental data of Parpura and Haydon (2000, Fig. 5A) is reproduced by our model in Figure 7.9. Thus it seems that we accurately model Parpura and Haydon's (2000) empirical findings with our representation of the astrocytic input to a CA1 neuron.

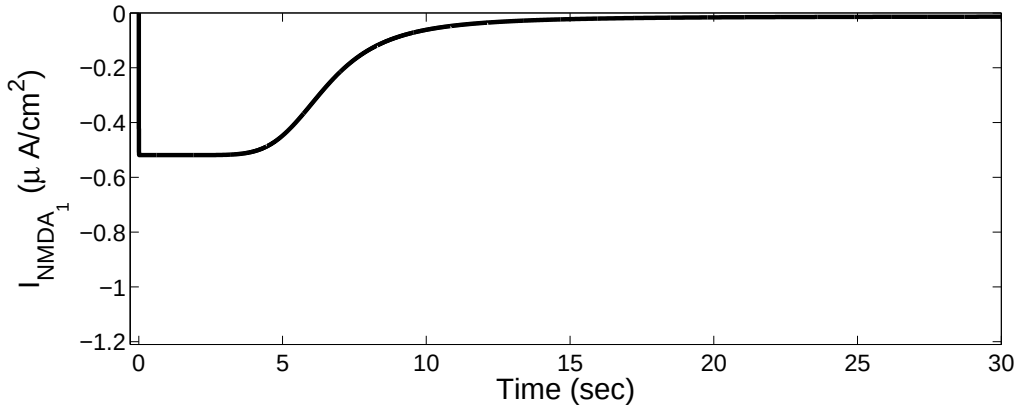

(a)

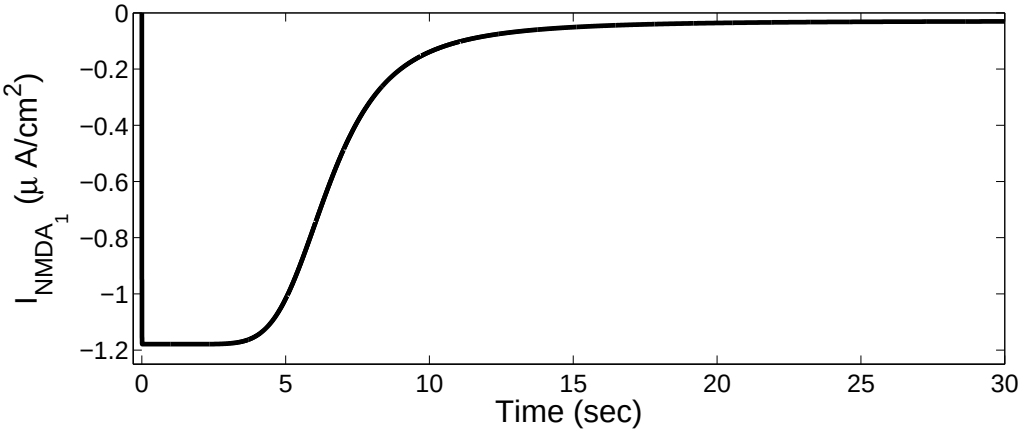

(b)

Figure 7.8: Using $pulse = 1.96$, a pulse of $[Ca^{2+}]_{astro}$ with peak 549 nM enduced a SIC. a) Using $\bar{g}_{NMDA_1} = 0.11\ mS/cm^2$, a SIC was produced with a peak of $-0.52\ \mu A/cm^2$, which was well below the desired range of $-1.23 \pm 0.332\ \mu A/cm^2$. b) The peak amplitude of the SIC could be adjusted to fall within the range given by Parpura and Haydon's (2000) by increasing the maximal NMDA conductance ($\bar{g}_{NMDA_1} = 0.25\ mS/cm^2$). With this new value, the SIC reached a peak of $-1.18\ \mu A/cm^2$. The shape of the peak of the SIC was inconsistent with the shape shown in Parpura and Haydon's Fig. 3C (2000).

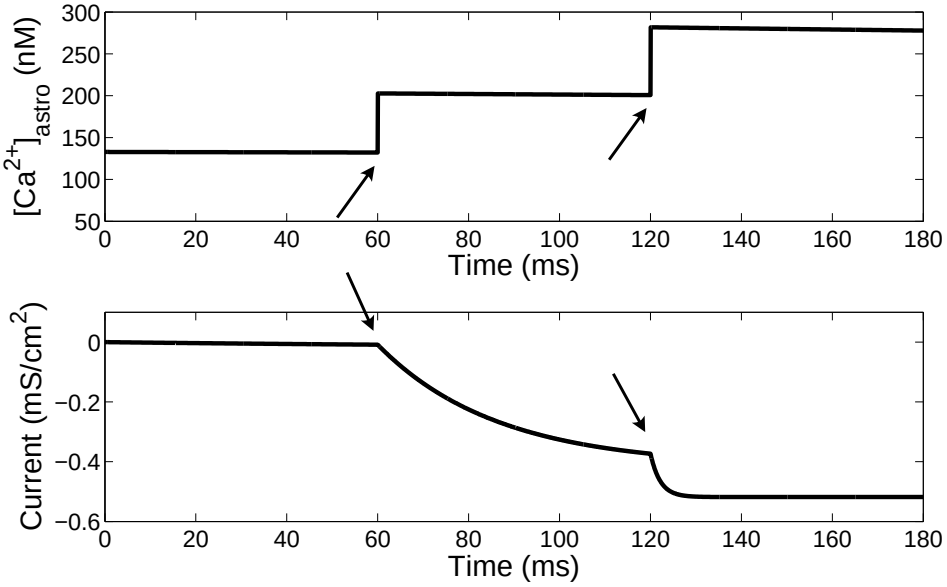

Figure 7.9: Our model reproduces the experimental result of Parpura and Haydon (2000, Fig. 5A). The parameter $k_2 = -0.065$ instead of its usual value of -0.0447, and $\bar{g}_{NMDA_1} = 0.11\ mS/cm^2$. These values are within a reasonable range of the parameters, and were chosen to fit Parpura and Haydon's experimental data. Arrows indicate when the pulse of $[Ca^{2+}]_{astro}$ occurred (at 60 and 120 ms). The voltage is clamped at 0 mV, and the SIC results from these pulses.

7.2.5 All-or-none astrocytes

We consider Parpura and Haydon's (2000) "all-or-none" astrocytes. These are astrocytes which either produce large SICs to the neighbouring neurons, or produce no signal at all. The corresponding plot from Parpura and Haydon (2000), with converted units from pA to $\mu A/cm^2$, was reproduced with "Engauge" and is shown in Figure 7.10. A notable quality of our NMDA synapse model its ability to adapt to different types of astrocytes: with a change in parameters, the data for these special astrocytic responses can be fit with our function $f([Ca^{2+}]_{astro})$ (given by Equation (7.4)). The implications of this are discussed in section 7.4.

7.3 NMDA receptors mediate depolarization shifts

Tian et al. (2005) state that glutamate (a neurotransmitter) released from astrocytes mediates the paroxysmal depolarization shifts (PDS) found in neurons. These PDSs are related to epileptiform activity, and are found in electroencephalogram (EEG) readings between seizures (Tian et al., 2005). Tian et al. perform a series of experiment to show that the signals producing the PDSs originate from astrocytes, and are mostly received by the neuron through the NMDA synapse. Tian et al.'s

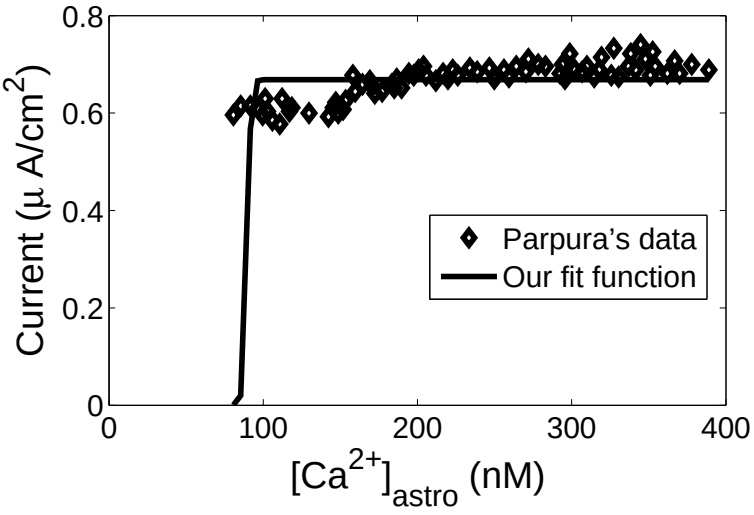

Figure 7.10: A reproduction of the "all-or-none" astrocytic response from Parpura and Haydon (2000, Fig. 5B), and its corresponding fit using $f([Ca^{2+}]_{astro})$ (Equation 7.4).

theories are commented on briefly in this section, but more details can be found in section 4.3.

In one particular experiment, Tian et al. (2005) show that synaptic activity among neurons is not required for PDSs. Epileptiform bursting activity was evoked in CA1 neurons by the application of a convulsant known as 4-aminopyridine (4-AP), a potassium channel blocker. Then a bath of tetrodotoxin (TTX), a sodium channel blocker, was applied. This caused the suppression of most neuronal activity. Surprisingly, the PDSs were largely resistant to the TTX. To confirm that neuronal synaptic activity had been inhibited, a variety of voltage-gated calcium channel blockers (VGCC blockers) were administered. Although communication among the neurons was suppressed, subthreshold ($< 40mV$) PDSs were still present. Using our model of a single neuron with I_{NMDA} from the synapse (with a pulse of $[Ca^{2+}]_{astro}$), we successfully reproduced these experimental findings (Figure 7.11) by simulating the events and comparing our results with Tian et al. (2005, Figure 1). To reproduce the channel blockers, the conductances of the individual channels were reduced. Certain parameters were more sensitive than others, and the amount of reduction varied to reproduce the empirical data. To simulate a potassium blocker, the conductances were altered as follows: $\bar{g}_{K-DR}$ was reduced from 17 mS/cm^2 to 15 mS/cm^2, $\bar{g}_{K-C,S}$ was reduced from 15 mS/cm^2 to 12 mS/cm^2, $\bar{g}_{K-C,D}$ was reduced from 5 mS/cm^2 to 4.6 mS/cm^2, and $\bar{g}_{K-AHP}$ was reduced from 0.8 mS/cm^2 to 0.6 mS/cm^2. For a sodium blocker, $\bar{g}_{Na}$ was reduced from 30 mS/cm^2 to 3 mS/cm^2, and for calcium blockers, $\bar{g}_{Ca,S}$ was reduced from 6 mS/cm^2 to 5.5 mS/cm^2 and $\bar{g}_{Ca,D}$ was reduced from 5 mS/cm^2 to 4.8 mS/cm^2. Unfortunately there is no literature on how to model blocked currents, and too large of a decrease in the conductances values caused the model to lose its behaviour.

Thus, in order to simulate the blockers, the conductances were diminished as much as possible without losing their qualitative relevance.

Although communication between the CA1 neurons has been cut off, through a series of channel blockers, most of the PDSs still exist. Surprisingly, Tian et al. (2005) noticed that these depolarizations are in fact synchronized! How do they synchronize when they are not sending synaptic signals to each other? There must be a connection between these neurons. The theory is that the neighbouring astrocytes serve as such a connection (Tian et al., 2005). In our next simulation, we consider two CA1 neuron models. These two cells both receive input through their respective NMDA synapses, representing the input from an astrocyte. One can easily argue that a pulse of $[Ca^{2+}_{astro}]$ will produce our desired simulation, yet it is simply easier to see the synchronization between the neuron models when a wave is used. We show that these neurons (and their PDSs) synchronize, even when the direct communication between them is cut off (Figure 7.12). In our model, the communication between the neurons can be cut off in two ways. First, the AMPA conductance, $\bar{g}_{AMPA}$, can be set to zero. Although one cell may produce a signal, the second can not receive it. Thus the only input to the two cells is through the NMDA channels, and although the cells are not identical, they will synchronize. This synchronization may be less obvious because of the differences in the cells dynamics, but the next method will make it more evident. In this method, the AMPA conductance may remain the same, but channel blockers are applied to prevent the neurons from sending a signal. The synchronization becomes more obvious when examining the PDSs. Both of these cases are shown in Figure 7.12. In this simulation, it is appropriate to model our $[Ca^{2+}_{astro}]$ as a wave (see section 7.2.2).

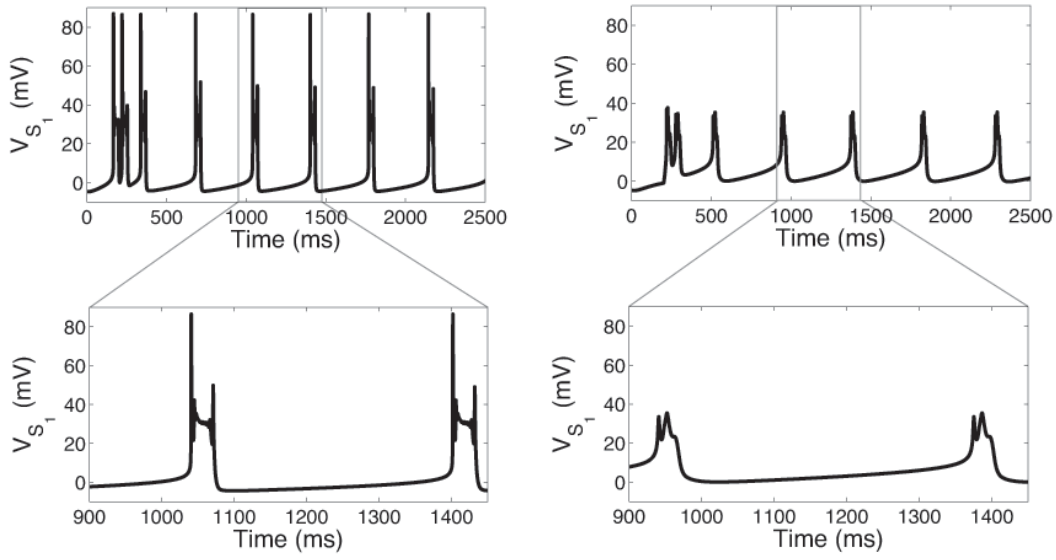

(a) (b)

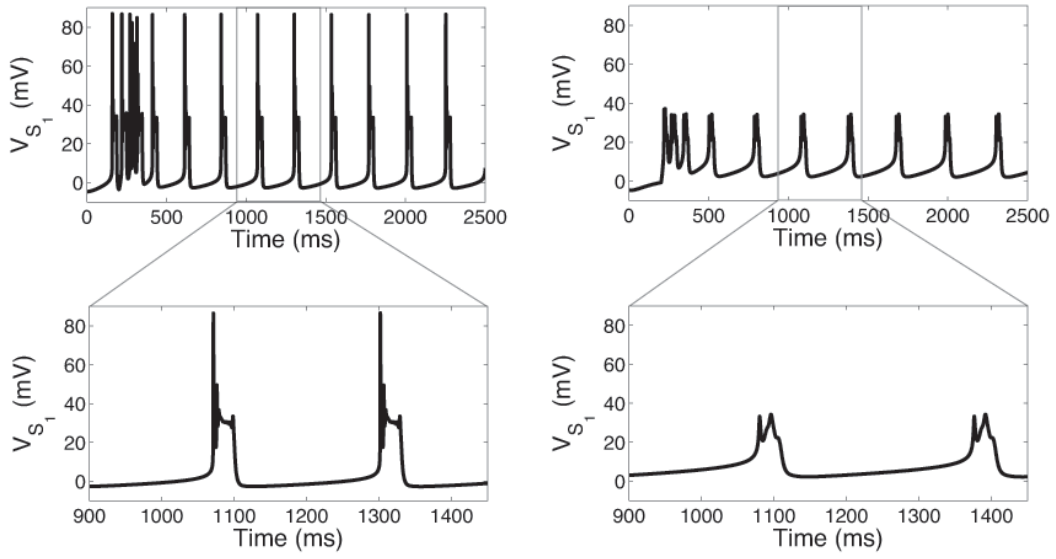

(c) (d)

Figure 7.11: Our model reproduces the experimental results of Tian et al. (2005, Figure 1): synaptic activity among neurons is not required for PDSs. We use $\bar{g}_{NMDA_1} = 0.4\ mS/cm^2$, and an astrocytic calcium pulse of $pulse = 1.25$. Each inset shows the behaviour over a smaller time window (550 ms). (a) An application of a potassium blocker, 4-AP, causes epileptiform bursting activity. A reduction of the potassium conductances replicates this finding. $\bar{g}_{K-DR} = 15\ mS/cm^2$, $\bar{g}_{K-C,S} = 12\ mS/cm^2$, $\bar{g}_{K-C,D} = 4.6\ mS/cm^2$, and $\bar{g}_{K-AHP,S} = \bar{g}_{K-AHP,d} = 0.6\ mS/cm^2$.(b) TTX, a sodium blocker ($\bar{g}_{Na} = 3\ mS/cm^2$), is added to the 4-AP (by reducing the conductances) and small subthreshold depolarizations (the PDSs) are prevalent. (c) 4-AP and calcium blockers ($\bar{g}_{Ca,S} = 5.5\ mS/cm^2$ and $\bar{g}_{Ca,D} = 4.8\ mS/cm^2$), VGCC blockers, are applied. Bursting activity still exists. (d) 4-AP, VGCC blockers and TTX are applied, and yet the PDSs are not supressed.

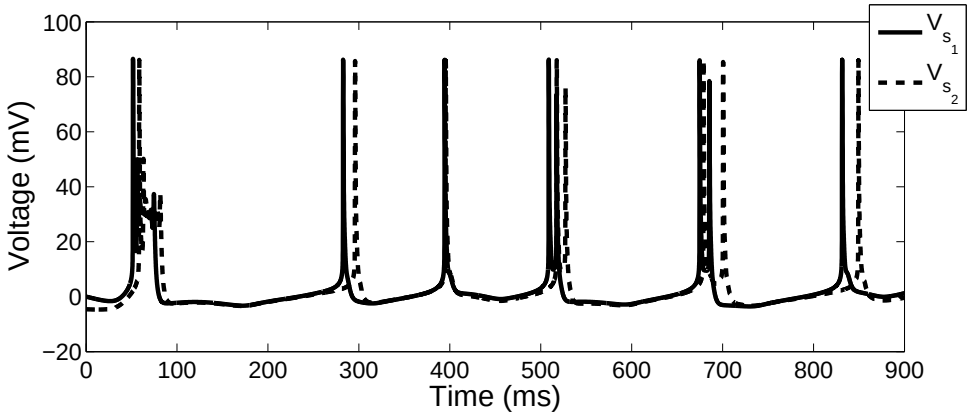

(a)

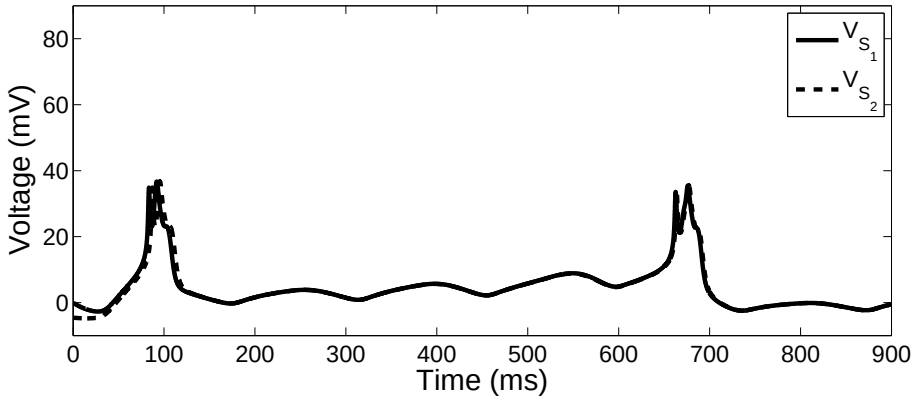

(b)

Figure 7.12: Simulations reproducing results found by Tian et al. (2005). A wave of intracellular astrocytic calcium, $[Ca^{2+}]_{astro}$, is used (as in section 7.2.2). (a) No AMPA input ($\bar{g}_{AMPA} = 0.0\ mS/cm^2$). The two cells, with slightly different dynamics, synchronize to the NMDA input. Here, $\bar{g}_{NMDA_1} = \bar{g}_{NMDA_2} = 0.3\ mS/cm^2$. (b) The cells can communicate through the AMPA synapse, as $\bar{g}_{AMPA_1} = \bar{g}_{AMPA_2} = 0.2\ mS/cm^2$. Potassium, sodium and calcium blockers are applied as in Figure 7.11, making the PDSs evident. The synchrony is obvious, as the signals from the two cells are difficult to distinguish. Since the PDSs are subthreshold ($< 40\ mV$), the AMPA synapses are not activated, and the cells do not communicate. Note that the simulation can be done with $\bar{g}_{AMPA_1} = \bar{g}_{AMPA_2} = 0.0\ mS/cm^2$ and the same results will ensue.

7.4 Physiological relevance and limitations

What does our NMDA synapse model mean physiologically? We model the correlation between the intracellular astrocytic calcium concentration, and the glutamate (a neurotransmitter) released from the astrocyte. We do so by directly relating the $[Ca^{2+}]_{astro}$ to the voltage and inward synaptic currents of the neighbouring neurons, which, according to Parpura and Haydon (2000), is physiologically affected by the glutamate release from the astrocytes. For this to be a justifiable model, we imply that this concentration of glutamate activating the neuron's synaptic current is related to the concentration of $[Ca^{2+}]_{astro}$, and this relationship is determined by fitting the plot of SIC vs. $[Ca^{2+}]_{astro}$ (Figure 7.4). This implies that the "all-or-none" astrocytes discussed previously (section 7.2.5) release glutamate in a steeply graded (or step) response. Thus we suggest that the difference between the two types of astrocytes lies in the amount of glutamate released for low intracellular calcium levels. If the "all-or-none" astrocytes release high levels of glutamate for any elevation in the cytosolic calcium concentration (above rest), then these high levels of glutamate in the extracellular space would result in large neuronal SICs. It seems that the all-or-none responses are not due to a change in the number of binding sites for glutamate on the neuronal membrane. If the number of glutamate binding sites were reduced, they would become saturated for low levels of extracellular glutamate, and the all-or-none threshold behaviour would be exhibited. However, the SICs would result from low levels of glutamate, and therefore we would expect that the amplitude of these currents would be decreased. This is not the case, as the amplitude of these SICs is higher than the amplitude of the SICs due to graded astrocytes. If the number of glutamate binding sites were increased, we would not expect to see the threshold behaviour of the "all-or-none" astrocytes, but instead a graded response. Thus, this analysis suggests that the step response of the "all-or-none" astrocytes is due to a large release of glutamate for any intracellular astrocytic calcium elevation.

We consider the possible astrocytic pathologies which could trigger epileptiform bursting activity. For example, an excess of metabotropic glutamate receptors (mGluRs) found on the extracellular surface of an astrocyte may "interpret" a small signal from a neighbouring CA1 neuron as a much larger signal. This would create an abnormal increase in $[Ca^{2+}]_{astro}$ for the size of the neuronal signal, resulting in an equally abnormally large glutamate release from the astrocyte, and hence excessive neuronal bursting. Similarily, an excess of binding sites for intracellular calcium may result an excessive amount of glutamate to be released from the astrocyte. Again this may result in epileptiform neuronal bursting. Since we do not consider the astrocytic mGluRs, the IP3 dynamics, nor astrocytic glutamate release in our model, we can not directly examine these possibilities. A more detailed description of the astrocytic response would be helpful to distinguish between these pathology possibilities. However, we can represent these potential pathologies in a qualitative and general way, by adjusting the function $f([Ca^{2+}]_{astro})$ such that low levels of $[Ca^{2+}]_{astro}$ lead to large SICs.

The limitation of this model lies in its simplicity. The relationship between the $[Ca^{2+}]_{astro}$ and the glutamate release is unmistakably more complicated than we have modeled. Improvements can be made by modeling the astrocytic response to glutamate in more detail. The dynamics of the postysnaptic receptor or the dynamics of the synapse itself may require more attention for particular problems. However, for our purpose, the model has accurately produced the desired results. A benefit of such a simple model is that it can be easily improved: the astrocytic input to the NMDA synapse may be replaced with a model of an actual astrocyte. Thus the model is flexible enough such that it can be adjusted to answer a variety of questions.

7.5 Discussion

The synaptic communication between a CA1 neuron and an astrocyte has been modeled through an NMDA synapse, following Tian et al. (2005). The voltage- and magnesium-dependence was modeled, as well as the link between the intracellular astrocytic calcium concentration ($[Ca^{2+}_{astro}]$) and the slow inward synaptic current (SIC) to neighbouring neurons. The $[Ca^{2+}_{astro}]$ was examined as a step, a wave, and an exponentially decaying pulse. Although there is evidence (Tian et al., 2005) that the $[Ca^{2+}_{astro}]$ occurs in oscillations, Parpura and Haydon (2000) showed that when administering a pulse of light to release this astrocytic calcium, the calcium decayed slowly and exponentially in time. Thus either representation of the $[Ca^{2+}_{astro}]$ is reasonable, depending on the question at hand. The physiological relevance of the model was discussed and predictions about the source of "all-or-none" astrocytes were made. Some limitations of the model were discussed, and recommendations were made to improve the model. A number of experiments from Parpura and Haydon (2000) and Tian et al. (2005) were reproduced, bringing light to the value of the model in a qualitative sense.

Chapter 8

Conclusion

Temporal Lobe Epilepsy (TLE) is a disease which affects millions of people worldwide, and it is characterized by recurrent and unprovoked seizures (World Health Organization, 2001). The hippocampus is often the focus of mesial temporal lobe seizures, and damage to this region may result in learning and memory defiencies. A particular type of neuron, found in the hippocampal CA1 region of the brain, is known to easily produce excessive and synchronous neuronal discharges (Tian et al., 2005), and thus is often the focus of epileptiform bursting studies. However, researchers have recently become more interested in the role of astrocytes, as they have been found to modulate the behaviour of neighbouring neurons (Tian et al., 2005). Tian et al. (2005) propose that during epileptiform bursting, calcium signalling from astrocytes leads to paroxysmal depolarization shifts (PDSs) in nearby neurons. According to them, these depolarizations are actually the root of the epileptiform bursts, as opposed to the neuronal discharges themselves. Thus they suggest that pathologies in astrocytes, not neurons, are responsible for seizure generation. They propose that anti-epileptic drugs should be made to focus on the astrocytic calcium signalling, which may stop the excessive bursting without obstructing neuronal transmission (Tian et al., 2005). To better understand this calcium signalling, we consider research done by Parpura and Haydon (2000), which suggests that the intracellular astrocytic calcium fluctuations may play a physiological role in neuron modulation.

Traub et al. (1991) produced a 19-compartment model of a pyramidal neuron, which accurately reproduces characteristic qualities of the neuron's structure and function. However, it would be helpful to have a reduced model which maintains a realistic representation of the cell's mechanics, while being simple enough to permit a detailed analysis of the key parameters. The reduced complexity and computational demand of the model allows us to focus on properly representing the synaptic currents. In particular, we aim to model the relationship between the astrocytic intracellular calcium concentration and the PDSs, as described by (Tian et al., 2005).

Using the conductance densities from Traub et al. (1991) as a starting point, we

reduced the Traub model and created a two-compartment model of a CA1 neuron. This mathematical model represents the membrane potential, ionic, applied and synaptic currents as well as the coupling between compartments. Five active ionic currents were considered: a sodium current (I_{Na}), three types of potassium currents (I_{K-DR}, I_{K-C},and I_{K-AHP}) and a calcium current (I_{Ca}). Since I_{K-C} is both a voltage and calcium dependent current, and the I_{K-AHP} is a slow calcium dependent current, the intracellular calcium concentration needed to be represented. It was modeled as a function of the inward calcium current, in accordance with Traub et al. (1991). Like Pinsky and Rinzel (1994), we identified two types of synaptic currents, I_{AMPA} and I_{NMDA}. The AMPA current was primarily responsible for the synchronization of the neurons, while the NMDA current (a magnesium and voltage-dependent current) represented the astrocytic input. We introduced a new way to model an NMDA current, representing the rate of activation of the NMDA gating variable, S_1, as proportional to a function of the cytosolic astrocytic calcium levels. This function was fit to experimental data provided by Parpura and Haydon (2000), showing the slow inward current (SIC) of the neuron with respect to the intracellular astrocytic calcium concentration. This calcium concentration was examined as a step, a wave, and an exponentially decaying pulse.

The model exhibits the characteristic behaviour of a CA1 neuron, as identified by Traub et al. (1991). That is, when the soma or proximal dendrites are stimulated with a current less than 1 nA ($I_S < 1\ nA$), a train of action potentials is exhibited. However, if the same current stimulates the distal dendrites ($I_D < 1\ nA$), a full dendritic calcium spike with somatic burst is produced, followed by low frequency action potentials. The bursting mechanisms were analyzed in detail, and the slow variables q and $[Ca^{2+}]$ were shown to influence the generation of a burst and the length of the interspike interval. We found that the coupling parameters (g_C and p), as well as the dynamics between the inward dendritic calcium current and the two outward dendritic potassium currents, were especially important to the generation of a burst. We were able to reproduce figures from voltage-clamp experiments done by Parpura and Haydon (2000) (Figures **??**, 7.9). Using our model, we successfully reproduced the experimental findings of Tian et al. (2005), which show that synaptic activity among neurons is not required for PDSs (Figure 7.11).

8.1 Physiological relevance and limitations

A basic assumption of compartmentalized models is that each compartment represents an isopotential section of the neuron. To minimize computational error, the compartmental dimensions should be a fraction of the characteristic length ($\leq 0.1\lambda$). However, comparing the size of our compartments with Traub et al. (1991), the "length" of our compartments was greater than 0.5λ. Thus our model should be considered as phenomenological rather than physiological. Since our model was able to reproduce a number of experimental results, perhaps the level of intracellular astrocytic calcium is related to the slow neuronal inward currents

(SICs). The relationship between the astrocytic calcium elevations and the release of glutamate has yet to be defined.

When creating such a reduced model, it is important to recognize the level of detail one wishes to obtain. We have focused our attention on modeling the characteristic behaviour of a CA1 neuron, concentrating on the synaptic influence from astrocytes. Certain limitations of the model were discussed, including its inability to produce small all-or-nothing spikes called d-spikes. Although Traub et al.'s (1979) model accounts for these small spikes, this level of detail was not required for our analysis. Since Traub et al. (1991) modeled 19 compartments instead of two, they are able to describe differences in the properties along the neuron in more detail. Therefore, if these differences are relevant to the question at hand, a more detailed model would be useful. In addition, the relationship between the intracellular astrocytic calcium concentration and the glutamate release is not modeled in detail. To analyse the astrocytic influence on seizure generation, it would be helpful to have a qualitative model of the astrocytic response to glutamate. That is, an improvement on our model could include a detailed model of the dynamics between the astrocytic mGluRs, the IP3 release, the cytosolic calcium fluctuations, and the release of extracellular glutamate. A detailed model of the synaptic dynamics, or of glutamate activation of the neuronal NMDA receptor, could prove useful when considering the astrocytic generation of epileptiform bursting. However, our simplified model has accurately produced the desired results, and thus such detail in our model was not essential to achieve our goal.

In our analysis in section 7.4, we consider the steeply graded or step response of all-or-none astrocytes. We suggest that graded astrocytes differ from "all-or-none" astrocytes by the manner in which intracellular calcium stimulates glutamate release. We imply that minimal increases in astocytic calcium results in a maximal release of glutamate. Thus, neurons indirectly respond to small changes in astrocytic calcium levels, by obtaining large SICs in a step-like manner.

8.2 Future directions

The benefit of our simplified model is that it can be expanded in a number of ways, and the method of expansion will depend on the question at hand. For example, a model of astrocytic calcium signalling may replace the current astrocytic calcium described by a step, pulse or wave. It would be interesting to see how a network of astrocytes and neurons interact, and how this affects epileptiform seizure generation. A detailed description of how the intracellular calcium elevations influence glutamate, and more information on how the NMDA receptors are activated by glutamate, would be helpful to expand the model of the synaptic NMDA currents. There are many possible astrocytic pathologies which may influence the generation of epileptiform bursting. For example, excess metabotropic glutamate receptors on the astrocytic membrane may contribute to the generation of seizure activity by creating strong responses to weak glutamate signals. Similarily, excess release

of IP3 may create large cytosolic calcium responses, which may also contribute to seizure generation. Our model does not consider these dynamics in detail, and thus can not distinguish between these different possible pathologies. Therefore, a more detailed description of the astrocytic calcium signalling of neighbouring neurons would be useful to determine how an astrocyte influences epileptiform bursting.

References

T.L. Babb and W. J. Brown. Pathological findings in epilepsy. In J. Jr. Engel, editor, *Surgical treatment of the epilepsies*, pages 511–540. Raven Press, New York, USA, first edition, 1987. 4

N.R. Carlson. *Physiology of Behaviour*. Allyn and Bacon, Needham Heights, Massachusetts, USA, seventh edition, 2001. 5, 6, 8, 10, 11, 13, 15

K.S. Cole. Dynamic electrical characteristics of the squid axon membrane. *Arch. Sci. Physiol.*, 3:253–258, 1949. 20

K.S. Cole. *Membranes, Ions and Impulses: A Chapter of Classical Biophysics*. University of California Press, Berkeley, CA, 1968.

K.S. Cole and H.J. Curtis. Electrical impedance of the squid giant axon during activity. *Journal of General Physiology*, 22:649–670, 1939. 18

H.M. Duvernoy. *The human hippocampus: functional anatomy, vascularization and serial sections with MRI*. Springer, third edition, 2005. 4, 5, 6, 8, 10

J. Jr. Engel and Pedley. *Epilepsy A Comprehensive Textbook*. Lippincott-Raven Publishers, Philadelphia, PA, USA, 1997.

Bard Ermentrout. *Simulating, analyzing, and animating dynamical systems: a guide to XPPAUT for researchers and students*. Society for Industrial and Applied Mathematics, Philadelphia, P.A., USA, 2002. 61

C.P. Fall and J.E. Keiser. Voltage gated ionic currents. In C.P. Fall, E.S. Marland, J.M. Wagner, and J.J. Tyson, editors, *Computational Cell Biology*, chapter 2. Springer-Verlag, New York, 2002. 18

D.E. Goldman. Potential, impedance, and rectification in membranes. *Journal of General Physiology*, 27:37–60, 1943. 20

M.R. Guevara. Dynamics of excitable cells. In A. Beuter, L. Glass, M.C. Mackey, and M.S. Titcombe, editors, *Nonlinear dynamics in physiology and medicine*, volume 25 of *Interdisciplinary Applied Mathematics*, chapter 4. Springer-Verlag, New York, 2003. 20

B. Hille. *Ionic channels of excitable membranes*. Sinauer Associates Inc., Sunderland, Massachusetts, USA, second edition, 1992. 18, 19, 22, 23, 28, 31

N. Hitiris, R. Mohanraj, J. Norrie, and M. J. Brodie. Mortality in epilepsy. *Epilepsy and Behavior*, 10:363–376, 2007. 3

A. Hodgkin and A. Huxley. A quantitative description of membrane current and its application to conduction and excitation in nerve. *Journal of Physiology*, 117: 500–544, 1952d. 17, 18, 26

A.L. Hodgkin and A.F. Huxley. Currents carried by sodium and potassium ions through the membrane of the giant axon of *Loligo*. *Journal of Physiology (London)*, 116:449–472, 1952a. 22, 23, 24, 25, 27, 28, 29, 30, 31, 32, 34, 35, 36

A.L. Hodgkin and A.F. Huxley. The components of membrane conductance in the giant axon of *Loligo*. *Journal of Physiology (London)*, 116:473–496, 1952b. 23, 24

A.L. Hodgkin and B. Katz. The effect of sodium ions on the electrical activity of the giant axon of the squid. *Journal of Physiology (London)*, 108:37–77, 1949. 20, 23, 27

A.L. Hodgkin, A.F. Huxley, and B. Katz. Ionic currents underlying activity in the giant axon of the squid. *Arch. Sci. Physiol.*, 3:129–150, 1949. 20

G. Marmont. Studies on the axon membrane. i. a new method. *Journal of Cell. Comp. Physiol.*, 34:351–382, 1949. 20

J.H. Martin. *Neuroanatomy: text and atlas*. McGraw-Hill, USA, third edition, 2003. 3, 4, 5, 6, 8, 13, 14, 80

J. Milton and P. Jung. *Epilepsy as a Dynamic Disease*. Springer, New York, USA, 2003. 3, 4

Suhita Nadkarni and Peter Jung. Synaptic inhibition and pathologic hyperexcitability through enhanced neuron-astrocyte interaction: A modeling study. *Journal of Integrative Neuroscience*, 4(2):207–226, 2005. 15, 16, 76, 77

M. Nelson and J. Rinzel. The hodgkin-huxley model. In J.M. Bower and D. Beeman, editors, *The book of GENESIS: exploring realistic neural models with the GEneral NEural SImulation System*, chapter 4. TELOS/Springer-Verlag, second edition, 1998. 28

Vladimir Parpura and Philip G. Haydon. Physiological astrocytic calcium levels stimulate glutamate release to modulate adjacent neurons. *PNAS*, 97(15):8629–8634, July 2000. 2, 11, 15, 38, 49, 50, 79, 80, 81, 82, 83, 84, 85, 86, 88, 90, 91, 95, 96, 97, 98

D.H. Perkel, B. Mulloney, and R.W. Budelli. Quantitative methods for predicting neuronal behavior. *Neuroscience*, 6(5):823–837, 1981. 80

Paul F. Pinsky and John Rinzel. Intrinsic and network rhythmogenesis in a reduced Traub model for CA3 neurons. *Journal of Computational Neuroscience*, 1:39–60, 1994. 1, 37, 38, 42, 50, 52, 53, 54, 58, 62, 63, 64, 70, 73, 98

Guo-Feng Tian, Hooman Azmi, Takahiro Takano, Qiwu Xu, Weiguo Peng, Jane Lin, NancyAnn Oberheim, Nanhong Lou, and Maiken Nedergaard. An astrocytic basis of epilepsy. *Nature Medicine*, 11(9):973–981, September 2005. 1, 2, 15, 37, 38, 46, 47, 49, 50, 79, 82, 90, 91, 92, 93, 94, 96, 97, 98

Roger D. Traub and R. Llinás. Hippocampal pyramidal cells: Significance of dendritic ionic conductances for neuronal function and epileptogenesis. *Journal of Neurophysiology*, 42(2):476–495, March 1979. 52, 54, 58, 64, 70, 99

Roger D. Traub, Robert K. S. Wong, Richard Miles, and Hillary Michelson. A model of a CA3 hippocampal pyramidal neuron incorporating voltage-clamp data on intrinsic conductances. *Journal of Neurophysiology*, 66(2):635–650, August 1991. 1, 2, 37, 38, 39, 41, 42, 43, 44, 45, 50, 52, 53, 54, 55, 57, 58, 59, 62, 63, 64, 65, 70, 74, 80, 81, 97, 98, 99

Roger D. Traub, Richard Miles, and György Buzsáki. Computer simulation of carbachol-driven rhythmic population oscillations in the CA3 region of the *in vitro* rat hippocampus. *Journal of Physiology*, 451:653–672, 1992. 40, 73, 77

H. V. Vinters, D. L. Armstrong, T. L. Babb, C. Daumas-Duport, Y. Robitaille, C. J. Bruton, and M. A. Farrel. The neuropathology of human symptomatic epilepsy. In J. Jr. Engel, editor, *Surgical treatment of the epilepsies*, pages 593–608. Raven Press, New York, USA, second edition, 1993. 3

H. G. Wieser and P. D. Williamson. Ictal semiology. In J. Jr. Engel, editor, *Surgical treatment of the epilepsies*, pages 161–172. Raven Press, New York, USA, second edition, 1993. 4

H. G. Wieser, P. D. Williamson, J. Jr. Engel, T. L. Babb, and P. Gloor. Surgically remediable temporal lobe syndromes. In J. Jr. Engel, editor, *Surgical treatment of the epilepsies*, pages 49–63. Raven Press, New York, USA, second edition, 1993.

P. D. Williamson, J. Jr. Engel, and C. Munari. Anatomic classification of localization-related epilepsies. In J. Jr. Engel and T. A. Pedley, editors, *Epilepsy - A Comprehensive Textbook*, pages 2405–2416. Lippincott-Raven Publishers, Philadelphia, PA., USA, 1997a. 4

P. D. Williamson, J. Jr. Engel, and H. G. Weizer. Mesial temporal sclerosis. In J. Jr. Engel and T. A. Pedley, editors, *Epilepsy - A Comprehensive Textbook*, pages 2417–2426. Lippincott-Raven Publishers, Philadelphia, PA., USA, 1997b. 4

World Health Organization. Epilepsy: aetiogy [sic], epidemiology and prognosis. World Health Organization, 2001. URL http://www.who.int/mediacentre/factsheets/fs165/en,2001. Available from http://www.who.int/mediacentre/factsheets/fs165/en, 2001. 1, 3, 97